Operational characteristics of a metal supported solid oxide fuel cell power generation system on methanol for naval applications

MSc. Thesis
Marine Technology
Y. Hoff

TU Delft

DAMEN NAVAL

Operational Characteristics Of A Metal Supported Solid Oxide Fuel Cell Power Generation System On Methanol For Naval Applications

by

Y. Hoff

in partial fulfilment of the requirements for the degree of

Master of Science
in Marine Engineering

at Delft University of Technology,
to be defended publicly on Thursday Februari 3rd, 2021 at 11:00 CET

Student number:	4319168	
Project duration:	Januari 11, 2021 – Februari 3, 2022	
Supervisor:	Assistant prof. Dr. Ir. L. van Biert	TU Delft (SDPO)
Supervisor:	Ir. G.J. Meijn	DAMEN Naval (DSNS)
Thesis committee:	Associate prof. Ir. K. Visser	TU Delft (SDPO)

ABSTRACT

The International Maritime Organisation intends to reduce the total greenhouse gas emissions with 50% by 2050 for the maritime industry relative to 2008. The operating lifespan of a vessel is between 15 - 30 years. This implies that a decade from now, most new-build vessels will contribute to the total emissions of 2050, forcing stakeholders to look for alternative solutions for fuels and power generation systems.

The Royal Netherlands Navy looks into the use of methanol as a short term solution for their fleet and has interest in fuel cell systems for naval applications. Therefore, Damen Naval, who builds vessels for the RNLN and stakeholder in this research, wants to explore alternative solutions for fuels and power generation systems for naval applications. Hence this research; what are the characteristics of the methanol fuelled metal supported solid oxide fuel cell based balance of plant for power generation applications on a hydrographical survey vessel. The HOV has a diesel electric power generation system and will be replaced in 2033.

The behaviour of the balance of plant with the MS-SOFC is the main focus of this research. The balance of plant exists out of the (methanol) pre-reformer, the FC system, the combustor, the heaters, and pipes connecting the system. The reformer and the FC system are modelled 1-D where the other parts are 0-D modules. The goal is to find the behaviour of the the system for various temperatures, fuel feeds, fuel flows and determine the power density, fuel utilisation and overall efficiency of the FC together with the BoP. This is bench marked against an ICE on MDO to determine if the system configuration is viable for marine applications regarding performance, efficiencies, power density, and emissions.

The main focus is on the 1-D reformer and FC system. The burner, heaters, pipes, pumps and turbines are considered 0-D units, which support the 1-D models.

The reformer is tested for various temperatures and various molar fractions of water and methanol for various volumetric flows. The reforming process is methanol steam reforming which is endothermic. The fuel feed is heated by the exhaust gasses via the solid of the reformer acting as a plate heater in a parallel flow system.

The MS-SOFC distinguishes itself because of the metal support layer at the anode electrolyte. Small holes in the metal support allow hydrogen to reach the electrolyte. The system operates at a maximum temperature of 873.15$[K]$ and is cooled via the air supply in the cathode. Two temperature states are assumed, the air temperature and the lumped stack and fuel temperature. The MS-SOFC internally reforms methanol via methanol decomposition. The distribution of the current density along the discretization units is determined by a numerical solver based on temperature, pressure, volume, molar fractions and total required current density.

The reformer and FC are both tested as stand alone units to determine their individual behaviour under different circumstances. The system as a whole is tested for four operational profiles and a 5000 nm transit, which are functional requirements for the HOV.

The reformer model showed promising results for fuel feeds of 50/50 methanol/water or less methanol. The system is able to reform up 80% relatively fast with a methanol molar fraction of $y_{me} = 0.5[\frac{mol}{mol}]$, a mass flow rate of $\dot{m}_{fuel} = 0.2[\frac{m}{s}]$, an exit temperature of $T_{reformer_{exit}} = 598.15[K]$, and a reformer length of $L_{reformer} = 1[m]$. However, to reform the last 20%, the reformer needs to be twice as long. Note that the amount of moles rise due to the decomposition of methanol, this results in higher volumetric flow rates and thus slowing down the reforming process relative to length of the reformer unit. The exhaust gasses carry enough heat to sustain the reforming process.

The FC model shows it performs best with 80% methanol reformed or more. The system shows great part load characteristics with system efficiencies of $\eta_{FC} \geqslant 0.551$ for $I_{tot} \leqslant 1900[\frac{A}{m^2}]$. However, due to the lower spatial distribution of hydrogen in the metal support, the FC system rapidly decreases in efficiency for higher current densities of $I_{tot} \geqslant 2500[\frac{A}{m^2}]$. The system also shows a 23% loss in performance when the exit temperature is decreased by 40 degrees.

The system as a whole shows to have an overall efficiency of $\eta_{FC} = 0.527$ regarding the four operational profiles. The system uses up to 73% of its own generated heat, leaving 27 % of the heat as exhaust gasses. The amount of methanol needed for a 14 day endurance is $L_{methanol} = 93.7[m^3]$, which is 4 times less than the available bunker space. The part load system efficiencies for $P_{required} \leqslant 0.55P_{max}$ are $\eta_{FC} \approx 0.551 - 0.645$. However, the high load system efficiencies for $P_{required} \geqslant 0.85P_{max}$ are $\eta_{FC} \leqslant 0.443 - 0.332$. As a result, the system is about 40% more efficient in part-load cases. The carbon dioxide produced is $\eta_{CO_{2,FC}} = 414.23g/kWh$, which is 30% less than a conventional system. The system produces no other emissions like NO_x or SO_x. For an ICE this is $\eta_{NO_{x,ICE}} = 12g/kWh$, equivalent to $\eta_{CO_{2,ICE_{equivalent}}} = 3576g/kWh$.

The system is viable to replace an ICE for marine applications regarding its performance. The study suggest three follow-up studies to further investigate the BoP together with the MS-SOFC on methanol.

First, a BoP design study about the 0-D system must be made. This gives insight in the actual size of the BoP and the actual power density of the total system. At the same time, due to the great part-load performance and poor high load performance of the FC system regarding fuel utilisation and total efficiencies, it is suggested to look further in the addition of a power generator which is great for peak loads and transient loads. An ICE using the hydrogen rich exhaust gas of the FC for example.

The model was not able to perform transient studies due to numerical errors. Therefore, a control study about the transient behaviour of the MS-SOFC is needed. The FC is sensitive for the change in temperature regarding its operational performance. It has been found that the actual temperature changes itself are not causing difficulties, it is changing the current drawn from the stack in relation to changing the fuel and air feed which makes it complex.

Lastly the methanol well-to-tank challenges need to be investigated. The emphasis of this study should lie in the compliance, the economic feasibility and the logistic challenges that methanol has. The fuel of the future depends as much on well-to-tank performance as for tank-to-wave performance regarding costs, safety and ease to use for a logistic fuel in general.

Acknowledgements

Sometimes you feel cheerful because something great happened. Sometimes you get dissatisfied because things are not as they should be. But most times you don't even bother.

That is why I once more want to be grateful to everyone who helped me achieving this.

Please if you read this, go to this Youtube link and be grateful for what you have.

https://www.youtube.com/watch?v=3L0dVaWq_tE

Thank you.

CONTENTS

NOMENCLATURE

A list of the acronyms and the symbols used in this thesis is shown in this section.

Tab. 1 | Table of all acronyms in this thesis

Acronym	Description
AFC	Alkaline Fuel Cell
ASC	Anode Supported Cell
ASU	Air Separation Unit
BOP	Balance of Plant
CSC	Cathode Supported Cell
CTE	Coefficient of Thermal Expansion
DEFC	Direct Ethanol Fuel Cell
DMFC	Direct Methanol Fuel Cell
DSNS	DAMEN Naval (DAMEN Schelde Naval Shipbuilding)
EEZ	Exclusive Economic Zone
ELOT	End of Life Type
EMF	Electromotive Force
EMS	Energy Management System
ESC	Electrolyte Supported Cell
FC	Fuel Cell
GHG	Greenhouse Gas
HFO	Heavy Fuel Oil
HOV	Hydrographic Survey Vessel
HT-	High Temperature -
ICE	Internal Combustion Engine
IMO	International Maritime Organisation
IT-	Intermediate Temperature
LD	Lethal Doses
LNG	Liquefied Natural Gas
MCFC	Molten Carbonate Fuel Cell
MDO	Marine Diesel Oil
MEPC	Marine Environment Protection Committee
MGO	Marine Gasoil
MSC	Metal Supported Cell
MSR	Methanol Steam Reforming
MS-SOFC	Metal Supported Solid Oxide Fuel Cell
nm	Nautical Mile
OCV	Open Circuit Voltage
O&M	Operations and Management
OMR	Oxidative methanol reforming

Acronym	Description
OPEX	Operational Expenditures
PEMFC	Proton-Exchange Membrane Fuel Cell
PEN	Positive electrode - Electrolyte - Negative electrode
POM	Partial Oxidation of Methanol
RNLN	Royal Netherlands Navy
SOFC	Solid Oxide Fuel Cell
TRL	Technology readiness level

Tab. 2 | Table of all symbols in this thesis

Symbol	Description	
$\dot{m}$	Mass flow rate	$[\frac{m}{s}]$
$\dot{V}$	Volumetric flow rate	$[\frac{m^3}{s}]$
η	Efficiency	[-]
σ	Electronic conductivity	$[\frac{S}{m}]$
τ	Thickness	$[m]$
ρ	Density of medium	$[\frac{kg}{m^3}]$ or $[\frac{mol}{m^3}]$
A	Surface	$[m^2]$
A	Pre-exponential factor	[-]
C_x	Molar concentration of species	$[\frac{mol}{m^3}]$
C_p	Heat capacity	$[\frac{J}{K}]$
C_2H_5OH	Ethanol	
CH_3OH	Methanol	
CH_4	Methane	
CTE	Coefficient of thermal expansion	$[\frac{ppm}{K}]$
CO	Carbon Monoxide	
CO_2	Carbon Dioxide	
D	Diameter	$[m]$
E_{act}	Activation energy	$[V]$
$e+/e-$	Positive-, negative electron	
F	Faraday's Constant	$[\frac{sA}{mol}]$
G	Gibbs Free Energy	$[J]$
g	Gravitational Acceleration	$[\frac{m}{s^2}]$
H	Enthaly	$[J]$
H_2	Hydrogen	
H_2O	Water	
i	Current density	$[\frac{A}{m^2}]$
i_0	Exchange current density	$[\frac{A}{m^2}]$
I_{tot}	Total current density	$[\frac{A}{m^2}]$
k	Rate constant	[-]
kts	Knots	
L	Length	$[m]$

Symbol	Description	
n_e	Amount of electrons	[-]
N_x	Molar flow	$[\frac{mol}{sm^3}]$
NH_3	Ammonia	
O_2	Oxygen	
P	Pressure	$[Pa]$
P	Power	$[\frac{W}{m^2}]$ or [W]
p_x	Partial pressure of species	$[\frac{molPa}{mol}]$
Q	Heat	$[J]$
q_x	Heat flux	$[\frac{W}{m^2}]$
R_{ohm}	Ohmic resistance	$[Ohm]$
R_u	Universal Gas Constant	$[\frac{J}{molK}]$
R_{MD}	Reaction rate of methanol decomposition	$[\frac{mol}{m^3}]$
R_{SR}	Reaction rate of methanol steam reforming	$[\frac{mol}{m^3}]$
R_{WGS}	Reaction rate of water gas shift	$[\frac{mol}{m^3}]$
S	Entropy	$[\frac{J}{gK}]$
t	Time step	$[s]$
t	Thickness	$[m]$
T	Temperature	$[K]$
v	Velocity	$[\frac{m}{s}]$
V_{act}	Activation losses	$[V]$
V_{con}	Concentration losses	$[V]$
V_{Nernst}	Nernst Voltage	$[V]$
V_{oc}	Open circuit voltage	$[V]$
V_{ohm}	Ohmic losses	$[V]$
$V_{operational}$	Operational voltage	$[V]$
x	thickness	$[m]$
y_x	Molar fraction of species	$[\frac{mol}{mol}]$
z	Hight	$[m]$

1

INTRODUCTION

In 2018, International Maritime Organization (IMO) adopted the IMO's Marine Environment Protection Committee (MEPC) greenhouse gasses (GHG) strategy. This strategy suggested, among other things, a reduction in total GHG emissions of at least 50% by 2050 compared to 2008 for the maritime industry. At the same time the industry should opt to eliminate GHG emissions entirely [1]. A vessel is a capital-intensive asset with a typical operating lifespan of 20-30 years, or sometimes even longer. This implies that a decade from now, most new-build vessels will contribute to the total emissions of 2050. Therefore, immediate focus is required to achieve this target by 2050 rather than taking it as a far-away ambition [2]. This can only be done if all stakeholders in the maritime industry work together.

According to DNV-GL, an international accredited registrar and classification society, it is expected that the maritime industry by 2050 will mostly be dominated by hydrogen based power systems whilst it is dominated by oil today [3, 4]. Hydrogen as a logistic fuel is less preferable compared to various alternative fuels like ammonia, methane or methanol for maritime applications due to the unfavourable gravimetric density, volumetric density and/or low temperature combined with high pressure storing [3, 5, 6]. In other words, the logistic fuel that has to replace oil based fuels has not yet been determined. For instance, the development of cheap sustainable electricity or cheap sustainable biomass are key parameters that influence future operational expenditures (OPEX). The former is favourable for ammonia and the latter for methanol [3]. The Royal Netherlands Navy (RNLN) participates in the consortium Green Maritime Methanol in which the possibilities for green methanol for internal combustion engines (ICEs) have been researched broadly for their fleet and will be further investigated for the replacement of the support vessels, in particular the hydrographical survey vessels [7–9].

The RNLN has interest in fuel cell (FC) systems for naval applications. Compared to the conventional ICE, it is expected that a FC system will have higher efficiencies, less noisy, operate smoothly, pollute less and require less maintenance. However, the technology readiness level (TRL) of fuel cells (FCs) for maritime applications has not yet matured. The RNLN cannot afford to install a power generation system which might not be able to deliver the required power for the operational design. Therefore the RNLN will most likely not install FC systems in the near future. This was discussed with an DMO engineer in april 2021. This has to do with complications that lead back to the two fundamental problems with fuel cells; [a] the development of large, reliable and powerful fuel cell systems have not yet been viably demonstrated and [b] hydrogen or hydrogen carriers are not readily available fuels. Many researchers have attempted to solve these problems by designing different FC types. However, each solution brings new difficulties of its own [10].

The alkaline FC (AFC) is one of the oldest types of FC. The main advantage is that it is a rather cheap system. The problem is that the AFC is easily poisoned by CO_2 and therefore only operates on pure hydrogen and pure oxygen. The purification of oxygen from air is costly [11].

Proton exchange membrane FCs (PEMFC) operate at relative low temperatures, have a good power density and are relatively light. The major drawbacks are that they require expensive catalysts, commonly platinum, and that they operate on pure hydrogen. Using alternative fuels requires reforming which is often at higher temperatures than the operating temperature of the PEMFC. This results heating and cooling parasitric losses. Besides, the althernative fuel needs to be reformed to a (nearly) pure hydrogen feed which is an expensive operation [11].

Molten carbonate FCs (MCFCs) reach high efficiencies with the use of non-precious metals and can scale up to >10MW systems. The MCFC operates on high temperatures and gives the possibility to capture the expelled heat and use it. Systems can reach up to 85% efficiency in total, using both the electrical energy as the thermodynamic energy from the FC system. Due to the high operating temperatures, the MCFC is able to internally reform fuels like methane, methanol and other light hydrocarbons which reduces costs and improves the fuel flexibility of such a system. The main disadvantage of MCFCs is the poor durability due to the corrosive electrolyte that damages the structure internally [12].

The solid oxide FC (SOFC) uses a non-porous ceramic electrolyte that transfers oxide ions. Like the MCFC the SOFC reaches high efficiencies, is scalable, operates on relative high temperatures and has an even better fuel flexibility, regarding sulphur poisoning. In contrast to the MCFC, the SOFC is not corrosive at all due to the nature of the system. The main disadvantages of the SOFC system are the poor transient capabilities, slow start-up time, high material costs for high temperatures and rather poor shock resistance [12].

The metal-supported solid oxide fuel cells (MS-SOFCs) seems to overcome many problems that the traditional SOFC copes with. Conventional SOFCs cope with problems like tolerance to rapid thermal cycling and redox cycling, material cost and ruggedness while maintaining high efficiencies, long lifetimes and scalability on temperatures ranging from $500-1000\,^{\circ}C$. The solution is as follows; the ceramic electrolyte is supported by a broadly available stainless steel layer. As a result, the operating temperature must not exceed $\leqslant 600\,^{\circ}C$ to sustain the integrety of the metal support. The major drawback is that reduced operating temperatures reach lower overall performances due to ion passing capabilities of the PEN structure and the higher activation and ohmic losses. Although the open circuit voltage will be higher, it does not compensate for the losses (yet) [13]. This is why it attracted (renewed) interest for the development of FC systems in the recent years.

For this research, it was chosen to go in a direction that both helps maturing the low TRL of FC systems and compliments the ambitions of the stakeholders. The Delft university of Technology does research in FC systems and DAMEN Schelde Naval Shipbuilding (DSNS) wants to meet the RNLN demands. At the same time, the MS-SOFCs are expected to commercialise in the near future, and the RNLN has a tendency towards green methanol as a logistic fuel [7]. A solution for sustainable maritime power generation applications could lie in the use of a MS-SOFC on methanol for the RNLN. To get a deeper understanding of the performance of a MS-SOFC on methanol for maritime applications, the system first needs to be analysed.

The fact that an SOFC is able to internally reform methanol does not yet mean that it is considered ideal [14], nor does it imply that either all methanol should be reformed or nothing. In figure 1.1 the power density of three types of low temperature SOFC types are depicted at several operating temperatures, the direct ethanol FC (DEFC), the direct methanol FC (DMFC) and a 'regular' H_2 fuelled SOFC.

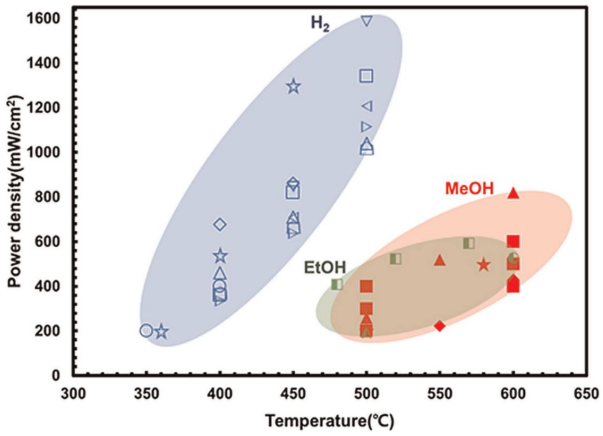

Fig. 1.1 | Summary of peak power densities of direct alcohol-fuelled and H2-fuelled LT-SOFC [14]

For DEFCs high coking is expected, which significantly reduces the lifetime, the operability and stability of this FC[14, 15]. Coking occurs when two carbon atoms react to a solid state and precipitate onto the FC stack and reducing its performance. Further explained in section 3.2.4. DEFCs are not further considered in this review due to their poor lifetime performances and their low current densities, shown in figure 1.1. The

DMFC and the H_2-fuelled SOFC are. As one sees in figure 1.1, the positive 'linear' relation between power density and temperature is higher with H_2 than CH_3OH. For this reason it would be obvious to supply pure hydrogen, reformed methanol, to the SOFC. The reforming process however is slow [16]. Thus, either the size of reforming system would be huge or the reformer is not able to supply the hydrogen demand. Note that the reformer is a parasitic system also, which draws heat from the system. However, there subtle balance between DMFC and fully reformed methanol feeds for SOFC systems which lies in between the H_2 fueled and $MeOH$ fueled FCs shown in figure 1.1.

From a design point of view, the power density of the total system is an important factor because it has a direct relation with the size of the system. One of the reasons why methanol is used relates to the inefficient storage of pure hydrogen [5]. So one way to optimise a DMFC system is to partly reform the methanol [17]. As a result the thermal stresses in the FC will be lower due to fewer endothermic reactions, the partial pressure of hydrogen at the inlet will be higher and this could lead to higher power densities [17]. How this works will be explained in chapter 3.3.

From this point in the research, methanol has been chosen as the logistic fuel, an MS-SOFC as the power generator and a reformer as the main BoP component supporting the MS-SOFC. The fuel is relatively easy to reform, it is slightly endothermic compared to methane. Methanol can be bunkered in liquid phase, it is has a high hydrogen yield and it is of interest to the RNLN. A LT-SOFC on hydrogen seems to have the power density to be viable for marine applications, however, not if it is fueled by pure methanol. Therefore a the interaction of a methanol reforming system and a LT-SOFC is reviewed. The MS-SOFC is a type of LT-SOFC which is a strong contender for future FC usage. The low temperature results in a higher change in molar Gibbs energy of formation which results in lower thermodynamic losses. Nevertheless, lower temperatures result in higher ohmic and activation losses also. The BoP composition is further reviewed in order to asses the viability of the MS-SOFC on methanol with reformer combination.

Since the considered SOFC system produces both heat, electric power and uses fuel pre-reforming, it would be nonsensical to observe the stack only for power generation. The total power generating system on board of the vessel is called the balance of plant (BoP). The components that constitute the balance of plant are fuel cell stacks, a heater, heat exchanger, start-up power source, steam recovery system, air blower, pumps, battery pack and more. Although the exact definition of a balance of plant is not defined, one could see it as all the systems needed to operate the entire power generation system properly [18]. In figure 4.1 the considered balance of plant is shown.

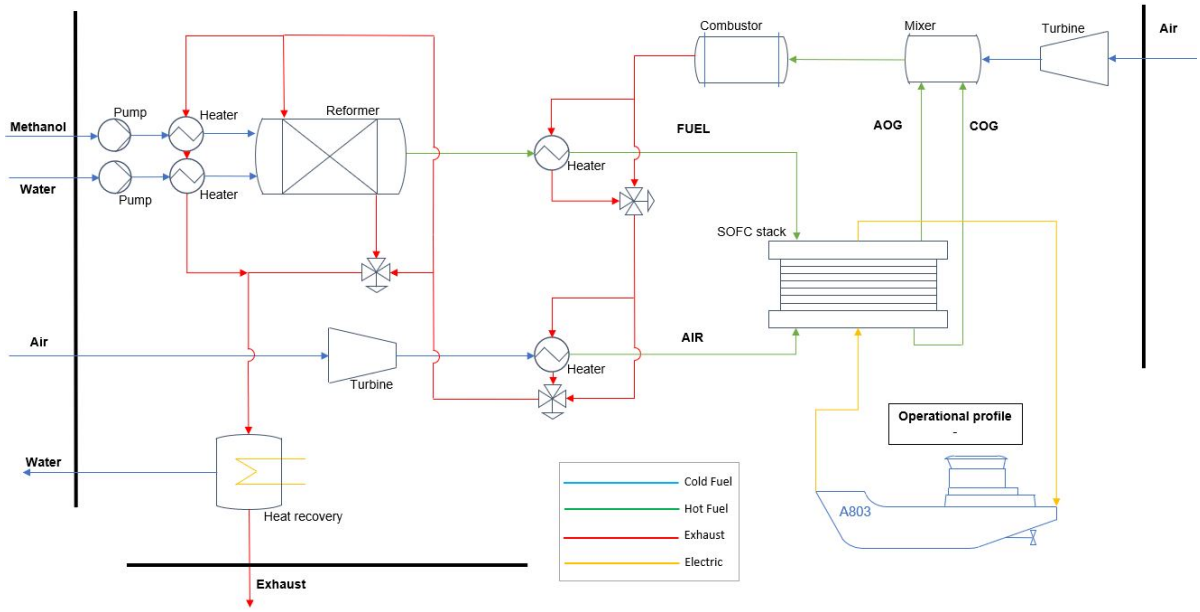

Fig. 1.2 | Schematic representation of the Balance of Plant considered in this research from Results in chapter 8

Water and methanol are mixed before the inlet of the reformer. This improves the methanol conversion rates and it helps to prevent or reduce coking. The methanol/water mixture is heated to $300-350\,^{\circ}C$ and then (partly) reformed in the reformer into hydrogen, water, carbon monoxide, carbon dioxide. Then the air and fuel are heated further to $400-450\,^{\circ}C$ to reduce thermal stresses in the FC stack. If the difference in

temperature between the entrance and exit of the FC stack are too high, materials could begin to inflect or crack due differences in characteristics of materials to what extend it expands upon heating. The fuel is then supplied to the anode. The cathode receives pressurised air that both supplies oxygen as it cools the stack internally. The anode off-gas contains unused hydrogen and carbon monoxide, which is combusted in the combustor together with the unused oxygen from the cathode and fresh air. The produced heat is used to heat the fuel in and after the reformer, the cathode air via a heat exchanger and lastly the heat is drawn in a heat recovery system. Such a recovery system could, for example, heat water and air for on board usage or drive another power generating system. Lastly, the exhaust gasses flow trough a steam recovery system which cools the exhaust gasses to extract the water. Pure water is produced and redirected to the inlet of the pre-reformer. The excess of water and other exhaust gasses are disposed via exhaust pipes.

The fuel cell stack produces electrical energy which is supplied to an energy management system. Due to the rather slow ramp-up, ramp-down and starting characteristics of the fuel cell system, an external power source is considered also. Such an external power source could be an ICE, a battery pack or another power generator. Although this is most certainly necessary, it is not further investigated in this research. The main reason for that is because it mainly a design challenge.

It is clear that the performance of MS-SOFC on methanol based BoP for maritime applications needs to be analysed entirely instead of the SOFC alone. To evaluate a BoP on its viability whilst the TRL of several components is low, it is advised to first model its behaviour [13]. Therefore, the system will be dynamically modelled to simulate operations of a vessel. This could give insights in the behaviour of the system. After reviewing the system, it can be evaluated with conventional systems in its overall performance. It is important to take the inter-relational behaviour of the reformer and FC system into account to determine the strengths and weaknesses of the BoP design.

2

RESEARCH OBJECTIVE

Simulations of various operations gives insights in the characteristics and the viability of an ms-sOFC on methanol based BoP as stated earlier. Most available models give insights in the behaviour and the performance of a single cell or a FC stack only, but relatively few to none on the level of a BoP containing sub-system level detail for maritime applications [19]. The main reason is that every BoP has to be tailored for its specific application. So even if such models were created, they would probably contain supplier confidential system data and/or system configurations to keep their market posititon.

As stated earlier, the fundamental problems of fuel cell systems for marine applications are that [a] the development of large, reliable and powerful fuel cell systems have not yet been viably demonstrated and [b] hydrogen or hydrogen carriers are not readily available fuels. It is suggested that an ms-sOFC system on methanol could potentially overcome these challenges. Therefore, in this research an ms-sOFC system on methanol will be analysed and reviewed on its behaviour for maritime applications trough dynamic modelling.

The model must cover all the relevant processes in a timescale that corresponds to daily operations of a naval vessel. Therefore subjects like the start-up time, ramp-up and ramp-down characteristics, the lifetime and durability of the system, the safety, reliability and maintenance of the system need to be analysed. The model must simulate full operations to address these problems thoroughly. This implies that the time step of the simulated outcomes of the FC system model are scaled to changes during an operation.

The outcomes of the model will be used to compare the FC system with a conventional ICE system also. This research aims to answer the following research question:

- *What are the characteristics of the methanol fuelled metal supported solid oxide fuel cell based balance of plant for power generation applications on a hydrographical survey vessel?*

In order to answer this question, the following sub-questions will be studied more in-depth.

- *What would the MS-SOFC on methanol based BoP for power generation applications on a naval vessel look like?*
- *Is the BoP a viable option for a naval vessel as a power generation system according to the 8 following parameters? [1] Efficiency in design and off-design conditions, [2] Power and energy density, [3] Load transients and system start-up, [4] Environmental impact*
- *Is an ms-sOFC based BoP on methanol for power generation applications competitive to an internal combustion engine system in terms of the previous listed parameters?*

This research is carried out from a marine engineering perspective. The outcomes do give insights in the flows, the heat and the electrical power of the system, and and the questions above. The actual design of the system is out of scope.

3

SCOPING AND THEORETICAL BACKGROUND

3.1. THE OPERATIONAL PROFILE: HYDROGRAPHIC SURVEY VESSEL

It may sound trivial, but a vessel fits a purpose. This purpose is characteristic to the vessel, defined by the user prior to building it to serve in certain operations. This translates into certain characteristics, for example; the measures of the vessel, the ability to sail certain areas, the speed, the on board instruments, the accommodating facilities, etc. The required performance of the vessel is partly defined in capabilities of the BoP; the torque demanded by the shaft to get certain speeds, the electricity for on-board equipment, heating, ventilation and air conditioning (HVAC) in the cabins and on the bridge. These are all supplied from a power source. This power source runs on a fuel and is restricted to a certain weight, volume, robustness, lifetime, etc. and in case of naval applications also to signatures like sound, vibrations or heat and shock resistance.

Due to the interests of Damen Naval as main supplier of vessels for the RNLN, a family of support vessels with an expected end life of type (ELOT) in the not too distant future is chosen as the reference for this study. The ELOT of hydrographic survey vessels (HOVs) is in ≈ 2033 and they already have a complete diesel-electric propulsion system with an installed power of 1546 kW [20]. There have been ambitions from the government to reduce emissions and search for greener solutions regarding the support vessels [8]. There even have been studies towards alternative fuels, however, they dismissed the option of using an SOFC power generation system due to its low technology readiness level (TRL). A high TRL for naval applications is considered a must [9].

3.1.1. REPLACEMENT OF THE SUPPORT VESSELS

Besides the replacement of the Hydrographic Survey vessels, the logistic support, submarine support, and the naval training vessels will be replaced as well. Several sources suggest that the replacement vessel will have a 'family hull design'. This suggest that the hull of all vessels are based on the same concept [21]. The dimensions and exact operational profile, shown in table 3.1, has not yet been defined, but the principal design characteristics are.

Tab. 3.1 | Principal design characteristics [9]

Parameter	Family	HOV
High speed transit	12 kts	8 kts
Maximum speed	15 kts	12 kts
Installed power	5000 kW	1546 kw
Range transit speed	5000 nm	5000 nm
Displacement	2400 t	1814 t
Payload	800 t	≈ 800 t
Design life	30 years	30 years
Endurance	14 days	14 days
Operational Days	200 p/y	200 p/y

The Hydrographic Survey vessels map the seafloor for civil and military purposes in the exclusive

economic zone (EEZ) of the Netherlands or in specific area's. Note that the RNLN is required to serve and protect the Netherlands Antilles and Aruba also, meaning that the HOVs need to be able to cross the Atlantic Ocean which explains the 5000 nautical mile transit range requirement.

COMPARE PERFORMANCE

Although it is likely that the operational profile could change for the new HOV, the current operational profile is chosen. The goal of this research is not to develop a BoP for the HOV, but to get insights in the characteristics of an FC based BoP.

De Gaaij [22] suggested in his MSc. thesis, which was verified by an engineer of the Defence Materiel Organisation (DMO), that the operational profile of the Snellius class could be reduced to a couple of main parameters to give a rough, but indicating, estimation of what the power system should be able to deliver. The operation profile of the current vessel is given in table 3.2 and the family design is given in table 3.3.

Tab. 3.2 | Operational profile HOV [23]

	Type of operation	Power	Time	Speed
1	Low speed	141 kW	15%	4kts
2	Operations	436 kW	40%	6-10kts
3	Economic transit	436 kW	15%	9kts
4	High speed transit	880 kW	25%	12kts
5	Maximum speed	1150 kW	5%	13kts

Note that the maximum speed operation requires $1150kW$ where the installed power is $1546kW$. The main reason is that the estimation of De Gaaij stems from the functional scoping of the RNLN. Thus the installed power of $\approx 1500kW$ at maximum speed operations to make sure the amount of power required for the operatoins matches the current design.

Tab. 3.3 | Operational profile family design [9]

	Type of operation	Power	Time	Speed
1	Low speed	33%	15%	4kts
2	Operations	52%	40%	6-10kts
3	Economic transit	52%	15%	9kts
4	High speed transit	82%	25%	12kts
5	Maximum speed	99%	5%	15kts

the amount of power required for the 5 operations which are shown in table 3.3. The operational profile in this research is based on the measures of the current Hydrographical Survey class and the operational requirements shown in table 3.3.

TOTAL USAGE OF POWER

The FC system generates all power for the vessel and the BoP components. Therefore it should be noted that even though the five types of operations with their power demand and percentage of time seem roughly estimated, it does represent a conservative power demand for the vessel [9]. The model, however, will be designed to run through various operations independent to the measures of the vessel and the amount of power required. This does give the opportunity to run simulations for off-design conditions, other vessels or even as a part of another system. This will be further elaborated in chapter 4.

3.2. THE FUEL: METHANOL

Methanol (wood alcohol) was discovered by Robert Boyle as a byproduct of the pyrolysis of wood in 1661. This is done by heating wood with the absence of air. Since then this method has been the most common way of producing methanol, although it is rather inefficient. In 1920 synthesis gas was discovered, a combination of carbon monoxide and hydrogen. The production of methanol was easier, faster and more efficient with the use of synthesis gas [24]. The reaction is given as follows in equation 3.1

$$CO + 2\,H_2 \rightarrow CH_3OH \tag{3.1}$$

Currently methanol is mainly produced by processes like methane reforming, synthesising bio-methanol from biomass or the production of e-methanol from hydrogen and carbon monoxide. Bio-, and e-methanol can be purely produced from renewable resources. This could add to the decarbonization of the industry when used as a fuel. At the same time, methanol produces CO_2 in the reforming process to hydrogen. Cumulatively this results in a carbon neutral cycle [3].

3.2.1. ALTERNATIVE FUELS FOR SOFC APPLICATIONS

The electrochemically oxidized fuel in an SOFC is mostly hydrogen. There are some major challenges with using hydrogen as a logistic fuel. Hydrogen needs to be contained at cryogenic conditions or at extreme high pressures up to 700 bar to achieve reasonable tank sizes. This gives way for other fuels that could act as a hydrogen carrier [10]. In table 3.4 various fuels are shown. The table shows the fuel, their formula, the percentage of their molar mass that consists out of hydrogen, the density, and the amount of fuel in litre needed to store one kg hydrogen. The tank sizes are not considered. They do add to size because of their storage conditions that vary due to high pressures and/or low temperatures. This adds to a more unfavourable density $kg * L^{-1}$ and unfavourable volume $L * kg^{-1}$ needed to transport some fuels, this holds mainly for liquid hydrogen, liquid methane and liquid ammonia. The reforming system of methane is also not considered, but certainly not negligible in size and weight [25]. This results in that both liquid methane and liquid hydrogen have considerable drawbacks for long distance transportation. In the case of the alcohols, from a renewable energy source point of view, methanol is produced more easily than ethanol, whilst the advantages for fuel cell applications are in favour of methanol also because of coking [25]. All in all, the choice of the most promising future fuels in long distance transportation is reduced to ammonia and methanol [4] from a tank-to-wake point of view relative to the emissions as shown in figure 3.2. From a well-to-tank perspective, the only fuel considered with an already existing infrastructure is methane. However, Maersk announced that they want to use methanol as a fuel for their merchant vessels in the near distant future in early 2024 [26], which could help building the methanol infrastructure more easily. Maersk announced to be leading in green ammonia also, but in the distant future. Both plans for methanol and ammonia are not directly related to the use of fuel cell applications.

Tab. 3.4 | Various fuels as hydrogen carrier [10]

Name	Formula	Percent hydrogen	Density kg L^{-1}	Vol.(L) to store 1 kg H_2
Liquid H_2	H_2	100	0.07	14
Ammonia	NH_3	17.76	0.67	8.5
Liquid NG	CH_4	25.13	0.415	9.6
Methanol	CH_3OH	12.5	0.79	10
Ethanol	C_2H_5OH	13.0	0.79	9.7

Ammonia is synthesised from nitrogen and hydrogen. Nitrogen is abundant in the air ($p_{N_{2atm}} = 0.781$) and hydrogen can be produced through electrolysis of water. The ammonia molecule knows no carbon atom, which is favourable for a carbon free future. The decomposition of ammonia to hydrogen is in theory very straightforward.

$$2NH_3 \rightarrow 2N_2 + 3H_2$$

Both ammonia and methanol are already widely produced for several applications. Both fuels are relative easy to store and have been widely shipped. Another advantage is that these fuels can be used for internal combustion engines (ICEs) as well. Although, in contrast to methanol ICEs, the TRL of ammonia ICEs have not matured yet. Both fuels are toxic, but big ammonia leaks are substantially more disastrous than methanol leaks [27]. According to DNV-GL the choice between the two fuels depends on input price. Methanol depends on the price of biomass and ammonia on the price of renewable energy[4].

It must be said that DNV-GL advises shipowners to look for dual-fuel LNG for the short-term investment. Conventional LNG, e-LNG and bio-LNG are also very promising as a transition fuel in the shipping market. Ammonia and methanol will gain ground in >2040 [3, 4]. As briefly touched in the introduction, the Royal Netherlands Navy expresses strong interest in methanol as a fuel for its support vessels [7, 8]. In 2023 the RNLN scheduled to commence the replacement of the hydrographic survey support vessels. The RNLN

already extensively studied the viability of methanol as shipping fuel for its support vessels and tends to further investigate it. However the RNLN is considering ICE applications in combination with methanol due to the low TRL of FC systems [9].

CHOICE OF LOGISTIC FUEL

Due to the uncertainties embedded in the search for the new future fuel for shipping, the most practical fuel has been chosen. Methanol is one of the most promising future fuels, the RNLN is moving towards methanol, and methanol is relatively easy to reform to hydrogen and relatively easy to store compared to liquid hydrogen, liquid ammonia, and LNG. Besides, the production, storage, and transportation of the fuel, also known as the Well-to-Tank depicted in figure 3.2, is quite favourable for methanol as shown in figure 3.1 [28].

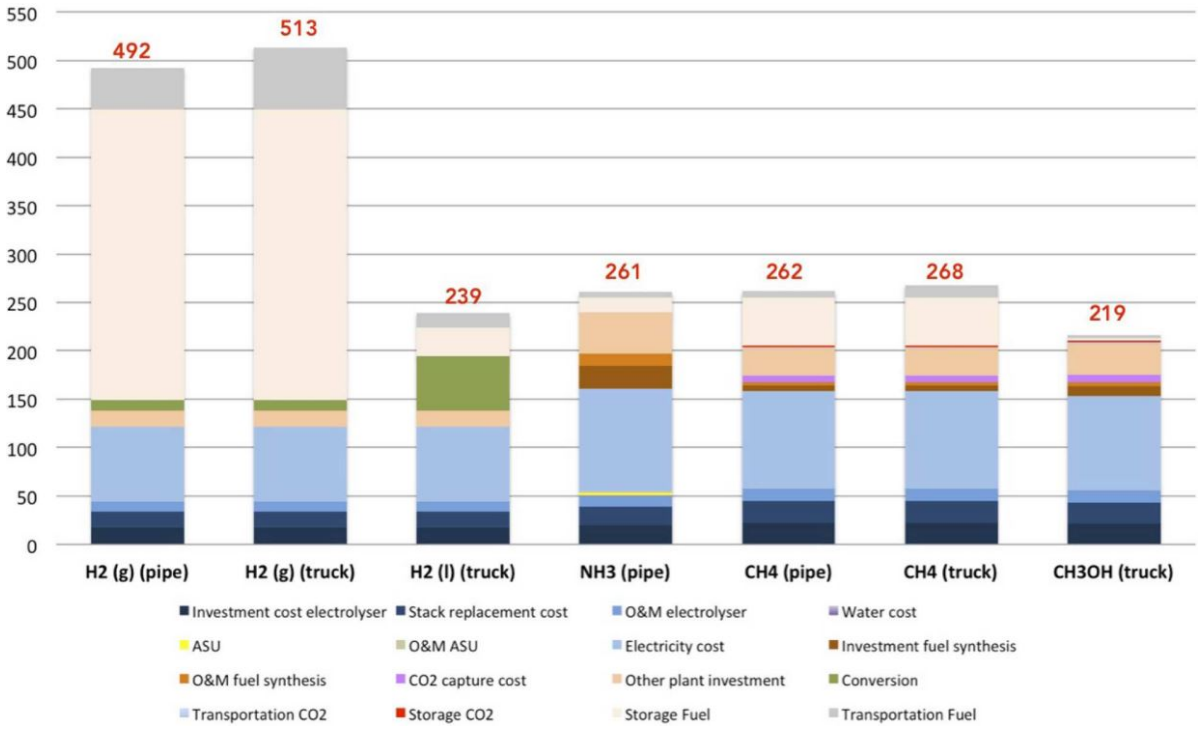

Fig. 3.1 | Global costs (production, storage, and transportation) for each fuel in €/MWh$_{fuel}$, with 30€/ton CO_2 [28]

The Air Seperation Unit (ASU) is considered expensive for the production of ammonia, the same for the Operations and Management (O&M) which is not that expensive for other future fuels considered. The largest portion of the price is determined by the amount of electricity used for the synthesis.

As a conclusion of the first findings regarding the logistic fuel for an intermediate temperature MS-SOFC in a balance of plant, methanol is favourable. Therefore methanol is chosen and other fuels are not further considered. The model, however, is built in such a manner that fuel flexibility is possible.

3.2.2. CHARACTERISTICS OF METHANOL

Methanol is the simplest alcohol molecule. It is poisonous to the human body. The median lethal dosses, LD_{50}, is 25 ml when it is absorbed through ingestion, breathing or skin. Methanol itself is not harmful, the human body naturally breaks methanol down to formaldehyde, formid acid and formate. These products cause the toxicity [29].

Methanol is considered a safer fuel because it develops less heat and burns more slowly, however, the flashpoint is lower. When spilled, methanol is broken down naturally if discharged into nature and can be diluted with water in the case of major discharges [30] which petrol can not.

Methanol is hygroscopic, this means that it absorbs moister, mostly water, directly from the atmosphere when it gets in contact with it. Since methanol vapour is heavier than air, it will linger close to the ground. When the concentration of methanol in the air is between 6-36% or higher (depending on the conditions), it

can be lit by a spark. When lit, it could cause an explosion when the temperature is > 12 °C, also refereed to as its flashpoint [10, 24].

3.2.3. METHANOL AS A LOGISTIC FUEL

Due to the flashpoint of > 12 °C, methanol is not allowed for use in merchant vessels as stated in IMO's IGF code (Code of Safety for Ship Using Gases or Other Low-flashpoint Fuels). The flashpoint threshold to be considered for a fuel is at > 60 °C, therefore methanol is considered an alternative fuel. To introduce a low flashpoint fuel on a merchant vessel, a risk assessment approach has to be taken. This is to ensure that the proposed system has an equivalent level of safety, from a fire safety perspective, as a conventional fuel oil arrangement [31]. As for other alternative fuels, methanol is one of the 'easiest' fuels to adapt to in the maritime industry due to its liquid phase at < 64.7 ° and slightly lower toxicity compared to petrol.

The ICCT estimates that the energy consumption in the marine industry will rise in the coming 10 years. As stated earlier, alternative fuels like ammonia or methanol will become viable in long term future. By then it is estimated that about 350 million metric tons of marine fuels a year are consumed which will be a mix of LNG, HFO, MDO, MGO etc. In other words, in order to supply the fuel demand with sustainable fuels, it has to be produced in extreme large quantities. For methanol a global production of 75 million metric ton a year already exists. Although a small percentage is completely green, it is estimated that the production of green methanol on such a large scale is possible [31].

As today, green methanol is about 2 - 4 times more expensive as the conventional fuels. Many reports have been written on the possibilities to scale up the green methanol production with the right kind of subsidies [3, 5, 30, 31]. By then, the price will decrease as well. The exact implementation of methanol from well to tank is extremely interesting. It will largely determine the feasibility of methanol as a logistic fuel in the marine industry. In this research the tank-to-wake technology is addressed only.

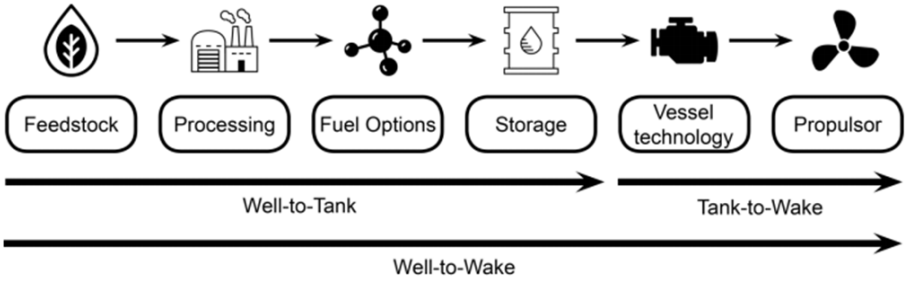

Fig. 3.2 | Definition of the Well-to-Wake approach of a fuel

As today, nearly every commercial green methanol application is focused on ICEs, due to the ease of transitioning towards methanol ICEs. Companies doing so do not want to invest in LNG ICEs since green LNG is more expensive and extracted gas is not carbon neutral. It must be said that even for future ammonia applications, most companies do consider ICEs as prime power generation system. The concluding remark is that FC systems are not readily considered as viable options. This has, as said earlier, mainly to do with the low TRL and uncertainties in what FC system to use.

3.2.4. METHANOL FOR POWER GENERATION

There are several types of fuel cell applications on methanol. Examples are direct methanol fuel cells (DMFC) [32], which have an oxygen ion passing electrolyte also, or high temperature proton exchange membaren fuel cells (HT-PEMFC) [33]. Methanol can be converted into syngas via the methanol decomposition (MD eq. 3.2) as shown below [34]. For a DMFC this is beneficial since it utilises both carbon monoxide as hydrogen. For HT-PEMFC the carbon monoxide needs to be converted to carbon dioxide via the water gas shift (WGS eq.3.3) reaction due to the toxicity of CO to PEMFCs. HT-PEMFCs, relative to other LT-PEMFCs, have the best resistance to CO but it is still rather poor, up to 3% [35]. These reactions together are often referred to as methanol steam reforming (MSR eq.3.4).

$$CH_3OH \rightleftharpoons CO + 2H_2 \qquad \Delta H_{298^\circ} = 90.64 \tag{3.2}$$
$$CO + H_2O \rightleftharpoons CO_2 + H_2 \qquad \Delta H_{298^\circ} = -41.17 \tag{3.3}$$
$$CH_3OH + H_2O \rightleftharpoons CO_2 + 3H_2 \qquad \Delta H_{298^\circ} = 49.47 \tag{3.4}$$

For the DMFC the main reaction is MD, shown in equation 3.2. Since this reaction is endothermic, but the process inside the FC is exothermic, the fuel cell copes with internal thermal stresses. The reaction rate is high because of the relative high temperature, this makes the DMFC a thermodynamically and fluid mechanically very complex machine [14]. Besides, there is a possibility to coking [15] as described in equations 3.5.

$$2CO_{(g)} \rightarrow CO_{2(g)} + C_{(s)} \qquad H_{2(g)} + CO_{(g)} \qquad \rightarrow H_2O(g) + C_{(s)} \tag{3.5}$$

To suppress this reaction, enough oxygen carrying molecules should be added to prevent this (slow) reaction from happening [15]. Such a carrier could be water -> steam. The addition of steam also helps with the conversion of methanol [36]. When enough water is added to the system, the amount of carbon monoxide is reduced quickly through the water gas shift reaction. Thus preventing carbon formation.

Besides MSR, Partial oxidation of methanol (POM) is another method to reform methanol to a hydrogen gas. In contrast to MSR, POM is a highly exothermic reaction. Some great advantages are that the reactor is faster, smaller, has fewer start-up problems and great response to transients [15]. However, the hydrogen yield is less as shown in equation 3.6. Besides, due to the large amount of heat generated, it can be problematic to control the temperature inside the reactor.

$$CH_3OH + \frac{1}{2}O_2 \rightleftharpoons CO_2 + 2H_2 \qquad \Delta H_{298^\circ} = -192.2 \tag{3.6}$$

Oxidative methanol reforming (OMR) is a combination of both MSR and POM. MSR is endothermic whilst POM is exothermic. It is possible to find a heat equilibrium between these reactions. However an optimal OMR reactor is slightly exothermic due to endothermic side reactions like the WGS (eq. 3.3) [15].

There has been a lot of research on the development of the right catalyst for these reactions. It happens to be that copper based catalysts perform great on reaction rate, lifetime and stability. For this research an in-dept research on what catalyst to use would be unnecessary since the quality and the performance is gaining quickly [37]. Although it is important to model the behaviour correctly.

For this study, it is irrelevant to consider OMR since MSR reformers have a higher yield, are less complex and addition heat is not necessarily a problem. Besides, MSR reformers have already been used commercially for transport applications.

3.2.5. REFORMER CHARACTERISTICS

Typically methanol is reformed between $200-350\,^\circ C$ into a hydrogen rich gas. In figure 3.3 the possible paths of methanol reforming are shown. The green box (CH_3OH) indicates the start of the reforming process, the red box ($2H_2 + CO$) indicates the step towards methanol decomposition, and the orange step ($H_2 + CO_2$) indicates the final step of the water shift reaction. Note that there are multiple pathways towards the orange box.

The dehydrogenation of methanol happens to be the slowest reaction that therefore cannot be omitted, also the rate determining step (rds). This is important to know for catalyst or reactor models [38]. The reaction is as follows;

$$CH_3OH \rightarrow HCHO + H_2$$

This dehydrogenation is the first step that takes place, the step from the green box towards $HCHO$. This step is an up-hill reaction ($\Delta_r G_m^\Theta > 0$ & $\Delta H > 0$), which means the reaction is not spontanious and it draws energy from the system [39].

A reformer for large fuel feeds in a small place, i.e. marine applications, must have a rather high volumetric flow rate. The fast paced reactions like MD (eq.3.2), WGS (eq.3.3) and MSR (eq.3.4) are considered. Methane formation is negligible due to its slow reaction rate at low temperature and high volumetric flow rate. Methanation is considered about 5000 times slower than methanol decomposition [34]. Lastly the coking is addressed by having a minimum amount of steam added to the fuel[15].

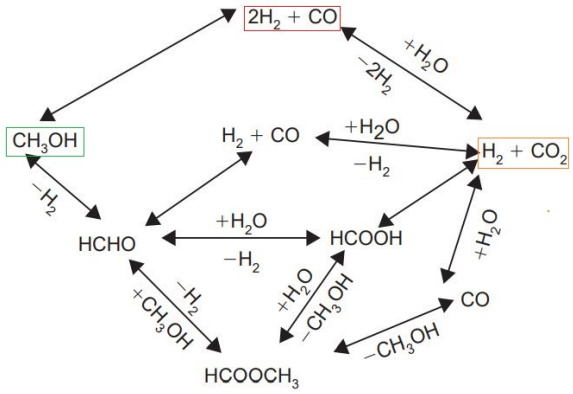

Fig. 3.3 | Reaction pathways of MSR (altered [15])

3.3. THE ENERGY TRANSFORMER: SOLID OXIDE FUEL CELL

In order to determine what FC system would suit in the operational profile of the Hydrographical Survey vessel on methanol, it is important to take a closer look to the FC system as the prime energy generation unit.

3.3.1. DEFINITION OF AN FC

The definition of an engine according to the Cambridge dictionary is as follows; *'A machine that uses the energy from liquid fuel or steam to produce movement'* [40]. To call an FC an engine would be wrong according to this statement since the system is not designed to produce any mechanical power. A fuel cell transforms chemical energy into electrical energy and heat by 'burning' or 'combusting' hydrogen and oxygen to water.

$$2H_2 + O_2 \rightarrow 2H_2O$$

In figure 3.4 one can see the simple principle of a fuel cell. On the left at *(a)* a current is added to the circuit and gaseous hydrogen and oxygen are created. At *(b)* one can see how a current is generated.

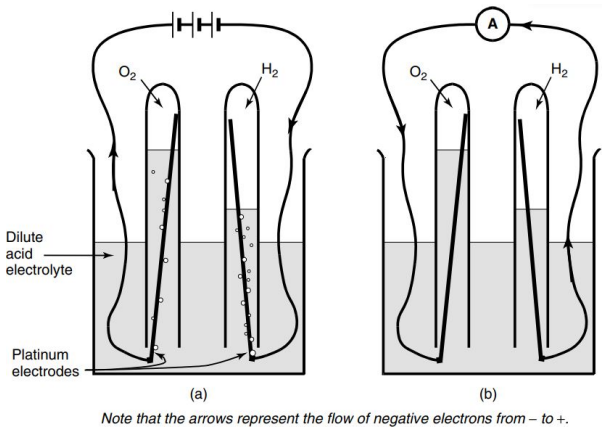

Fig. 3.4 | (a) yields electrolysis and (b) energy generation [10]

To elaborate on what happens in experiment *(b)*, which is a conceptual fuel cell, the phenomena is separated in two chemical reactions. At the right stick of the glass, the anode, gaseous hydrogen is ionised releasing electrons and liquid H^+ ions. These liquid ions diffuse through the acid electrolyte. At the left stick, the cathode, the gaseous oxygen reacts with the liquid H^+ ions to water while the electrons are drawn through the circuit due to the path of least resistance.

$$2H_2 \rightarrow 4H^+ + 4e^-$$
$$O_2 + 4H^+ + 4e^- \rightarrow 2H_2O$$

Which logically leads back to;

$$2H_2 + O_2 \rightarrow 2H_2O$$

This experiment shows a rather weak current which can be optimised in two fundamental ways. First by enlarging the contact area between the gas, the electrodes and the electrolyte. This will increase the amount of reactions which potentially could lead to a higher current. Secondly by minimising the space between the electrodes and diminishing flow resistance of the electrolyte. This is achieved in the structure as shown in figure 3.5.

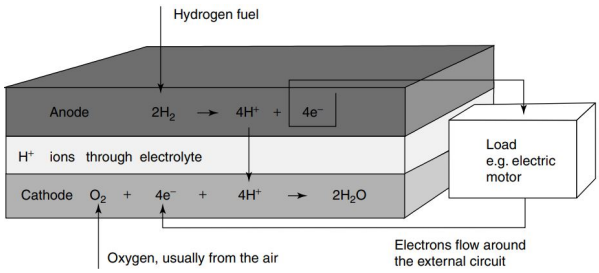

Fig. 3.5 | A single cell of an acid electrolyte fuel cell

Conceptually this works the same as in figure 3.4(b). To maintain a stable current, the hydrogen fuel should be supplied at the anode side whilst oxygen is supplied at the cathode. The electrolyte must pass through the free liquid H^+ ions. Beside acids, some polymers could do the job as well. This is the basic principle of an PEMFC.

The current produced in an FC is subjected to the amount of reactions that take place and the amount of electrons that pass through the circuit from a single reaction. From a classical approach the reaction can be interpreted by an activation energy that must be 'paid' and an amount of released energy as shown in figure 3.6. Some ways to increase the reaction rate are to use a catalyst to decrease the activation energy, to increase the temperature, to increase the area of the electrodes to facilitate more reactions, or to optimise composition of the fuel [10].

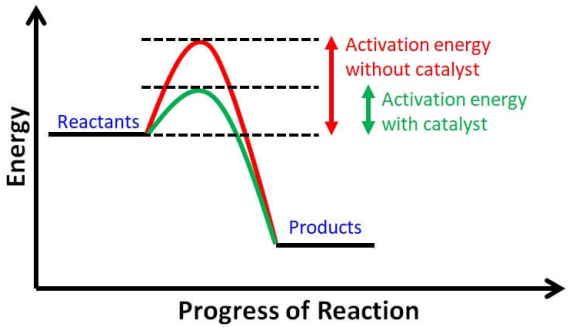

Fig. 3.6 | Classical approach activation energy

3.3.2. AN OXYGEN ION PASSING ELECTROLYTE

The SOFC works a little different then the previous described PEMFC. Nernst found in 1899 that an electrolyte made out of stabilised zirconia conducts oxide ions at higher temperatures, around 800 °C. This implies that the cathode reduces gaseous oxygen (O_2) to oxygen ions within the electrolyte phase [10].

$$\frac{1}{2}O_2(g) + 2e^-(c) \rightleftharpoons O^{2-}(e) \tag{3.7}$$

This charge-transfer reaction transfers electronic charge from one phase to another. This happens at the triple phase boundary (tpb) of the electrode-electrolyte interface which is exposed to the gas. Here (g) represents the gas phase, (c) the cathode phase, and (e) the electrolyte phase. The phase identification is

important in evaluating charge-transfer reaction rates [41].

As shown in figure 3.7a and 3.7b the oxygen reduction reaction facilitates absorption of oxygen ions at the cathode. Due to the potential chemical energy imbalance the oxygen ion travels through the electrolyte where it oxidises with hydrogen to form water (and carbon dioxide).

$$H_2(g) + O^{2-}(e) \rightleftharpoons H_2O(g) + 2e^-(a) \tag{3.8a}$$
$$CO(g) + O^{2-}(e) \rightleftharpoons CO_2(g) + 2e^-(a) \tag{3.8b}$$

Note that the electrons are generated in the anode phase (a). Theoretically the carbon monoxide could be reduced to carbon dioxide by reacting with the oxide ion from the electrolyte, but practically hydrogen oxidation is faster which makes it the dominant charge-transfer pathway [41]. Besides, the production of water due to the combustion of hydrogen favours the reaction of carbon monoxide and water to hydrogen and carbon dioxide. Therefore it is assumed that no carbon monoxide reacts with oxide ions at the tpb.

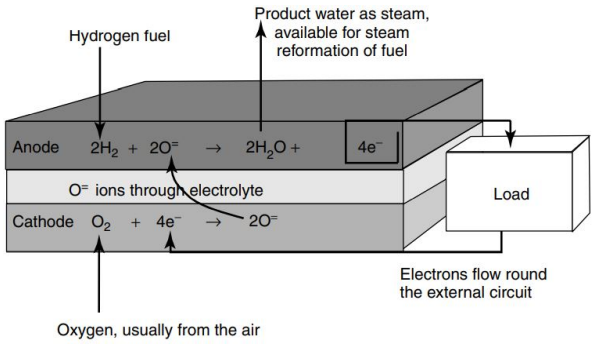

(a) Hydrogen is used as a fuel

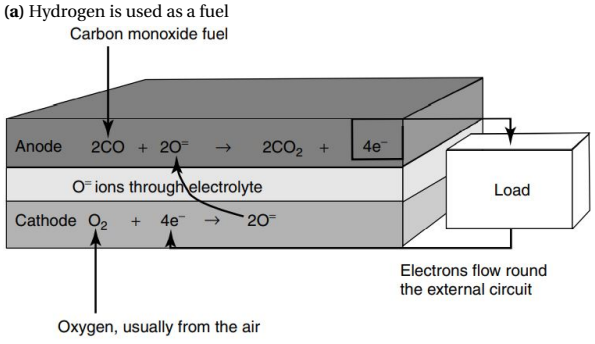

(b) Carbon monoxide is used as a fuel

Fig. 3.7 | A Schematic representation of using hydrogen and carbon monoxide as a fuel with an oxygen passing electrolyte

SOFC PEN STRUCTURE

In figure 3.7a and 3.7b a positive electrode - electrolyte - negative electrode (PEN) structure is shown. Such a structure has a typical thickness between $0.15 - 1.0mm$. This structure is often strengthened with a support layer. This can be an anode-, cathode- or electrolyte-supported cells (ASC, CSC or ESC). Around this PEN structure bipolar plates are placed which seal the cell. These cells can be stacked to form a multiple cell stack. On one side of such a stack hydrogen is supplied and anode-off gas is retrieved while on the other side the same is done with oxygen supply and cathode-off gas. On both ends there are current collectors which can be connected to the electricity grid [41].

3.3.3. METAL-SUPPORTED SOLID OXIDE FUEL CELL

The development of SOFCs is going on for many decades. The operational achievements are very promising, yet successful commercialisation has not preceded. This has mainly to do with four problems: [1] high costs of cell materials, [2] unreliable cell sealing, [3] susceptibility of the cell to failure due to rapid thermal

transients, mechanical shock, or oxidation of the anode, [4] manufacturing issues associated with the production of large, complex ceramic parts. These problems can be overcome by changing/optimising the geometry of a fuel cell [13, 42–44].

An electrolyte supported cell is able to support a very thin anode and cathode. To reduce the ohmic impedance of the electrolyte, temperatures reaching $800-1000\,^{\circ}C$ are required. The PEN structure becomes more expensive in order to resist higher temperatures. An anode- or cathode-supported cell is not able to operate on such high temperatures, but has lower ohmic impedance due to a smaller electrolyte. All these types of supported cells contain brittle ceramic or cermet materials for mechanical support, which deal poorly with the four problems described previously.

This is where a metal-supported cell (MSC) could help. The MSC is, most often, a type of ASC where the support layer is made from inexpensive and robust porous metal on which the active PEN layers are applied [44] instead of a ceramic or cermet support.

Main advantages of the MSC are mechanical ruggedness which is preferred for transportation applications where the cell is likely to endure shock, vibration or mechanical load. Ruggedness eases the production of the cells also, since it can withstand rougher or faster handling which would fracture a ceramic cell. Tolerance to redox cycling is improved significantly as well. Last but not least, thermal cycling is improved significantly which is also desirable for many SOFC applications [13].

The main reason why thermal cycling is a problem within SOFCs is because of the mismatch between the coefficient of thermal expansion (CTE) of the support layer and the PEN structure. A metal-supported anode has a nearly identical CTE as the possible electrolyte materials. It is expected that the remaining indifference in initial thermal stresses dissipates via metal creep [13].

Tab. 3.5 | Candidate support metals

Metal support	CTE ($ppmK^{-1}$)
NiCrAlY	15-16
Hastelloy-X	15.5-16
Ni	16.5
Ni-Fe (1:1)	13.7
300 SS	18-20
400 SS	**10-12**
Electrolyte	CTE ($ppmK^{-1}$)
YSZ, CGO, LSGM	10 - 12

Lastly, the price of a metal-support is very low since the 400-series of stainless steel is widely used in automotive exhaust manifolds and mufflers because of their low-cost and high-temperature oxidation resistance [13]. The major drawback of an MSC is that the operating temperature is limited and therefore the power density is lower than conventional HT-SOFC systems.

3.3.4. THEORETICAL MODEL FOR A SOLID OXIDE FUEL CELLS

The exact phenomena occurring inside the SOFC have been analysed thoroughly for many years. Nevertheless some phenomena are often simplified with empirical relations because they are not yet fully understood or it takes too much computational power for a negligible addition of precision in the model. The assumptions made in modelling an FC stack have a major influence on the outcomes. Therefore it is of upmost importance to describe and understand the underlying principles of the assumptions.

The electromotive force (EMF) or reversible open-circuit voltage (OCV or V_{OC}) of a fuel cell can be described by equation 3.9. V_{OC} is the voltage, ΔG is the free Gibb's energy, n_e is the amount of electrons passed around the circuit, and F is Avogadro's number [41].

$$V_{OC} = \frac{-\Delta G}{n_e F} \tag{3.9}$$

The OCV is a theoretical electric potential of the system since it only holds if there are no losses at equilibrium condition. It does give insight on the efficiency limit of an FC is bounded to which is bedded in the change of the Gibb's free energy [41]. When a hydrogen fuel cell is considered, the V_{OC} is typically assumed to be equivalent to the equilibrium Nernst potential V_{Nernst} for the overall reaction $H_2 + \frac{1}{2}O_2 \rightarrow H_2O$ [45].

$$V_{OC} \approx V_{Nernst} = \frac{-\Delta G^0}{n_e F} + \frac{R_u T}{n_e F} \ln\left(\frac{p_{H_2} p_{O_2}^{\frac{1}{2}}}{p_{H_2O}}\right) \tag{3.10}$$

The first term of the Nernst equation gives the standard potential of the system. The second term holds the change in activation throughout the system. The R_u is the universal gas constant, T is the temperature, p_x is the partial pressure of the gas product x. Note that at the entrance of the stack the partial pressure of hydrogen and oxygen will be larger than at the exit of the stack since it is reformed to water. This affects the V_{OC} and therefore the overall efficiency. This assumption neglects any irreversible processes such as reactant and electronic electrolyte crossover (internal short-circuiting), and electrode-electrolyte parasitic reactions [45].

During operation, the operating voltage $V_{operating}$ moves away from an equilibrium state at the open circuit voltage V_{OC} and the voltage drops due to irreversibilities associated with internal charge transfer, conduction, and diffusion processes. These are categorised in activation (ΔV_{act}), ohmic (ΔV_{ohmic}) and concentration (ΔV_{con}) voltage losses. This gives the following equation 3.11 [10, 41, 45].

$$V_{operating} = V_{OC} - \Delta V_{act} - \Delta V_{ohmic} - \Delta V_{conc} \tag{3.11}$$

The losses shown are distinctive to the FC and are functions of the current density. The behaviour of the losses proportional to the current density are as follows.

$$\Delta V_{act} \propto \ln\left(\frac{i}{i_0}\right) \tag{3.12}$$

$$\Delta V_{ohmic} \propto i \tag{3.13}$$

$$\Delta V_{conc} \propto \ln\left(1 - \frac{i}{i_0}\right) \tag{3.14}$$

$$\tag{3.15}$$

The i_0 is the exchange current density, which is the current density at the equilibrium state. The i is the electrode current density, the amount of electric current flowing when operating. In figure 3.8 a representation of the $V_{Nernst} = V_{operating}$ is shown together with the theoretical V_{OC}. The x-axis represents the change in i and the y-axis the change in $V_{operating}$. Note that the convex dip is due to a strong increase of the activation losses V_{act}. The linear part is mainly a combination of activation losses and ohmic losses V_{ohmic} and the concave dip is due to the increasing concentration losses V_{conc}. In high temperature FCs the activation losses V_{act} are often less [42]. This results in a smaller convex dip at high voltage and low current, the relation then becomes more linear.

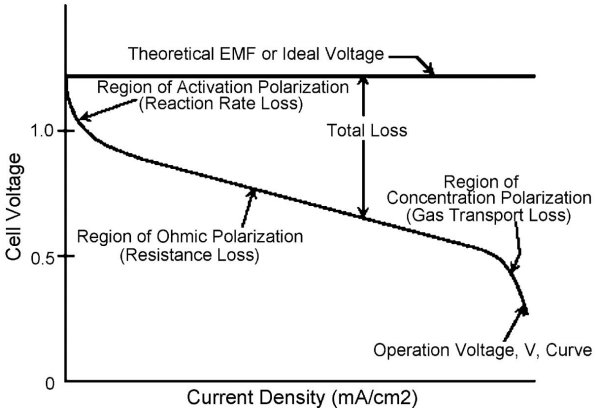

Fig. 3.8 | Ideal and actual fuel cell voltage-current characteristics from [42]

INFLUENCE ON OPEN-CIRCUIT VOLTAGE

As shown in equation 3.10, there is a term in the OCV which is affected by the change in activation throughout the system. This term is given again below;

$$\Delta E = \frac{R_u T}{n_e F} \ln\left(\frac{p_{H_2} p_{O_2}^{\frac{1}{2}}}{p_{H_2O}}\right)$$

The amount of electrons passing per reaction are $n_e = 2$ since oxide ions are considered. The partial pressures of hydrogen (p_{H_2}) and oxygen (p_{O_2})are the reactants and the partial pressure of water (p_{H_2O}) represents the products in the electrochemical process. Along the process the amount of reactants decrease and the amount of water increases. This results in ΔE becoming increasing negative. Note that the higher the temperature, the larger ΔE becomes, but this is negligible with the decreasing partial pressure of hydrogen and the increase partial pressure of water. This is a serious issue with high temperature fuel cells since the voltage drop due to this relation affects the efficiency [45]. Note that the amount of hydrogen reduction relates more to this voltage drop than the oxygen reduction due to the quadratic term in $p_{O_2}^{\frac{1}{2}}$. All in all this voltage drop affects the operability of the fuel cell stack and should not be neglected.

MODELLING ACTIVATION LOSSES

One of the governing equations for a fuel cell are the activation losses at both the electrodes due to the oxygen reduction at the cathode and hydrogen oxidation at the anode. These activation losses V_{act}, part of equation 3.11, can be represented in the Butler-Volmer (B-V) equation [45];

$$i = i_0 \left(e^{a_1 (F/R_u)\Delta V_{act}} - e^{-a_2 (F/R_u)\Delta V_{act}}\right) \tag{3.16}$$

F is the Faraday's constant, R_u is the universal gas constant and T stands for the temperature in Kelvin. The reference exchange current density i_0 is often estimated as a function with an Arrhenius-type relation in the form of;

$$i_0 = A e^{-E_{act}/R_u T} \tag{3.17}$$

This function depends on the cell material, the temperature and the geometry. The term A is generally a function of cell temperature and product and reactant partial pressures [45]. The reduction and oxidation transfer coefficients, α_1 and α_2 respectively, represent the electron transfer processes at the electrode-electrolyte interface. These constants are hard to define since the exact reaction mechanism is difficult to identify. However, some approximations have been made to determine the transfer coefficients as follows [46]

$$\alpha_1 = \frac{n-\gamma}{\nu} - s\beta \tag{3.18a}$$

$$\alpha_2 = \frac{\gamma}{\nu} + s\beta \tag{3.18b}$$

Where n gives the total number of electrons transferred per reaction and γ the number of electrons transferred *before* the rate determining step (rds). The rds is the slowest step in the chemical reaction process that determines the speed of the reaction. The ν stands for the number of times the rds occurs in one complete oxidation or reduction reaction. The s is the number of electrons transferred in the rds (0 or 1) and the β is the symmetry factor [45].

First of all, it is assumed that the oxidation and reduction processes happen in an instant before an electron is transferred. This holds that $\frac{n-\gamma}{\nu} = 1$ and $\frac{\gamma}{\nu} = 0$ since $\gamma = 0$, and $s = 1$. This simplifies the equation of eq. 3.16 to;

$$i = i_0 \left(e^{(1-\beta)(F/R_u)\Delta V_{act}} - e^{-\beta (F/R_u)\Delta V_{act}}\right) \tag{3.19}$$

The value of β in ideal cases is equal to 0.5, but experiments show values ranging from 0.3 to 0.6 [45]. When β is assumed to be 0.5 and the B-V equation is rewritten, then the logarithmic term becomes a hyperbolic sinus function and the following equation is obtained;

$$\Delta V_{act} \cong \frac{R_u T}{\alpha_1 F} \sinh^{-1}\left(\frac{i}{2 i_0}\right)$$

This equation is only valid for either the anode or the cathode as $\alpha_1 = \beta = 0.5$. When both have to be modelled one gets equation 3.20. This relation is empirically the most practical representation that describes the behaviour related to the activation losses.

$$\begin{aligned}\Delta V_{act,total} &= \Delta V_{act,A} + \Delta V_{act,C} \\ &= \frac{R_u T}{\alpha_{1.A} F} \sinh^{-1}\left(\frac{i}{2i_{0,A}}\right) \\ &+ \frac{R_u T}{\alpha_{1.C} F} \sinh^{-1}\left(\frac{i}{2i_{0,C}}\right)\end{aligned} \tag{3.20}$$

MODELLING OHMIC LOSSES

The ohmic losses V_{Ohm} have a (somewhat) linear relation to the change in current as stated in equation 3.13. The main contributors to this loss are the resistance in conducting oxygen ions through the electrolyte, the electrons passing through the electrodes and the current collectors, and the contact resistance between cell components [47]. The ohmic losses can be expressed by equation 3.21

$$V_{Ohm} = jR_{Ohm} \tag{3.21}$$

Where j is the current density and R_{Ohm} the internal resistance of the cell including the prior summed components of resistance. The internal resistance could be obtained from experimental data, but it can also be determined by calculating the conductivity of the individual layers also. The expression of R_{Ohm} can be express by equation 3.22

$$R_{Ohm} = \frac{\tau_a}{\sigma_a} + \frac{\tau_e}{\sigma_e} + \frac{\tau_c}{\sigma_c} \tag{3.22}$$

Where τ_x is the thickness of the anode, electrolyte or cathode layer and σ_x the electronic conductivity of the three cell components. In this equation it is assumed that the contact resistance, cross-plane charge flow and resistance due to series connection are negligible [47].

MODELLING CONCENTRATION LOSSES

The concentration of reactants at the TPB differs from the concentration in the gas channels due to diffusion. Diffusion is a mass transport phenomena that has to be considered in the gas channels and at the porous structure of the electrode. The ΔV_{con} in equation 3.11 could be described as follows[48];

$$\Delta V_{con} = \frac{R_u T}{n_{e_1} F} ln\left(\frac{p_{H_{2,tpb}} p_{H_2O}}{p_{H_2} p_{H_2O,tpb}}\right) + \frac{R_u T}{n_{e_2} F} ln\left(\frac{p_{O_{2,tpb}}}{p_{O_2}}\right)^{1/2} \tag{3.23}$$

where n_{e_1} and n_{e_2} are the number of exchanged electrons which are 2 and 4 respectively, and the $p_{x,tpb}$ are the partial pressures of species x at the triple phase boundary. These can be expressed assuming that there is no diffusion in the gas channel, only at the reacting site and that the electrochemical reactions only occur at the electrode - electrolyte interface, and no where else. This gives the opportunity to relate the partial pressures to the local current density i through the Faraday's law as shown in the following equations [49].

$$p_{O_{2,tpb}} = 1 + (y_{O_2} - 1) exp\left(\frac{i R_u T t_c}{n_{e_2} F D_{eff,c} P}\right) \tag{3.24}$$

$$p_{H_{2,tpb}} = y_{H_2} - \frac{i R_u T t_a}{n_{e_1} F D_{eff,a} P} \tag{3.25}$$

$$p_{H_{2,tpb}O} = y_{H_2O} - \frac{i R_u T t_a}{n_{e_1} F D_{eff,a} P} \tag{3.26}$$

where t_c and t_a are the thickness of the electrode and $D_{eff,c}$ and $D_{eff,a}$ the effective diffusion coefficients [49].

HEAT PRODUCED

A fuel cell generates both heat and electricity. The maximum theoretical efficiency can be estimated by change in Gibb's free energy ΔG divided by the change in enthalpy ΔH [10].

$$\text{Maximum efficiency possible} = \frac{\Delta G}{\Delta H} \tag{3.27}$$

Note that the Gibbs free energy ΔG is related to the change in enthalpy ΔH and the change in entropy ΔS in

$$\Delta G = \Delta H - T\Delta S \tag{3.28}$$

Both the entalpy and the entropy change when the temperature and partial pressure change. The largest influence on the Gibbs free energy is the change in temperature T. These two relations combined, equation 3.27 and 3.28, show that there is a negative relation in theoretical maximum efficiency to temperature. Although this is true, there are many factors that thrive on high temperatures also, like lower ohmic resistance, and lower activation losses for example. All in all, bluntly assuming that high temperature FC systems are less efficient due to a lower theoretical maximum efficiency from this relation would be nonsensical [10].

3.4. SUBSYSTEMS

The BoP contains many subsystems that support the pre-reformer and FC stack. The efficiency, size and cost of the total system is significantly influenced by the subsystems, therefore it is unwise to neglect these systems when analysing the BoP. The level of detail of components in a BoP could be analysed up to sensor level. In this research the large consumers and the dynamically influencing subsystems will be described as they are considered most important [18].

3.4.1. COMBUSTOR

The combustor recieves both the anode and the cathode exhaust gasses. It is very likely that not all methanol, hydrogen and carbon monoxide has been reduced to water and carbon dioxide in the FC stack. The remaining reactants could be burned together with the remaining oxygen from the cathode to carbon dioxide and water while realising heat.

Lower heating values	
Fuel	Kj/mol
Hydrogen	244.00
Carbon Monoxide	283.24
Methanol	638.55

3.4.2. HEAT EXCHANGER

Managing heat between BoP components is a vital aspect. To emphasise the importance of adequate heat exchangers, some examples are given below. The cathode air is pre-heated to prevent thermal shock, but at the same time it still needs to be cool enough to draw heat from the FC stack. The internal temperature of the pre-reformer varies due to mass flow differences, which could results in more endothermic reactions and even cooling the fuel too much to enter the FC stack. The water recovery system cools the exhaust gasses in order to extract water. If the amount of exhaust gasses increases and the internal energy is too high, the steam cannot be cooled enough to extract water, which is disastrous for the fuel feed. Therefore, specific heat exchangers must be designed for each application [18]. At the same time this shows the importance of a dynamic model since these problems would not occur when the system is statically analysed.

Probably the most difficult heat exchanger is the steam generator since this incorporates a phase change. This could lead to pressure fluctuations. A method to solve this problem is by assuming a heater in which the fuel does not change phase and a flash evaporator which instantly changes the phase of the fuel [18].

3.4.3. FUEL AND WATER PUMP

Most often positive displacement pumps are used for fuel and water feeds in liquid form. These pumps operate by trapping a volume of liquid and push it through the system. Such pumps are relatively easy to control and must be compatible with the fuel. The governing equation of such a pump could be described as follows

$$P = \frac{\Delta p_{total} Q}{\eta} \tag{3.29}$$

Where P is the required power, Δp the change in total pressure, Q the fluid flow rate in $\frac{m^3}{s}$ and the η is the pump efficiency. The change in pressure could be described rewriting Bernoulli's equation

$$\Delta p_{total} = \frac{v_2^2 - v_1^2}{2} + \Delta z g + \frac{\Delta p_{static}}{\rho} \tag{3.30}$$

Where v_1 and v_2 are the incoming and outgoing velocities, Δz the change in height, g the gravitation acceleration, Δp_{static} the change in static pressure and ρ the density of the medium [50].

3.4.4. AIR BLOWER

Air blowers are used for positive displacement of air. Mainly the cathode air needs to be pressurised. The air functions both as a fuel and as a coolant in the cathode. An air blower could, like the fuel pump, also be described by a derivation of the Bernoulli equation.

$$\frac{v_1^2}{2g} + \frac{p_{total_1}}{\rho_1 g} + h = \frac{v_2^2}{2g} + \frac{P p_{total_2}}{\rho_2 g} \tag{3.31}$$

Where h is a generic friction loss and ρ_1 and ρ_2 are the densities of the medium. At the pump incompressible fluid is assumed, this does not hold for air blowers. Therefore, a different density prior and after the blower is assumed. If the air blower is not strong enough, air pumps or compressors could be used. Moving air is an energy consuming process, so increasing the pressure of air will significantly add to the parasitic losses [18]

3.4.5. ENERGY MANAGEMENT SYSTEM

The power demand of a vessel varies during, for example, transit, operating or being idle in the harbour. This is described in the operational profile in chapter 4. The ability to meet ramp-up and ramp-down requirements of an SOFC power system is generally too slow. Besides, the start-up and shut-down capabilities are unfavourable slow too, compared to conventional systems [18]. In the automotive industry, where PEMFC applications have been commercially sold, small battery systems are used for starting and transient requirements [15].

An Energy Management System (EMS) is introduced to transport applications for various reasons. Especially for systems with large load variations, short high peak loads and long low base loads. An EMS could provide peak shaving, load levelling, frequency control, improving quality of power supply, and enable switching off power generation systems and function as a fuel reducing system for operation power optimisation [51]. For vessel applications an EMS is used for Equivalent Consumption Minimisation Strategies (ECMS) to reduce fuel [52].

In this research an EMS is introduced not necessarily to reduce fuel usage, although it could do so if optimised, but mostly to meet the operational requirements of power demand. Therefore it is an addition to the system rather than a required component.

ENERGY STORAGE SYSTEM

An Energy Storage System (ESS), e.g. batteries, flywheel, or super-capacitor, is the physical system of which the EMS manages the energy storage and withdrawal. For transport applications, it is safe to assume that the system should always be optimised to be as small as the operational boundary conditions allow it to be. For marine applications a lithium-ion battery energy storing system (BESS) is chosen due to its optimal combination of energy density, charge and discharge rapidly, being robust and reliable, and to hold energy for a longer period.

4

MODELLING METHOD

The principles of the systems in the model are discussed in the previous chapter. This research focuses on the interactions between systems to obtain the characteristics of the MS-SOFC based BoP on methanol. The goal is to prove if the assumptions made in chapter 3 are indeed as promising as theory describes and if the research questions of chapter 2 could get promising results.

To do so it is extremely important to understand what the model should look like and how the systems interact with each other. Therefore, the objective of this research will be analysed first.

4.1. OBJECTIVE DERIVATION

The objective of this research is;

– *What are the characteristics of the metal supported solid oxide fuel cell on a methanol based balance of plant for power generation applications on a hydrographical survey vessel?*

It is chosen to answer this research question by modelling various operations of the vessel in order to evaluate systems for their capabilities. An operation by a Hydrograhpical Survey vessel is given by the functional scoping given in table 4.1 and 4.2. Further elaboration on these values is given in section 3.1.

Tab. 4.1 | Principal design characteristics [9]

Parameter	Family	HOV
High speed transit	12 kts	8 kts
Maximum speed	15 kts	12 kts
Installed power	5000 kW	1546 kw
Range transit speed	5000 nm	5000 nm
Displacement	2400 t	1814 t
Payload	800 t	≈ 800 t
Design life	30 years	30 years
Endurance	14 days	14 days
Operational Days	200 p/y	200 p/y

Tab. 4.2 | Operational profile HOV [23]

	Type of operation	Power	Time	Speed
1	Low speed	141 kW	15%	4kts
2	Operations	436 kW	40%	6-10kts
3	Economic transit	436 kW	15%	9kts
4	High speed transit	880 kW	25%	12kts
5	Maximum speed	1150 kW	5%	13kts

The endurance is 14 days, the transit range is 5000 nautical miles and the 5 types of operations are given in kW required per percentage of time. Therefore, it is chosen to evaluate this system on a timescale of the entire operation. All notable effects on this timescale should be modelled, which are effects ranging from second to second and hour to hour. For this reason it is chosen to model steady state operations and transitions between the operations.

4.1.1. MODEL MAP

The components of the BoP considered can be split in two categories, the 1-D models and the 0-D models. The 1-D models are the reformer, which includes a heater, and the SOFC stack. The 0-D models are pipes, the combustor, the turbines, the pumps, other heaters, the EMS, the mixing nodes, and the inputs and outputs of volume flows. To components listed can be found in figure 4.1.

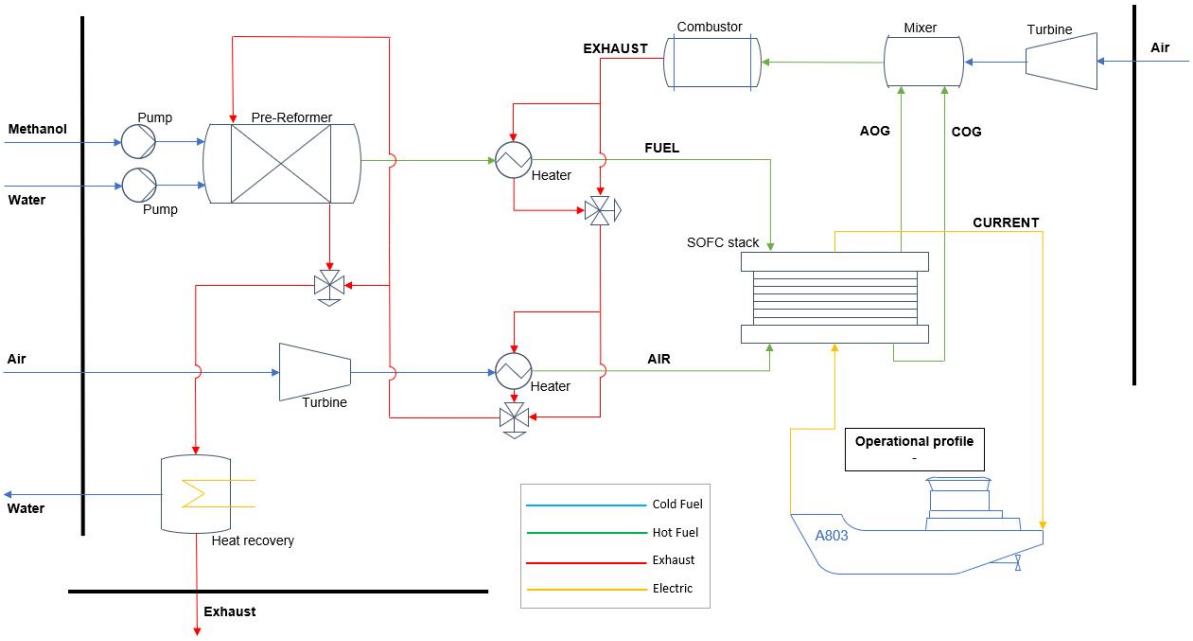

Fig. 4.1 | Balance of Plant

Some components are neglected, like the fuel tank, the water recovery tank the water recovery system. This is either because they hardly add to the dynamical behaviour of the system or because of the uncertainty how the system would look like. This is further elaborated in chapter 7.

DIFFERENTIATION BETWEEN 1-D AND 0-D SYSTEMS

The most interesting components in this model are the reformer, containing a fuel reforming and fuel heating part, and the FC stack. Both the entire reformer and the FC stack change significantly due to dynamic interactions throughout operations.

The most interesting interactions between these systems are the change in temperature in the FC stack due to higher or lower fuel and air input, the amount of heat produced by the combustor from exit gasses of the FC stack for heating the reformer, the inlet fuel and inlet air, and the amount of heat and electrical energy produced by the system during steady operations and transits between operations.

Understanding these components and their interactions shows that the reformer and the FC stack model are the most import systems. They need to show what it is like to operate under different states, while the other systems, often referred to as subsystems, should support the reformer and FC stack. The main goals as stated in chapter 2 are the main focus. To understand the interaction between 1-D systems, detailed components like multi-dimensional pump-, heater-, turbine-, or combustor models are not needed. Therefore they are kept to a 0-D system.

4.2. DESIRED OUTPUTS

To develop a balance of plant model representing an actual vessel is already a though and time extensive research, let alone a BoP existing of components which have not been commercialised yet. Therefore it is of upmost importance to derive clear objectives to research before modelling. The main objectives of this research are partly theoretical and literature driven and partly model based. In this section a clear distinction is made on what the model is going to provide on top of the literature.

4.2.1. REFORMER MODEL

Given that the spatial distribution throughout the reformer unit is relevant, the reformer unit is modelled using an 1D-approach. As literature suggested, it takes relatively long to reform all methanol to hydrogen, carbon monoxide/dioxide, and water. For this specific application however, not all methanol needs to be reformed. To understand how the reforming process looks like and how the reaction rates behave inside the reformer, it is important to have a clear view of the length of the reformer. It is in the scope of this research to elaborate on the performance of the reformer and what it can deliver and what it needs to deliver. The change in heat and mass is calculated for every time-step inside a discretization unit which contains the spatial distribution. Therefore as a result, every piece of the reformer can be tracked and shown.

The temperatures inside the reformer are important to track since they change of the length over the reformer unit, while having a major impact on the behaviour of the reformer. Together with the heating of the exhaust this is an interesting interaction to observe. The Arrhenius like reaction rates of the methanol steam reforming process already suggest that the majority of the reforming will take place at the beginning of the reformer. Note that this means this part will be the coolest part. Therefore parallel flow of the exhaust heat is needed to heat the reformer unit. Methanol steam reforming has a strong endothermic part, the methanol decomposition, and a weaker exothermic part, the water gas shift. As a result, the most optimal temperature to reform is around $275 - 325^{\circ}C$. The higher the temperature, the less favourable the water gas shift equilibrium becomes. Another note is that the exhaust gasses will be added to the system in such manner that the reformer will keep a equilibrium temperature around $300 - 325^{\circ}C$. This means however, that when the exhaust gasses change in temperature, the volumetric rate of the exhaust gasses through the system need to change also. As a result, if the temperature rises and the volumetric rate decreases, the system will be heated differently along the length of the reformer when the temperature is low and the volumetric flow is high. In summary, the changing temperature along the reformer unit, the temperature dependent behaviour of the reaction rates and an dynamic heat source give strong reason to model the reformer 1-D.

The interaction between the length, the width, and the volumetric flow of the fuel is another extremely interesting topic to research. However, the reaction rates are volume derived relations. As a result, this research is unable to enlarge the system in width while keeping proper results. The length and the volumetric flow, are variables. Considering the need for the FC system, a partly reformed methanol feed for example, it could be that the system has a relative short reformer unit with moderate volumetric flow rates or a longer reformer unit with a high volumetric flow rate. Note that the difference in length and volumetric flow rate influences the residence time of the fuel which. The behaviour of the reformer could influence the design of the system.

4.2.2. FUEL CELL MODEL

The main power generation system of the BoP is the FC system. One of the main problems of commercialisation of FC systems for high power solutions is the ability to perform transients. Especially in a BoP, where all systems work together, the transients of the main power generation system is determining the requirements for other components. It is important to asses how the temperature changes, how the mass balance changes and how the electric current drawn changes along the FC unit. These changes vary along the length of the model, which is can be spatially distributed in a model. Therefore, a 1-D approach istake for the FC model. Even some 2-D effects are key to the system; as the spatial distribution of the hydrogen in the bulk fuel and the anode, or the heat distribution in the solid structure and the gasses. These effects however, are tackled per discretization unit internally. At the same time, an MS-SOFC is a really specific FC system. For this research however, it is not the objective the particularly research the MS-SOFC as a viable FC system. Nevertheless, choosing the MS-SOFC as the main power generation system yields obligations to showcase

why the system works, what is special about it and what are its shortcomings.

4.2.3. OTHER BOP COMPONENTS

Great care is taken for the main components, the reformer and the fuel cell. Other components, burners, pumps, turbines etc., are 0-D models or even just input variables. There are two reasons why these other components are undervalued. The first is that a BoP design is extremely dependent on the requirements of the vessel and the performance of the FC. Therefore, it has been chosen to determine the input parameters only and leave the actual subsystems to simple interpretations.

4.3. MODULAR DYNAMIC MODELLING

The added value of this academic research is that it models dynamic interactions between underdeveloped systems for marine applications. Therefore it is of upmost importance to carefully consider what type of model is preferred. Three major choices have been made to model this project.

- *[1] All systems should be modular components so the model can be re-used and components can be optimised separately.*
- *[2] All modular components are connected through state space variables*
- *[3] The programming language matches the requirements as a foundation on which the model is built*

4.3.1. MODULAR COMPONENTS

Many choices have been made prior to the first step of actual modelling A BoP for the hydrographical survey vessel; methanol as a fuel, MS-SOFC as an FC, the layout of the BoP, and more. Therefore, it is convenient to have a model which can be altered easily. For example, if other fuels are preferred, like LNG, ammonia or liquid hydrogen, one can change the fuel or remove the reformer, change the combustor, and more. In order to do so, all components have been modelled to scale in volumetric flows, flows are modelled as vectors, and all material components have been assigned their characteristics through a master file. This is not only favourable for this study alone, but also for future studies when certain technologies tend to develop in different ways so the systems change. However, it must be said that this particular BoP is considered on methanol specifically. Using a different fuel alters the behaviour of the entire system, which most probably results in a new BoP design.

4.3.2. FEED FORWARD NETWORK

For this research a feed forward modelling technique has deliberately been chosen. Changes in volumetric flow, temperature, and moles will result in changes in pressure, which has to be accounted for. In every component the pressure drop is accounted in the pipes only, while the temperature, volumetric flow and change in moles is accounted in the systems itself. Sudden changes in pressure that would also result in a pressure gain in the previous system in reality are neglected. Internal changes in temperature in a component are taken into account, also for components prior to the temperature change. Feed forward systems are less numerically complicated then feedback systems. Also, the ODE's are less complex and modular components are more easily coupled. The biggest drawback is that dynamic behaviour does not necessarily respect causality. Upstream downstream components may be affected by upstream changes.

4.3.3. PROGRAMMING LANGUAGE

Three programming languages were considered. Python, Dymola (Modelica), and Simulink (MATLAB). It was found that Dymola from Modelica is not a compatible programming language. Modelica's purpose is to model dynamic systems with causality, which is a proper way of modelling dynamic models. The major problem *is* the causality based modelling technique that is embedded in Dymola. Since non of the people who worked on this project knows how to programme with Dymola and since very specific modules should be written, it was a too high risk to start with it. Besides, Dymola is far from the maturity of MATLAB's Simulink. The second to fall was Python. The major drawback is that every time step, the model differentiates every state for every discretization unit in every modular component, and this should be written from scratch or derived from an open-source party. Something Simulink has build-in applications for. At the same time, Simulink has build in ODE solvers like ODE45, ODE23, and more, which can vary the time step while respecting the

numerical stability of the explicit system. Thus maximising the time step on any point which results in shorter runs. Lastly, Simulink is therefore the easiest to use, most accurate, quickest, and most mature modelling software of all. This is why Simulink is chosen.

4.3.4. 1- AND 0-DIMENSIONAL MODULES

In this section all modules will be thoroughly explained. Every subsection is written in the following structure; short introduction of what the module does, analysis of the ODE's and their complementary equations, geometrical analysis, and expectation in performance. The following systems are considered, look at table 4.3

Tab. 4.3 | Module grouping in 1-D and, or 0-D.

Module	1-D	0-D
Reformer	X	-
Fuel Cell stack	X	-
Heater	X	X
Combustor	-	X
Blowers and pumps	-	X
Pipes and mixing nodes	-	X
Energy Management System	-	-
Fuel and air input	-	-

4.3.5. NUMERICAL ODE SOLVER

The system contains equations that tend to change in mili-seconds while other equations are made to change in the order of seconds to 10 seconds. As a result, the model can become extremely stiff. This means that when the input for the (first order) differential equations yield numerical unstable solutions, the solver needs to take a smaller step size, but with this model, that could imply that the stepsize goes from 20 seconds per second to 0.01 second per second in this case.

Because of this observation in advance to the modelling, a numerical solver given by MATLAB was chosen. The three main candidates for this model were ode45, ode23, and ode15s. The first two solvers are Runge-Kutta based solvers and the last named is a fifth order numerical differential equation.

Simply put, ode23 is the quickest due to its simplified version of the Runge-Kutta algorithm and the ode15s is the slowest. ode45 is the most accurate and the ode15s is the most rigid solver which is capable of solving very stiff models. The solvers are ranked from 1 (best) to 3 (worst), this is depicted in table 4.4.

Tab. 4.4 | Comparing solvers from 1 (best) to 3 (worst)

Solvers	Quick	Accuracy	Stiff
ode45	2	1	2
ode23	1	3	3
ode15s	3	2	1

During the modelling phase ode45 was used, since it is the safest choice and the most thoroughly engineered solver that MATLAB supplies according to the MATLAB Mathworks Help Center. After the model was finished all three solvers were used. As a result the ode23 couldn't cope with transients and became unstable too many times to safely use. Both ode45 and ode15s worked fine. Because ode45 is way faster when the model surpasses the initial transient (the most numerical stiff phase) than the ode15s, the final choice is the ode45 solver.

RUNGE-KUTTA

The algorithm behind the ode45 solver is known as the Runge-Kutta method or the RK4 method. It works greatly for approximating the value at the next time step t_{n+1} while considering input of t_n only. So suppose there is an initial value problem of

$$\frac{dy}{dt} = f(t, y), \quad y(t_0) = y_0$$

then the Runge-Kutta method looks as follows

$$y_{n+1} = y_n + \frac{1}{6}h(k_1 + 2k_2 + 2k_3 + k_4) \tag{4.1}$$
$$t_{n+1} = t_n + h \tag{4.2}$$
$$k_1 = f(t_n, y_n) \tag{4.3}$$
$$k_2 = f(t_n + \frac{h}{2}, y_n + h\frac{k_1}{2}) \tag{4.4}$$
$$k_3 = f(t_n + \frac{h}{2}, y_n + h\frac{k_2}{2}) \tag{4.5}$$
$$k_4 = f(t_n + h, y_n + hk_3) \tag{4.6}$$

The outcome of equation 4.1 then gives the value of y_{n+1}. The h is the variable timestep which is determined by the Dormand-Prince method. This is done by writing the $k_{1,2,3,4}$ as is a matrix via a modified Butcher tableau. This method is ingenious and widely used by many MATLAB and SIMULINK users. It is important to understand the roots of the numerical solver since this helps by understanding why the model is running slow or why outcomes oscillate while in reality the outcomes are stable. However, it would be trivial to further explain the roots of the solver since there is no need to optimise the solver yet.

4.3.6. MODEL CONVENTIONS

The entire SIMULINK model has colours attached to the blocks which makes it easier to grasp the purposes of components quickly. The explanation is given in table 4.5

Tab. 4.5 | Model colour conventions

Colour	Purpose
Orange	Input
Cyan	Output
Green	Function block/Matlab function
Red	Integrator
Magenta	1-D systems
Yellow	0-D systems
Grey	Pipes & connections
Blue	Model-check extensions

The top layer of the model is shown in figure 4.2. The purpose of the figure is to get comfortable with the colours assigned as described in table 4.5. Note that on the top-layer the green function blocks and the red integrators are absent. Logically, these are found in the 1-, and 0-D components of the model.

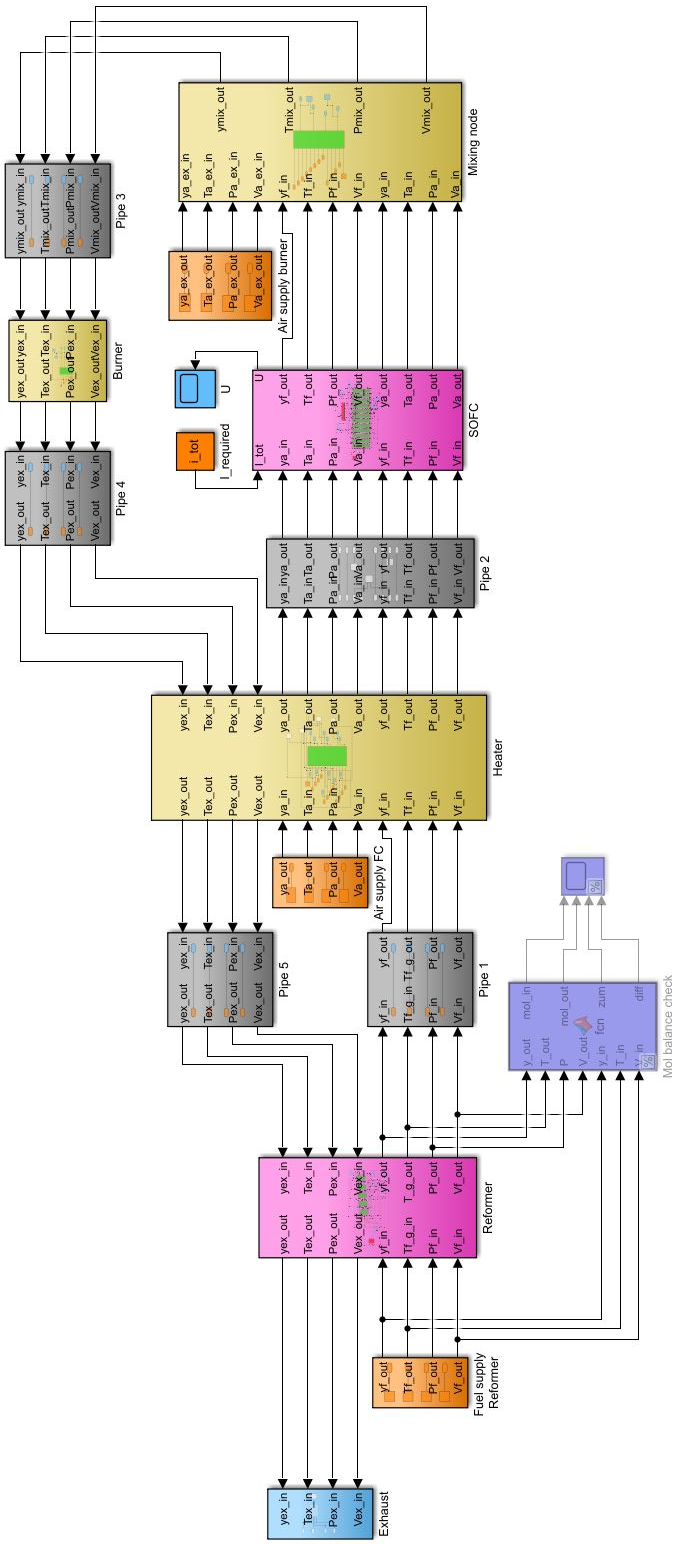

Fig. 4.2 | Top layer of the model, colour conventions are explained in table 4.5

5

1-D REFORMER

The reformer module, shown in figure 5.1, exists of an pre-heater, the yellow part, the reformer, the blue part, and the heater, the outer orange part. It is a tubular unit where the inner tube has a fuel flow from I to II and the outer tube a parallel exhaust flow from IV to VI. In the fuel receiving end, the fuel is a mix of water and methanol on ambient temperature of $25°C$. The reformer operates on temperatures ranging from $250-350°C$ and the the fuel flow is assumed to be in gas phase. To make sure the reformer receives heated gas, a pre-heater is needed.

The pre-heater is a 0-D unit where heat in transferred from the heat flow to the fuel flow through a heat conducting metal. Then the 1-D reformer exists out of multiple discretization units for the reforming process of methanol to hydrogen.

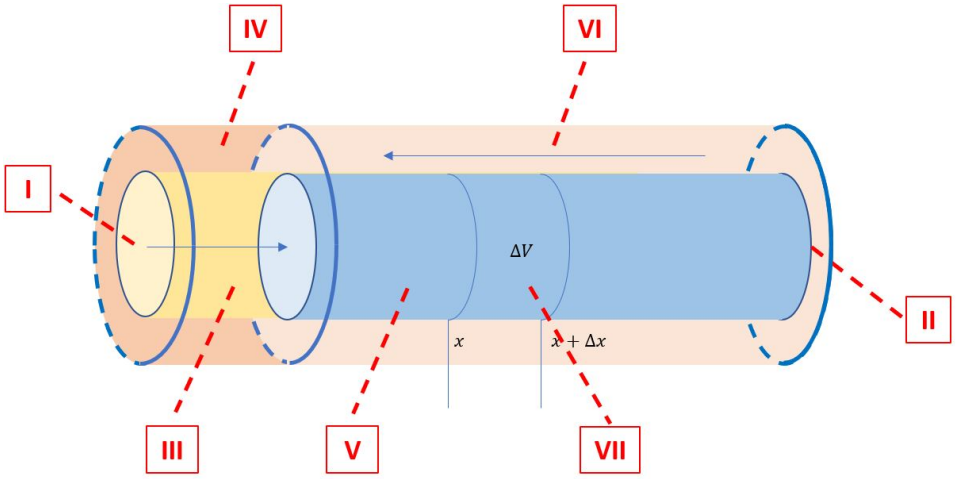

Fig. 5.1 | Schematic representation of the pre-heater and reformer model

In figure 5.3 a representation of a discretization unit is shown. This is also shown schematically in figure 5.1 between x and $x+\Delta x$. A single descretization contains the following values shown in table 5.1.
Figure 5.3 and table 5.1 gives all the information that goes into the function-block, the large white block in the middle. This function-block should be seen as if there is is one function evaluation in one time-step depending on [(all orange values)] = $\boldsymbol{F}$([(all light blue values)]). After the function-block evaluation, four values are integrated first to become output. This happens in the same time-step as the function-block evaluation.
During this chapter, all values will be explained in further detail.

5.0.1. THE REFORMER MODEL

First of all the reformer model itself looks like this, shown in figure 5.2. This picture is not meant to observe closely, however it shows the green elements, which are the discretization units, the orange elements which

are the input values of the system, the blue elements which are the outgoing values and the output of the system, and lastly the red element which is the active control system which throttles the exhaust gas to make sure the targeted heat value is reached at the end of the reformer.

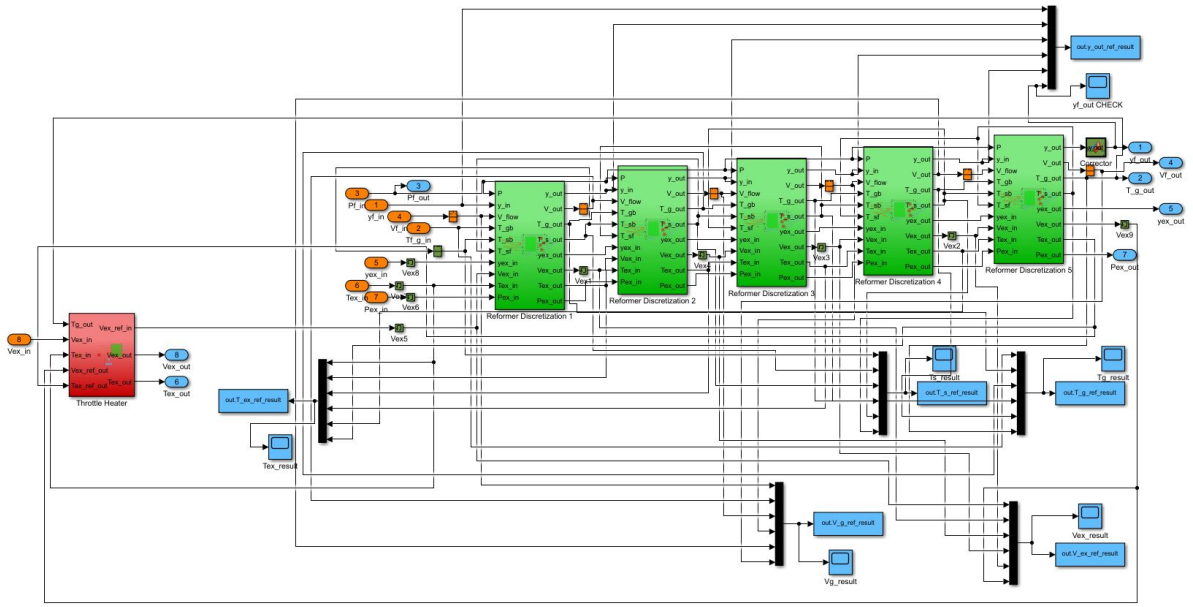

Fig. 5.2 | Representation of the reformer model

Tab. 5.1 | Input and output explanation of descretization system shown in figure 5.3

Name	Input	Output	Vector	Unit	Description
y_in_u	X	-	5x1	$[\frac{mol}{mol}]$	molar fraction of fuel gas into system
y_out	X	-	5x1	$[\frac{mol}{mol}]$	molar fraction of fuel gas leaving the system
T_g	X	-	1x1	[K]	Temperature fuel gas in this system
T_gb	X	-	1x1	[K]	Temperature of fuel gas in previous system
T_s	X	-	1x1	[K]	Temperature of solid in this system
T_sb	X	-	1x1	[K]	Temperature of solid in previous system
T_sf	X	-	1x1	[K]	Temperature of solid in next system
GV	X	-	15x1	-	Geometric Values of single discretization unit
V_in	X	-	1x1	$[\frac{m^3}{s}]$	Volumetric flow of fuel gas into the system
P	X	-	1x1	[Pa]	Pressure of fuel gas in this system
yex_in	X	-	4x1	$[\frac{mol}{mol}]$	molar fraction of exhaust gas into system
Pex_in	X	-	1x1	[Pa]	Pressure of exhaust gas in this system
Tex	X	-	1x1	[K]	Temperature of exhaust gas in this system
Tex_b	X	-	1x1	[K]	Temperature of exhaust gas in previous system
dydt	-	X	5x1	$[\frac{mol}{mol\,s}]$	Change in molar faction of fuel gas leaving the system per second
V_out	-	X	1x1	$[\frac{m^3}{s}]$	Volumetric flow of fuel gas leaving the system
dT_gdt	-	X	1x1	$[\frac{K}{s}]$	Change in temperature of fuel gas in the system per second
dT_sdt	-	X	1x1	$[\frac{K}{s}]$	Change in temperature of solid in the system per second
Vex_out	-	X	1x1	$[\frac{m^3}{s}]$	Volumetric flow of exhaust gas leaving the system
dTexdt_out	-	X	1x1	$[\frac{K}{s}]$	Change in temperature of exhaust gas in the system per second

5.1. GEOMETRIC VALUES OF THE REFORMER

Many different types of methanol reformers have been developed and commercialised already. Nevertheless, it has rarely been used for feeding hydrogen rich gas to an SOFC. This has been tackled in section 3.2.4 already. The most important notion however is; it is unnecessary to use valuable catalysts to lower the

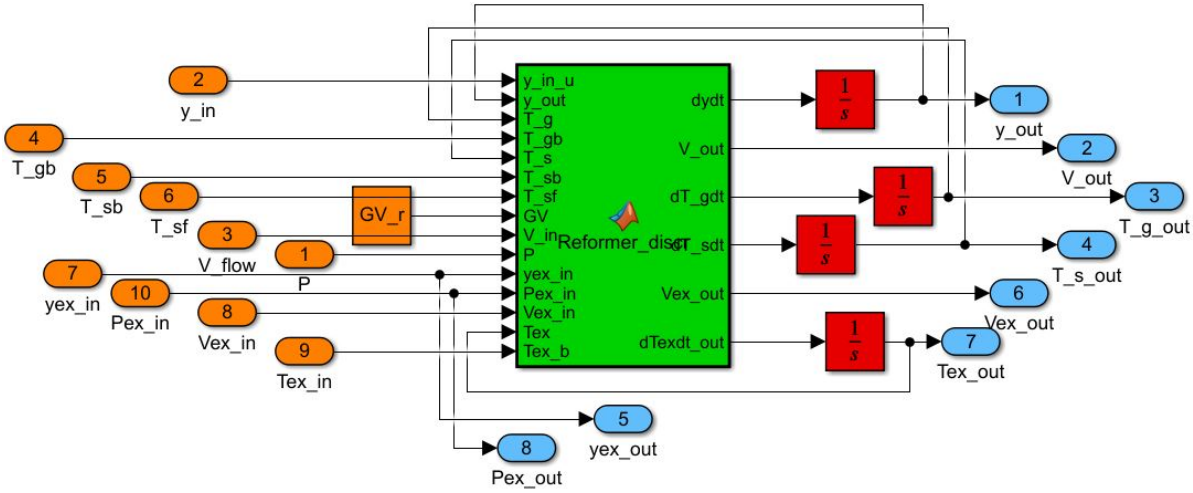

Fig. 5.3 | Simulink representation of reformer model with heater

activation energy for effective reforming temperatures of $< 250°C$ and removal of carbon monoxide. The IT-SOFC used has an entrance temperature of about $475°C$, therefore higher temperatures are allowed, and carbon monoxide is a fuel for the SOFC. The most important aspect of the reformer is thermal management to maintain a temperature of $300-350°C$. Therefore, an efficient heat conducting material is used. The geometric values of the reformer is given in table 5.2. Note that there are values of the inner solid and outer solid. The inner solid exchanges heat between the exhaust gas and the fuel gas. It is assumed that the outer solid exchanges 0 energy, i.e. heat, with the outer world.

Tab. 5.2 | Geometric values reformer unit, the material properties are used from Song et al. [53]

Variable	Value	Unit	Name
Length_{total}	1	[m]	L
Diameter_{outer}	0.5	[m]	D_{outer}
Diameter_{inner}	0.4	[m]	D_{inner}
Discretization	5	[-]	j
Density of inner solid	8055	$[\frac{kg}{m^3}]$	ρ_s
Heat capacity of inner solid	480	$[\frac{J}{molK}]$	
Thickness of inner solid	$2.1*10^{-3}$	[m]	x_s
Heat transfer coefficient inner solid	15.1	$[\frac{W}{m^2K}]$	k_s
Heat loss coefficient outer solid	3	[%]	Q_{loss}

5.2. MASS BALANCE MODEL

There are four ODE's that form the spatial system in one discretization unit. These ODE's describe quasy-static mass and energy models of the reformer. This means that the change in mass and the change in temperature is evaluated every time-step. Together they describe the dynamic change in the discretization unit for a forward flow of fuel, a parallel flow of exhaust gasses, the change in heat of the fuel, exhaust gasses and the intermediary tube. First the mass balance ODE given in equation 5.1. It is assumed that the mass and the molar fraction of the exhaust gas does not change. The molar fraction of the fuel gas does. Therefore, all values given in equation 5.1 refer to the fuel gas flow.

$$\frac{dy_{fuel}}{dt} = (C_{in}V_{in} - C_{out}V_{out})\frac{R_u T_g}{PV_j} + \sum R_{react}\frac{R_u T_g}{P} \tag{5.1}$$

The $y_{fuel}[\frac{mol}{mol}]$ are the molar fractions of the system, $C_{in,out}[\frac{mol}{m^3}]$ is the molar concentration of species, $V_{in,out}[\frac{s}{m^3}]$ is the volumetric flowrate, R_u is the universal gas constant, T_g is the fuel gas temperature, P is the local pressure and V_j is the local volume, $\sum R_{react}[\frac{mol}{m^3 s}]$ are the reaction rates. The following equations from

5.2-6.7 making up the values given in equation 5.1. Some equations need some elaboration. For example in equation 5.5 reveals a crucial assumption made, i.e. the ideal gas law, stating $\dot{n} = P\dot{V}/(R_u T)$, is assumed. Besides, it is assumed that the pressure P is constant, the volume V is constant, the ideal gas constant R_u is constant throughout a single discretization unit. Due to changes in temperature and mass, the only value that is able to change is the volumetric flow $\dot{V}$ in order to respect the ideal gas law. This results in an increase in flow speed. The change in the volumetric flow is calculated from the change in temperature and mass from the previous time-step. This results in a very small error in actual mass, temperature and volumetric flow in real time during dynamic behaviour only.

$$C_{in} = \frac{y_{in} P}{R_u T_{g(j-1)}} \tag{5.2}$$

$$C_{out} = \frac{y_{out} P}{R_u T_{g(j)}} \tag{5.3}$$

$$V_{in} = \frac{D^2 \pi}{4} \frac{m}{s} \tag{5.4}$$

$$V_{out} = V_{in} \frac{T_{g(j)}}{T_{g(j-1)}} \sum y_{out} \tag{5.5}$$

$$R_{react_1} = R_{sr} = k_{SR} P y_{CH_3OH_{out}} y_{H_2O_{out}} \exp\left(\frac{-E_{SR}}{R_u T_g}\right) \tag{5.6}$$

$$R_{react_2} = R_{WGS} = k_{WGS} P y_{CO_{out}} y_{H_2O_{out}} \exp\left(\frac{-E_{WGS}}{R_u T_g}\right) \tag{5.7}$$

$$R_{react_3} = R_{MD} = k_{MD} P y_{CH_3OH_{out}} \exp\left(\frac{-E_{MD}}{R_u T_g}\right) \tag{5.8}$$

The three reactions; steam reforming R_{SR}, water gas shift R_{WGS} and methanol decomposition R_{MD} are assumed to be present in the reformer combined to R_{react}. As stated earlier in section 3.2.4, other formation equations have been considered negligible. The formation of CH_4 is very unfavourable due to the low pressure and relative low temperature of the reformer and therefore neglected (reaction time about >5000x slower then SR [34]). The carbon decomposition is assumed negligible as well due to the amount of water present during the reaction which enables the water gas shift to remove all of the CO. Direct carbon decomposition from CH_3OH is considered negligible since the dehydrogenation from methanol to $HCHO$ is the only route towards a smaller molecule in the steam reforming reaction. From here the decomposition of carbon through reaction with another $HCHO$ to $2H_2O + C_2$ is extremely unlikely.

The only two outputs generated from the mass balance reaction are the molar change per second and the corresponding volumetric flow, lagging one time-step. Since equation 5.1 is a first order differential equation, the integrator block is placed afterwards as shown in figure 5.3. The outcome of the integrator block is then passed to the next discretization unit and redirected as an input for the next time-step.

5.2.1. REACTION EQUATIONS

To model an accurate methanol steam reformer for this specific application has three difficulties. These are the overheating of local spots near the end of the reformer tube (hot spots), sizing towards larger reformers with a volumetric scaler, and finding proper reaction rate equations for the specific model.

HOT SPOTS

The methanol decomposition, which is the most endothermic reaction of the three reactions, has a cooling effect on the reformer. Methanol decomposition also takes place mostly at the beginning of the reformer. The water gas shift then rises the temperature of the reformer due to its exothermic nature. When all methanol is reformed, one can imagine that the tube warms up due to the water gas shift more towards the end. If this is uncontrolled, hot spots occur. The strategy to cope with hot spots is maintaining a flow high enough to not reform all of the methanol and to keep the temperature below $325°C$ by throttling the heater. It is deliberately chosen not to reform all the methanol, which is done by enlarging the volumetric flow to a certain extend so methanol decomposition can take place in the FC stack also. Cooling the FC stack is another problem which is explained in section 3.3, but the methanol decomposition reaction is one 'tool' to do so. Therefore, not reforming all methanol, and thus making sure that there is a controlled environment of both endothermic and exothermic reactions at the end of the reformer, is an easy and great way to cope and prevent hot spots.

REACTION RATE EQUATIONS

The reaction rates are given in table 5.3.

Tab. 5.3 | Reaction rates reformer from Song et al. [53]

Type of reaction	**A** $[\frac{mol}{m^3 s}]$	$\mathbf{E}_a[\frac{J}{mol}]$	**Chemical equation**
Methanol Steam Reforming	$1.43 * 10^6$	$1.22 * 10^5$	$CH_3OH + H_2O \rightarrow CO_2 + 3H_2$
Water-gas shift	$5.115 * 10^4$	$8.77 * 10^4$	$CO + H_2O \rightarrow CO_2 + H_2$
Methanol Decomposition	$2.002 * 10^6$	$9.27 * 10^4$	$CH_3OH \rightarrow CO + 2H_2$

There are many papers on reactions. There are two reasons why this particular paper,[53], was chosen for reaction rates. The first and most important reason is that the rates have the same units, namely $[\frac{mol}{m^3 s}$ for temperatures around $300°C$ from the same paper . There are many more papers which use specifically this set of reaction rates also [34]. This means that the rates have been combined in other scientific work for the same application. Therefore, using these reaction rates is a validation to the use of a hypothetical system.

The second reason is that many methanol reformers purify the reformed gasses from everything but hydrogen to prevent poisoning PEMFCs. This is a difficult and costly step (both financially due to the expensive catalysts and chemically because of precision of filtering other molecules) which is disadvantageous for SOFC based BoP application like this research. In most other papers the reactions rate encapsulate the purifying step and therefore are sub-optimal to this research. The equation of [53] however, give insights to the reforming of methanol only, which is wanted.

SIZING OF THE REFORMER

In the main script of this model, specific geometric values are assigned to the reformer, see table 5.2. Although the geometric values can easily be enlarged to the size required, the reaction rates cannot. To reform methanol at $\approx 300°C$, a girdler G66B catalyst is used [34]. The catalyst is placed on the surface of the tube and has a characteristic reforming capability that is embedded in an Arrhenius equation. The Arrhenius equations used are proportional to $R_{reaction} \propto m^3$ while the catalyst has a m^2 surface. Therefore, a m^3 reaction rate is scaled by a m^2 catalyst surface. The paper [53] assumes volumetric dependent reaction rates nevertheless, but the sizing of these reaction rates for a much larger reformer, which is used in this model, is done by respecting the relative size of the reformer in the paper and by enlarging the amount of single tubes in one reformer. A representation is given in figure 5.4

Note that the relative size of the reformer is somewhat enlarged, but the width of an inner single tube is estimated to be $70mm$ while the inner diameter of the total tube given in table 5.2 is the size of all tubes combined like if there were no inner tubes. The model itself, however, is made non-dimensional to prevent physical boundaries.

5.3. HEAT BALANCE MODEL

The reformer model has three different temperature states. The fuel gas, the exhaust gas, and the solid. As described earlier, it is assumed that the boundary layer of the exhaust gas does not transfer any heat towards the outer world. The only heat transferring routes are the inlet and outlet of both the fuel gas and the exhaust gas, as between the solid layer of the reformer. However, it is assumed that the system as a certain heat dissipation factor. This is addressed in the $Q_{loss_{outer}}$ in the T_{solid} ODE. The three state equations are described in equations 5.9, 5.11 & 5.12.

These three first order differential equations give the change in temperature per second. The first differential equation to break down is the T_{solid} of equation 5.9. This is the ODE with the most terms.

5.3.1. TEMPERATURE OF THE SOLID

As a recap, the solid contains the thin tubes between the fuel gas and the exhaust gas. Note that one temperature is calculated for one volumetric quantity. It is assumed that multiple tubes form this volume together as shown in figure 5.4. The solid transfers heat from the exhaust and the fuel. The temperature of the solid is given in equation 5.9

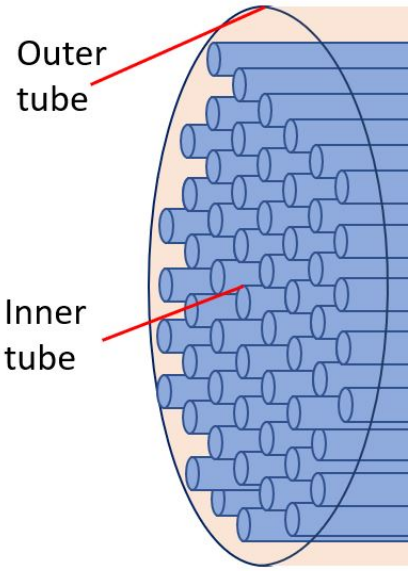

(a) Reformer tubes schematic representation

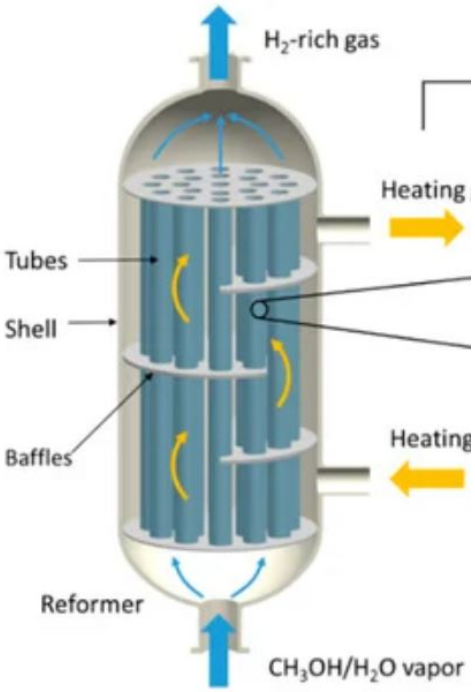

(b) Reformer tubes representation [54]

Fig. 5.4 | Molar fraction in reformer with different discretization units

$$\frac{dT_{solid}}{dt} = \frac{1}{\rho_s c_{p_s} x_s}\left(k_s(T_{fuel} - T_{solid}) + k_s(T_{exhaust} - T_{solid}) + k_s x_s \frac{d^2 T_{solid}}{dt^2} - Q_{loss_{outer}} - \sum \Delta HR_{react}\right) \tag{5.9}$$

The first term, $\frac{1}{\rho_s c_{p_s} x_s}$ is proportional to $\propto \frac{m^2 K}{J}$. Where ρ_s is the density of the solid, c_{p_s} the heat capacity of the solid and x_s the thickness. So all terms between the brackets should be in the form of $\propto \frac{J}{m^2 s}$ in order to have the change in temperature per second $\frac{dT_{solid}}{dt} \propto \frac{K}{s}$. The first two terms are the difference in temperature between the solid T_{solid} and T_{fuel} times the heat transfer coefficient k_s as the difference in temperature between the solid T_{solid} and the exhaust $T_{exhaust}$.

CENTRAL FINITIE DIFFERENCE FOR CONVECTION OF SOLID TO SOLID

Then a second order term is added to describe the conduction of heat between the two neighbouring discretization Unit$_{j-1}$ and Unit$_{j+1}$, this goes by the equation 5.10. The idea is to derive the first order ODE describing the conductive heat transfer. A visualisation is given in figure 5.5. Here the x-axes is the length between the central point of each discretization unit and the y-axis is the local temperature. To get a grip on the change in energy due to conduction, the slope of the local temperature is needed. The central finite difference method is the most accurate method of the numerical finite difference methods to do so. Note that at the first and last discretization units $J = 1$ or $J = J$, there is no following or previous unit. At these boundary elements, the unit itself is substituted instead.

$$\frac{dT_{solid_{convection}}}{dt} = k_s x_s \frac{d^2 T_{solid}}{dt^2} = k_s x_s \left(\frac{T_{solid_{j-1}} + T_{solid_{j+1}} - 2T_{solid_j}}{L_j^2}\right) \tag{5.10}$$

HEAT LOSS TO OUTER WORLD

A loss of heat to the outer world is defined as $Q_{loss_{outer}}$. This is estimated to be 0 for this study. However the parameter $Q_{loss_{outer}}$ is added to the model itself. This is a bold assumption, however, the size of $Q_{loss_{outer}}$ is unknown and therefore it would devalue the results.

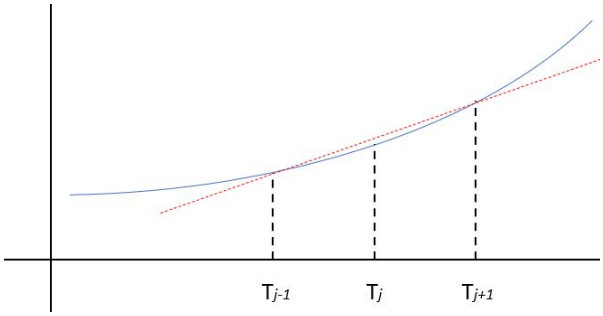

Fig. 5.5 | Visualisation of the central finite difference method

HEAT OF FORMATION TO THE SOLID

Lastly the term $\sum \Delta HR_{react}$ is added, this term describes the change in temperature of the solid due to the formation reactions. It is the sum of all the heat developed during the formation of molecules. For example, lets assume that methanol decomposition takes place.

$$CH_3OH = CO + 2H_2$$

Then the heat added to the system is given by the standard change in enthalpy due to formation $\Delta_f H°$. The values of the example reaction are given below. Note that the stoichiometric value is the amount of molecules that react.

Molecule	$\Delta_f H°$ $[\frac{kJ}{mol}]$	**Stoichiometry**
CH_3OH	-205. ± 10.0	1
CO	-110.53 ± 0.17	1
$2H_2$	0	2

The change in enthalpy is calculated by substracting the enthalpy of formation of the reactants from the products gives the change in enthalpy of methanol decomposition $\Delta_f H° = (-110.53 \pm 0.17 + 0) - (-205.0 \pm 10.0) \approx 90.640$. Now substituting in the term $\sum \Delta H_{MD} R_{MD}$, i.e. the change in enthalpy times the amount of reactions that took place due to methanol decomposition results in a increment of heat. In principle this works the same for steam reforming and water-gas shift.

Reaction	$\Delta_f H°$ $[\frac{kJ}{mol}]$
Methanol Decomposition	90.640
Water-Gas Shift	-41.170
Steam Reforming	49.470

There are two reasons why it is assumed that all the heat of these reactions is put on the solid only. First of all is because the heat capacity of the solid material is way bigger than the heat capacity of both gasses. Since the time-scale of interest is in the order of ≈ 10 seconds, it is not preferred to stiffen the model by adding these highly dynamic terms to the gasses during transits. The second reason why this assumption is viable, is because most of the reactions actually will take place at the solid due the presence of a catalyst on the surface. Therefore the majority of the heat would already be transferred to the solid anyway.
The major drawback of this assumption for a methanol reformer is that the exothermic water-gas shift actually does not take place at the reformers surface mostly, but it is spontaneous and takes place in the entire cross-section of the mass-flow. As a result, the model predicts that the solid rapidly increases heat towards the end while the fuel gas only heats due to heat transfer of the solid, while in reality it is the other way around. The major consequence is that the fuel gas leaves the system carrying less heat than it should in reality. This results in a conservative assumption regarding the amount of heat added to the fuel gas, and it means that the heater between the reformer and the FC unit needs to add less heat in reality. The phenomena of hot spots is not described correctly also due to the low temperature of the gas, but since all the heat is already put on the solid, the critical heat difference in a solid should be evaluated in order to conclude if hot spots would occur.

5.3.2. TEMPERATURE OF THE GASSES

Both gasses go by the form of a term $\frac{1}{\sum c_{p_{species}} C_{out}}$ which is proportional to $\propto \frac{m^3 K}{J}$. Note that this term, in contrast to the first term for the temperatures of the solid, is proportional to a volume instead of a surface.

$$\frac{dT_{fuel}}{dt} = \frac{1}{\sum c_{p_{fuel}} C_{out}} \left(q_{in} - q_{out} + 4k_s \frac{T_{solid} - T_{fuel}}{D_{reformer_{eff}}} \right) \tag{5.11}$$

$$\frac{dT_{exhaust}}{dt} = \frac{1}{\sum c_{p_{exhaust}} C_{out}} \left(q_{in} - q_{out} + 4k_s \frac{T_{solid} - T_{exhaust}}{D_{exhaust_{eff}}} \right) \tag{5.12}$$

$c_{p_{species}}$ INSTEAD OF $c_{v_{species}}$

First of all, the heat capacity is the amount of energy that is stored in a medium to raise it with one kelvin. In the case of $c_{p_{species}}$, it is assumed that the pressure stays constant during the change in temperature. For $c_{v_{species}}$ it is assumed that the volume stays constant. Actually, both are true in the case of this research since it is assumed that the pressure does not change inside a system and the boundary conditions of the volume do not change either. However, the specific heat $c_{p_{species}}$ of the gas is used deliberately. This is due to the fact that a modular unit is considered an open system with a variable volumetric flow $\dot{V}$. Therefore $c_{p_{species}}$ is used.

To determine $c_{p_{species}}$, the library of NIST for gaseous heat capacity is used [**WelcomeWebBook**]. This library supplies an 5^{th} order equation that goes by the following form;

$$c_p = A + Bt + \frac{Ct^2}{2} + \frac{Dt^3}{3} - \frac{E}{t^2} \tag{5.13}$$

Where $A-E$ are constant, t is the temperature in kelvin divided by 1000. For all species, the equation holds from $298K$ or the moment it becomes gaseous at ambient pressure until $1300-1500K$. Except for methanol, which is referred to as methyl alcohol by NIST. NIST does provide a set of data points where the $c_{p_{Me}}$ is measured at different temperatures at ambient pressure. The line is assumed to be captured by the relation given in equation 5.14

$$H^\circ = A\left(\frac{T_{fuel}}{100} - 2\right)^2 + B\left(\frac{T_{fuel}}{100} - 2\right) + C \tag{5.14}$$

Where $A-C$ are constants and T_{fuel} is the temperature in Kelvin resulting in the following empirically derived equation 5.15. The result of the equation is shown in figure 5.6.

$$c_{p_{methanol}} = -0.3113\left(\frac{T_{fuel}}{100} - 2\right)^2 + 9.353\left(\frac{T_{fuel}}{100} - 2\right) + 34.69 \tag{5.15}$$

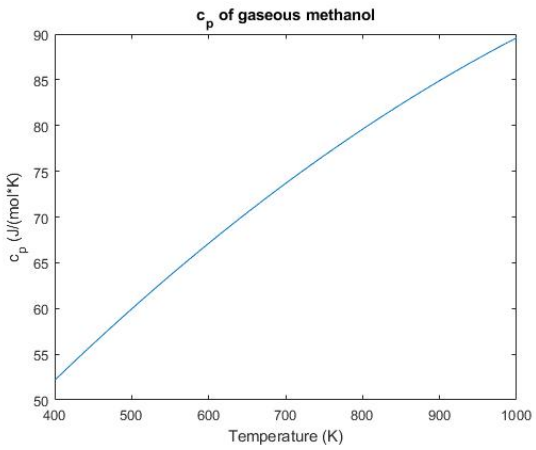

Fig. 5.6 | c_p of gaseous methanol

Note that the curve acts nearly linear, therefore it is assumed that this curve can be extrapolated beyond temperatures also. In the case of the other species, NIST provides another set of equations that go by the form

of equation 5.13, but than with temperatures ranging up to $1800-2000K$. This is not used in the reformer however, but it will be mentioned again in the combustor model.

Another important remark regarding the use of $c_{p_{species}}$, is that $c_{p_{species}}$ is related to the change in enthalpy in the system. That is why all thermodynamic equations in this model are related to enthalpy.

C_{out} AS CENTRAL MASS FLOW

In this model only the incoming mass states and the outgoing mass states are defined. Because the change in temperature given to the outgoing mass is calculated in $\frac{dT_{gasses}}{dt}$, the outgoing mass used also. Note that $C_{out} = [\frac{mol}{m^3}]$, which is the amount of mass inside the system at time-step t. This is determined through the outgoing molar fraction. This also means that C_{out} contains a time-step delay. The error in mass of the descretization unit will be lower with a higher amount of discretization units J. Possible effects are most noticeable in transit behaviour.

$$C_{out} = y_{out}\frac{P_{fuel}}{R_u T_{fuel}}$$

HEAT FLUXES q_{in} AND q_{out}

The heat fluxes of both gasses are calculated via q_{in} and q_{out}, which are defined by the sum of the molar flow of each specie N_{in_j} multiplied with its change enthalpy H_j as shown below

$$q_{in} = \sum_{species} N_{j-1}H_{j-1}$$
$$q_{out} = \sum_{species} N_j H_j$$

The molar flow is defined by multiplication of the molar fraction y_j, the local pressure P, and the local volumetric flow $\dot{V}$, devided by the universal gas constant R_u, the local temperature T_{gas_j}, and the local volume. Note that the pressure and the volume are not specified per discretization unit since they are constant.

$$N_{j-1} = y_{j-1}\frac{P}{R_u T_{gas_{j-1}}}\frac{\dot{V}_{j-1}}{V}$$
$$N_j = y_j\frac{P}{R_u T_{gas_j}}\frac{\dot{V}_j}{V}$$

As for the heat capacity c_p, the change in enthalpy H° is calculated from the open source NIST library [55]. For this equation 5.16 $A-F$ are constants, t is the temperature in kelvin devided by 1000. Note that this term does not include the enthalpy of formation. This is only accounted for in the term $\sum \Delta H_{react} R_{react}$ as elaborated in section 5.3.1. Since the change in entalpy is what matters, it does not influence the ΔH° if the formation enthalpy is calculated somewhere else. The same temperature range for c_p holds for H° also, i.e. for all species, the equation holds from $298K$ or the moment it becomes gaseous at ambient pressure until $1300-1500K$.

$$H^\circ = At + \frac{Bt^2}{2} + \frac{Ct^3}{3} + \frac{Dt^4}{4} - \frac{E}{t} + F \tag{5.16}$$

For methanol, no library was given by NIST. But since the nature of the equations NIST provided for the other species, the magnitude of the enthalpy change could be estimated. This is is done by altering the equation of methanol to the following relation

$$H^\circ = \left(A\left(\frac{T_{fuel}}{100}-2\right)^3 + B\left(\frac{T_{fuel}}{100}-2\right)^2 + CT_{fuel}\right)/1000$$

Although this relation is not empirically proven, it does match the magnitude of enthalpy change regarding other species. As depicted in figure 5.7, the upper line follows the trajectory of the others. Note that the position relative to the y-axis is not of any importance due to the fact that the difference in enthalpy is, i.e.

the slope is important. Although this derivation could be seen as a flaw in the thermodynamic model, it is not of that big of an impact. The only cells that have high concentrations of methanol are the first discretization units of the reformer, furthermore in this model, the fraction of methanol is of upmost 15% to mostly ≈ 1%. If the slope would be 20% off, which about the difference of the steepest slope to the most shallow slope in figure 5.7, this would make up for an heat transferring error of < 3% in worst case scenario. Understanding this, it is decided to not further investigate the change in enthalpy for methanol.

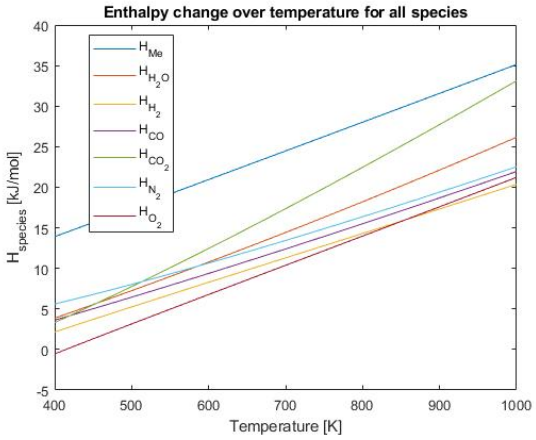

Fig. 5.7 | Enthalpy change over Temperature

HEAT TRANSFER THROUGH SOLID

The last term in the derivation of the change in heat of the gasses is the heat transfer from solid to gas. Note that both in both equation 5.11 and 5.12 the diameter used is not equal to the diameter of the total cylindrical volume. The reason is that the term is as follows.

$$\left(4k_s\frac{T_{solid}-T_{gasses}}{D_{eff}}\right)\propto\frac{J}{m^2sK}\frac{K}{m}=\frac{J}{m^3s}$$

The heat transferring surface area, for which $k_s \propto \frac{W}{m^2K}$ is defined, is not on the entire volume, but on every single tube, as shown in figure 5.4. Therefore to go from the lateral cylindrical surface to a volume, the diameter of a single tube is used. This is done by adding $\frac{4}{D_{eff}} \propto \frac{1}{m}$ to the term as shown bellow.

Lateral surface cylinder	$2\pi rh=\pi Dh$
Volume cylinder	$\pi r^2h=\frac{\pi D^2h}{4}$

5.4. DISCRETIZATION OF REFORMER

The reaction rates of the reformer model uses the partial pressure of the outgoing gasses and the temperature as input. Therefore, the outgoing partial pressure and the local temperature are the only variables that influence the reaction rate. The temperature changes due to reaction heat drawn or expelled and due to the convective heat of the solid. The latter is heated by the exhaust gasses from the burner. Note that the bigger a discretization unit is, the larger the step in temperature change and molar change will be.

The outcome of the system does look quite the same. The unit that uses more discretizations in figure 5.8b reforms more methanol then the one with fewer in figure 5.8a. There are some reasons that explain this occurence, but the most critical variable is the change in velocity of the gas. It is assumed that the volumetric flow rate changes due to change in the amount of moles and change in temperature. The volumetric flow of the entire unit is determined at the end of the unit. Therefore, the internal flow is estimated to be too high. The biggest result is that the residence time of the gas is relatively lower with fewer discretization units. As a result, there is relatively less time to change the constitution of the fuel gas. More discretization units will result in a more accurate reforming process.

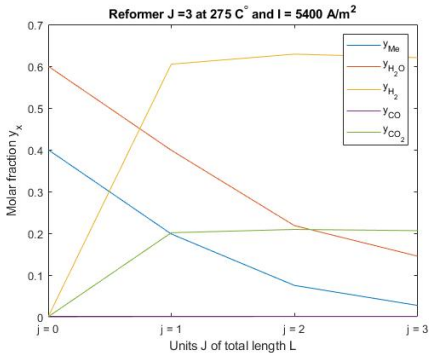

(a) Reformer with J=3

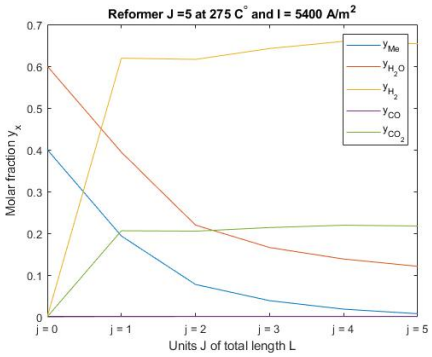

(b) Reformer with J=5

Fig. 5.8 | Molar fraction in reformer with different discretization units

Another difference in discretization units is the temperature of the fuel gas and the solid. The temperature decreases at the beginning of the reformer, this is due to the endothermic methanol decomposition reaction.

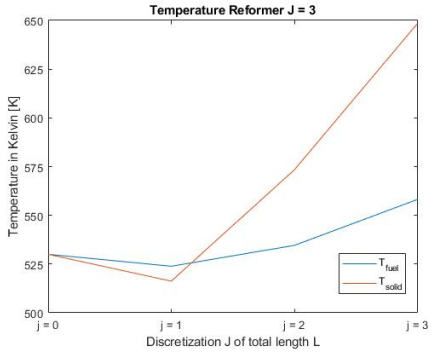

(a) Temperature in reformer with J=3

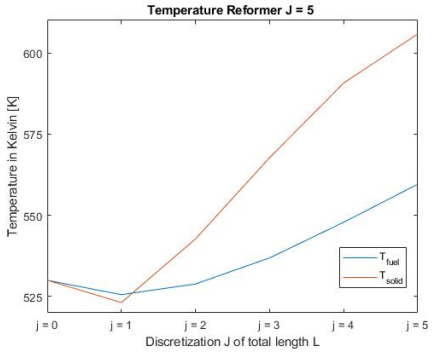

(b) Temperature in reformer with J=5

Fig. 5.9 | Temperature differences in reformer with different discretization units

6

1-D Solid Oxide Fuel Cell

In figure 6.1, a representation of a single cell is given. In this research a metal supported solid oxide fuel cell is used. Note that the anode support, given in grey, is a porous metal layer that is in between the fuel and the anode. In figure 6.1b the red arrows are the anode fuel and the blue arrows the cathode air, as explained earlier.

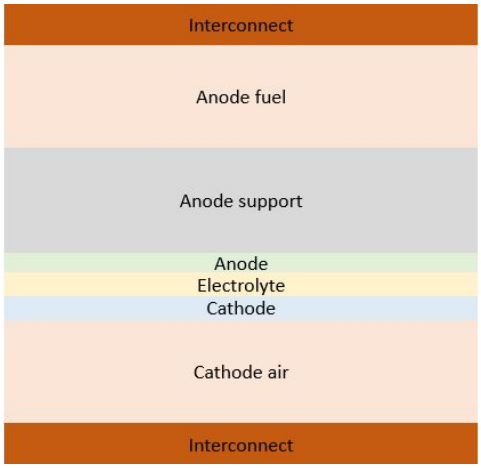

(a) Single cell of FC stack

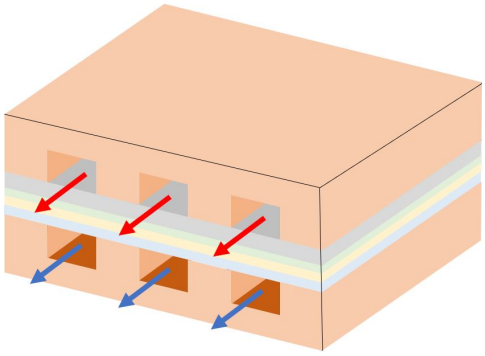

(b) Single cell of FC stack 3D

Fig. 6.1 | Schematic of a single cell

The main reason why an FC should be a one dimensional unit is because of the many interactions that take place along the length of the FC stack. But first some assumptions are made; it is assumed that a stack exists out of multiple cells that are identical. In reality this is not the case since outer cells are relatively cooler than inner cells. Nevertheless, the main losses in electrical efficiency in a fuel cell occur due to events inside the cell structure. Another simplification is that it is assumed that every channel is identical in receiving fuel, air, oxidizing hydrogen, temperature differences etc. In reality this is not the case since a single fuel cell has a central fuel and air feed which is then distributed in the different channels. As a result, the outer channels are likely to be colder and are relatively longer. The channels sometimes sling inside the cell to cope with this problem. However, in this research it is assumed that there is a uniform flow from 0 to 1 L_{FC}. As for the stack losses, these assumptions are not governing losses. Lastly, 2-D and 3-D effects are neglected, the main reason is that the outcome of the stack model should give insight in the behaviour in the balance of plant and this is not necessarily a highly in dept research on how the FC stack behaves on its own. It is suggested that when one finds an optimal work point or a preferred configuration of this balance of plant, one should research single units more in dept.

6.0.1. MATCHING OF FC STACK TO METHANOL

The metal supported SOFC needs to operate at lower temperatures due to metal support. This support will lose its structural integrity if the temperatures rise towards $650°C$, therefore it is suggested that the maximum allowed temperature in this FC stack should be $600°C$ at max.

Right now a commercial unit of this particular stack is readily available in the market running on a mixture of natural gas (methane) and water which is used for households as a replacement for a conventional central heating boiler. Methanol however, is easier to reform, less endothermic, and lower coking problems. Besides, the reforming process happens favourable at lower temperatures also, around $300°C$, while methane reforming happens at best at temperatures of $> 600°C$.

Another result of the less endothermic reaction inside a stack is that the maximum temperature gradient in the solid structure is lower, the main reason is that the cooling is less so the stack relies more on air cooling from the cathode.

6.1. THE FUEL CELL MODEL

The fuel cell model itself is shown in figure 6.2. This picture is not meant to observe closely, however it shows the green elements, which are the discretization units $j = 1,2,3,..,12$, the orange elements which are the input values of the system, the blue elements which are the outgoing values and the output of the system, and lastly the red elements receive the required current density and then calculate the corresponding power and voltage output to make sure the targeted inputs are met.

The main reason 12 discretization units are chosen instead of 5 like the reformer model has, shown in figure 5.2, is because of multiple phenomena that occur in specific parts of the FC unit. Namely; the FC model reforms methanol internally, it has three governing losses; ohmic-, concentration-, and activation losses, and has a variable temperature along the path length. It is expected that both the internal reforming and the activation losses will be most present at the beginning of the FC. The temperature peak and the concentration losses will be present at the end of the FC. The highest local current densities will be somewhere at $L_{fc} = 0.6$ on the non-dimensional length. To make sure that all these phenomenons can be observed separately, more discretization units are used.

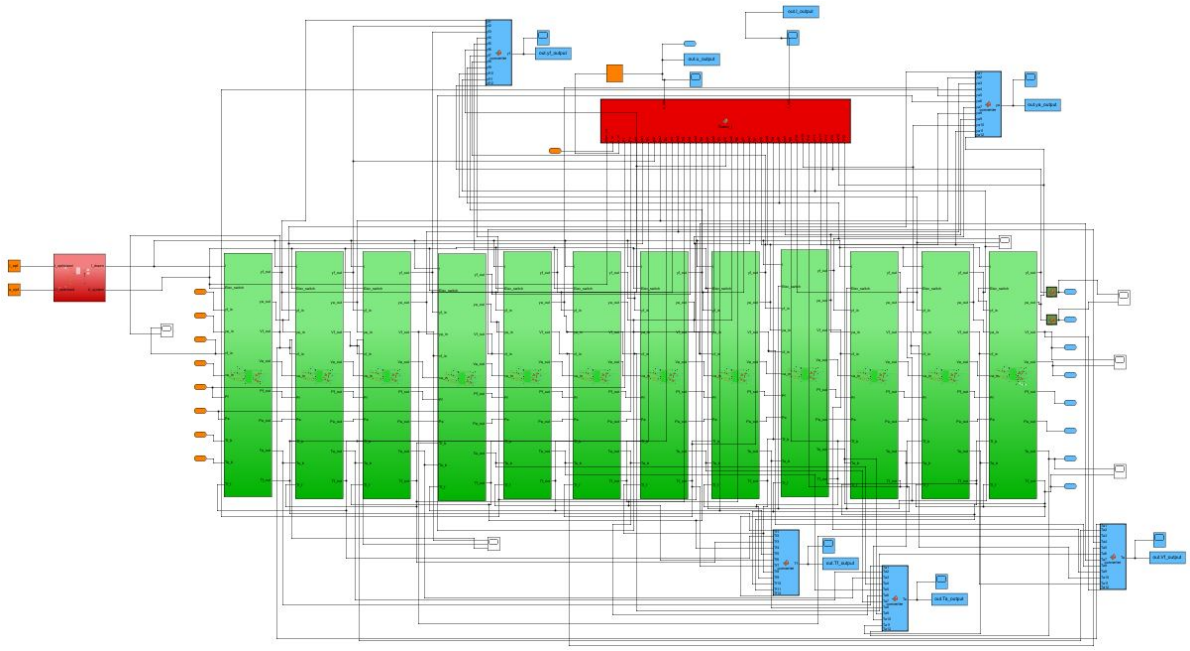

Fig. 6.2 | SIMULINK representation of the FC model

6.1.1. DESIGN OF FUEL CELL STACK

The stack exists out of multiple models that work together to form the total unit. As shown in figure 6.3, the stack is made up out of four different models, the thermodynamic, the electric, the mass and the geometric model. Note that the geometric model is a set of parameters, but it most definitely is an important piece since it highly influences the behaviour of the other 3 models.

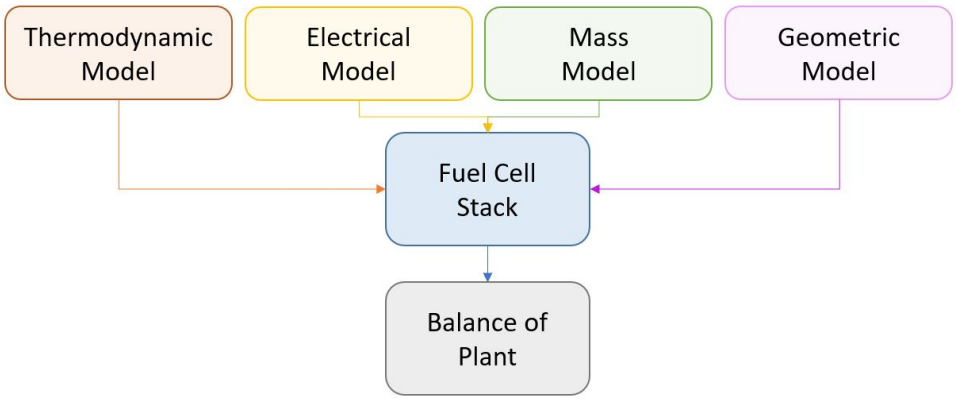

Fig. 6.3 | Schematic structure of models working together

In SIMULINK, 12 discretization units have been used to model one FC. One cell is given in figure 6.4. All the orange parts are input, blue is output, red are integrators and green is a MATLAB environment containing all equations. Note that the I_{in}, which is the optimised current density for this specific unit j, produces an output U. However the output U is already known since the input I_{in} is chosen in such a way that for all I_j $U = U_j$. The reason why U is still calculated is because not all factors are taken into account in the numerical optimiser for I. The change in hydrogen oxidation due to transients for example has been neglected in the numerical optimiser, therefore it is important and interesting to recalculate the offset of U to measure the deviation.

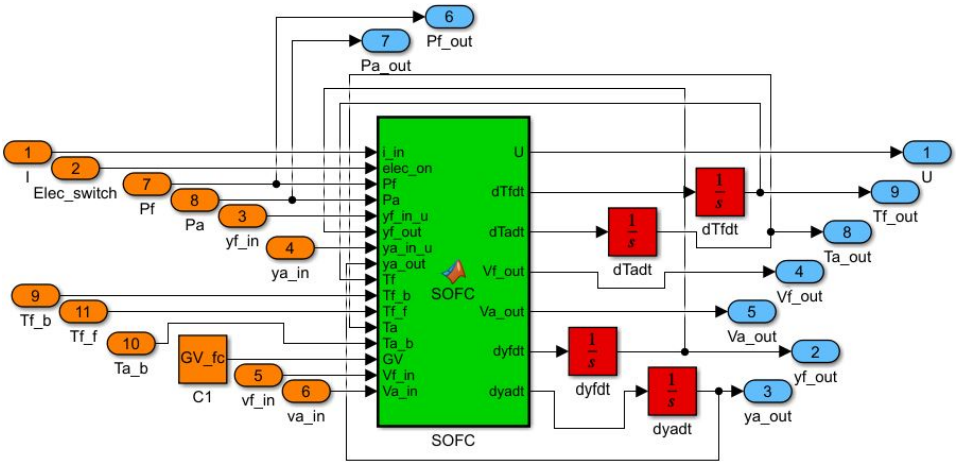

Fig. 6.4 | SIMULINK representation of discretization unit SOFC

In table 6.3 all visible variables of figure 6.4 are given and explained briefly. The intergrators have not been listed in the table, this is because they integrate the output value with respect to time as an first order ODE. There are two specific cases in which the discretization unit looks different, and that is at the boundaries of the system. In the entrance of the system, the temperature of the fuel and gas of the discretization unit does not exist, therefore the temperature of the fuel gas from the heater is used. This, however, comes with complications since the fuel gas temperature, Tf_b, is lumped with the solid temperature, which is explained further in section 6.4. For the last discretization unit, the temperature of the fuel in the next unit does not exist, instead the temperature of this unit is used as if it was the next unit. This choice will be elaborated on in section 6.4 also.

Tab. 6.1 | Input and output explanation of descretization system shown in figure 6.4

Name	Input	Output	Vector	unit	Description
i_in	x	-	12x1	$[\frac{A}{m^2}]$	local current density of unit
elec_on	x	-	1x1	[-]	switch to turn electrical model on or of for numerical efficiency
Pf	X	-	1x1	[Pa]	Pressure of fuel gas in this system
Pa	X	-	1x1	[Pa]	Pressure of air gas in this system
yf_in_u	X	-	5x1	$[\frac{mol}{mol}]$	molar fraction of fuel gas into system
yf_out	X	-	5x1	$[\frac{mol}{mol}]$	molar fraction of fuel gas leaving the system
ya_in_u	X	-	2x1	$[\frac{mol}{mol}]$	molar fraction of air gas into system
ya_out	X	-	2x1	$[\frac{mol}{mol}]$	molar fraction of air gas leaving the system
Tf	X	-	1x1	[K]	Temperature of fuel gas in this system
Tf_b	X	-	1x1	[K]	Temperature of fuel gas in previous system
Tf_f	X	-	1x1	[K]	Temperature of fuel gas in next system
Ta	X	-	1x1	[K]	Temperature of air in this system
Ta_b	X	-	1x1	[K]	Temperature of air in previous system
T_sf	X	-	1x1	[K]	Temperature of solid in next system
GV	X	-	15x1	-	Geometric Values of single discretization unit
Vf_in	X	-	1x1	$[\frac{m^3}{s}]$	Volumetric flow of fuel gas into the system
Va_in	X	-	1x1	$[\frac{m^3}{s}]$	Volumetric flow of air gas into the system
U	-	X	1x1	[V]	Voltage rproduced by the system
dTfdt	-	X	1x1	$[\frac{K}{s}]$	Change in temperature of fuel gas in the system per second
dTadt	-	X	1x1	$[\frac{K}{s}]$	Change in temperature of air gas in the system per second
Vf_out	-	X	1x1	$[\frac{m^3}{s}]$	Volumetric flow of fuel gas leaving the system
Va_out	-	X	1x1	$[\frac{m^3}{s}]$	Volumetric flow of air gas leaving the system
dyfdt	-	X	5x1	$[\frac{mol}{mols}]$	Change in molar faction of fuel gas leaving the system per second
dafdt	-	X	2x1	$[\frac{mol}{mols}]$	Change in molar faction of air gas leaving the system per second

6.2. THE MASS MODEL

The mass model describes a change in molar composition throughout the fuel cell from 0 to 1 L_{FC}. The major effects on the molar mass are the reforming reforming reactions like methanol decomposition, methanol steam reforming, and the water gas shift and the oxidation of hydrogen and reduction of oxygen due to the electrochemical reactions. A result of the reforming reactions is that the amount of molecules grows which will lead to an increase in volumetric flow since the pressure is assumed to be constant. Note that the ideal gas law is assumed to be applicable. A result of the hydrogen oxidation and oxygen reduction is a mass surplus on the anode side, the bulk fuel, and a mass deficit on the cathode side, the bulk air. The two governing equations are the following 6.1 & 6.2.

$$\frac{dy_{fuel}}{dt} = (Cf_{in}\dot{V}_{fin} - Cf_{out}\dot{V}_{fout})\frac{R_u T_f}{P_f V_f} + \sum R_{f_{react}}\frac{R_u T_f}{P_f} \tag{6.1}$$

$$\frac{dy_{air}}{dt} = (Ca_{in}\dot{V}_{a_{in}} - Ca_{out}\dot{V}_{a_{out}})\frac{R_u T_f}{P_f V_f} + \sum R_{a_{react}}\frac{R_u T_f}{P_f} \tag{6.2}$$

Both equations are the governing equation in the change of mass in $[\frac{mol}{mols}]$. All variables used in the governing equations 6.1 & 6.2 have are given in the equations below. The left column are the fuel related mass equations, and the right column for the air. The $C_{channel_{direction}}$ flows are the molar flows inwards and outwards the system, the $\dot{V}$ is the volumetric flow in the system, and the R_{react_x} are the reaction equations of certain reactions. The five reaction equations are put in two vectors, $R_{f_{react}}$ and $R_{a_{react}}$. The first vector contains the second to forth reactions and the latter the fifth. The first reaction, which is methanol steam reforming in the reformer, is neglected. Note that MSR is a combination of MD and WGS, but in the literature it is suggested to not lump the SR equation and keep them separate for direct SOFCs, mainly because the WGS equilibrium shifts disproportional to MD equilibrium [56].

$$C_{f_{in}} = \frac{y_{f_{in}} P_f}{R_u T_{f_{j-1}}} \qquad C_{a_{in}} = \frac{y_{a_{in}} P_a}{R_u T_{a_{(j-1)}}} \tag{6.3}$$

$$C_{f_{out}} = \frac{y_{f_{out}} P_f}{R_u T_{f_j}} \qquad C_{a_{out}} = \frac{y_{a_{out}} P_a}{R_u T_{a_j}} \tag{6.4}$$

$$\dot{V}_{f_{out}} = \dot{V}_{in} \frac{T_{f_j}}{T_{f_{j-1}}} \sum y_{f\,out} \qquad \dot{V}_{a_{out}} = \dot{V}_{in} \frac{T_{a_j}}{T_{a_{j-1}}} \sum y_{a\,out} \tag{6.5}$$

$$R_{react_2} = R_{WGS} = x_{tuner_2} k_{WGS} P_f y_{CO_{out}} y_{H_2O_{out}} \exp\left(\frac{-E_{WGS}}{R_u T_g}\right) \tag{6.6}$$

$$R_{react_3} = R_{MD} = x_{tuner_3} k_{MD} P_f y_{CH_3OH_{out}} \exp\left(\frac{-E_{MD}}{R_u T_g}\right) \tag{6.7}$$

$$R_{react_4} = R_{OX} = \frac{I_j}{2F} \frac{1}{V_{f_j}} \tag{6.8}$$

$$R_{react_5} = R_{RED} = \frac{I_j}{2F} \frac{1}{V_{a_j}} \tag{6.9}$$

The reaction rates are derived from a direct methanol SOFC at $> 800°C$. They use a reaction rates with tuners like $x_{tuner_{2,3}}$ to minimize numerical errors and for more accurate representations. Most SOFC models assume a near instantly WGS reaction if water is available because this is the case in reality, therefore the rate of R_{WGS} is tuned so it approaches 0 more slowly instead of being empirically right. This makes the model faster. This assumption is negligible for the final result. The other tuning factor does influence the system heavily, that is why this factor is set at 1. The materials available in the fuel cell for direct reforming, however, could influence the reaction rate. Therefore, the tuning factor is available for research purpose. Another notation is that the reaction rates are calculated on the leaving species. Since the change in species is calculated, this is the only possibility to get the formation of molecules in equilibrium with the feed of molecules. The reaction rates are given in table 6.2.

Tab. 6.2 | Reaction values FC unit

Type of reaction	**k** $[\frac{mol}{m^3 s}]$	**E**$_a$ $[\frac{J}{mol}]$	**Chemical equation**
Water-gas shift	$5.115 * 10^4$	$8.77 * 10^4$	$CO + H_2O \rightarrow CO_2 + H_2$
Methanol Decomposition	$2.002 * 10^6$	$9.27 * 10^4$	$CH_3OH \rightarrow CO + 2H_2$

6.3. THE GEOMETRIC MODEL

As explained earlier, the fuel cell exists out of a module of multiple cells, 140 cells each. Each cell has a schematic representation which is already given in figure 6.1. Note that the anode support is a metal porous plate that connects the fuel feed to the anode of the PEN structure. This plate however has influence on the amount of hydrogen that is actually able to reach the anode, and the amount of water (steam) it can drain back to the fuel feed. A representation of this porous metal is given in figure 6.5

The effect of the diffusive behaviour of hydrogen and water through the porous metal is a two dimensional effect. Since this model does not model two dimensional effects actively a spatial distribution of hydrogen and water is used. This is done by rewriting the local partial pressures averaged to a steady state solution given in equations 6.11 & 6.10 [57].

$$p^{inter}_{H_2} = p^0_{H_2} - \frac{R_u T_{f_j} (\tau_{holepitch} + \tau_{substrate})}{2FD_{eff,anode}} I_j \tag{6.10}$$

$$p^{inter}_{HO_2} = p^0_{HO_2} + \frac{R_u T_{f_j} (\tau_{holepitch} + \tau_{substrate})}{2FD_{eff,anode}} I_j \tag{6.11}$$

The $p^0_{species}$ is the local partial pressure in the bulk fuel, the R_u is the universal gas constant, the T_{f_j} is the local temperature of the fuel and PEN structure, the $\tau_{holeptich} \& \tau_{substrate}$ are half the distance between holes

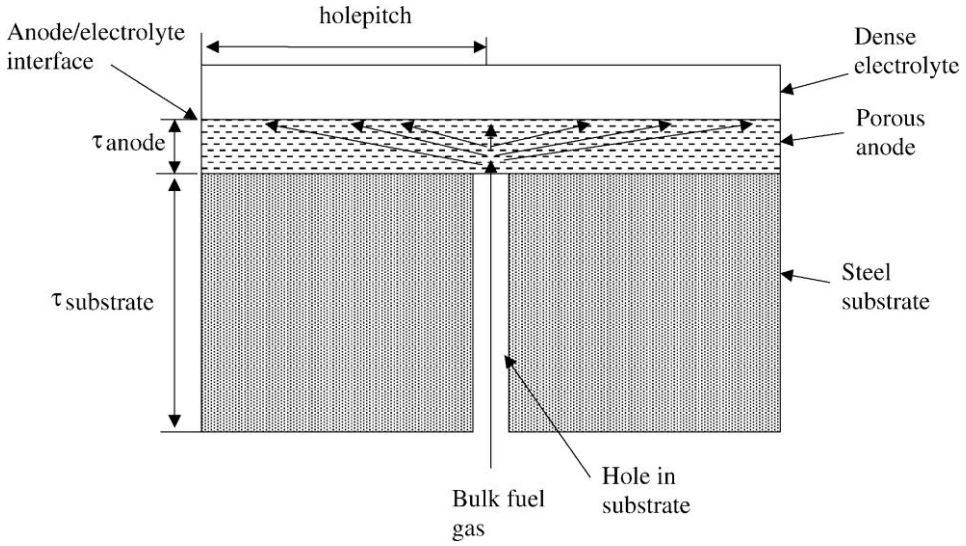

Fig. 6.5 | Schematic representation of porous metal inside the fuel cell (not to scale) [57]

and the total length of a hole from bulk fuel to the anode respectively, F is Faraday's constant and $D_{eff,anode}$ is a constant that takes the effective porosity of both the anode and the substrate, in other words, the limitations on the maximum hydrogen and steam transport from and towards the bulk fuel gas and the PEN structure.

Note that the distance $\tau_{holepitch}$ is the distance between the hole in the substrate and half the distance to the next hole. This does not only affect the local partial pressure of hydrogen, but also the partial pressure of oxygen in the PEN structure. Although this could be compensated with another spatial compensation, this is neglected since its contribution is very small. If, however, this is considered important, the equation, 6.12, would look like this. Notice how the factor n in the denominator has become 4 instead of 2 because of the amount of electrons passing, and how the length of the $\tau_{cathode}$ is way smaller than $\tau_{holepitch}$ and $\tau_{substrate}$ in the numerator.

$$p_{O_2}^{inter} = P_a - (P_a - p_{O_2}^0) \exp \frac{R_u T_{f_j}(\tau_{cathode})}{4FD_{eff,cathode}P_a} I_j \tag{6.12}$$

EFFECTIVE WIDTH

Even though it is assumed that there is a volumetric flow, which effectively runs through the entire width of the FC, there has to be compensation for the solid structure of the interconnect which is connected to the PEN structure. This is visible in the schematic representation of figure 6.1b. It is assumed that the connection is about half the width of the system, therefore an effective width is added to the system W_{eff}. Note that the channels of bulk air and bulk fuel are identical. However, the effective width could be changed in different geometries or different models, therefore it this parameter is easily changed.

METAL PROPERTIES

The solid is lumped as one material, including the PEN structure, the metal support, and the interconnect. This is easier because the specific material properties are either confidential or optimised for specific purposes. A metal supported SOFC main advantage is the coping with thermal stresses because of the absence of large ceramic or cermet parts. The exact thermal conductivity and the density have been averaged with the following equations

$$\alpha k_{nickel} + \beta k_{SS400} + \gamma k_{CGO} + \delta k_{LSCF-CGO} = 23[\frac{W}{m^2 k}]$$
$$\alpha \rho_{nickel} + \beta \rho_{SS400} + \gamma \rho_{CGO} + \delta \rho_{LSCF-CGO} = 7700[\frac{kg}{m^3}]$$

The sum of the Greek letters α, β, γ & δ are equal to 1. Note that these values can vary per configuration or optimisation, and these are very specific. For the thermal conduction holds that the higher this value is, the better it is able to lose temperature near the exit of the structure to the entrance part. This is favourable

since the the maximum temperature is capped because of the properties of the metal, but the higher the average temperature to the maximum value, the lower the ohmic resistance for example. For the density the biggest contribution can be found in the first order ODE. Namely the bigger the value of the density, the higher the amount of heat the solid can carry, due to the relation of heat capacity that is $[\frac{J}{kgK}]$. In other words, the amount of joules per kelvin a medium can carry per kilogram. The lower the density, the higher the temperature transients. This can both be desirable as disadvantageous. As a result this it could result in more extreme minimum and maximum temperatures, but is is also easier to change in operational state due to relatively fast temperature changes.

6.3.1. TABLE OF CHARACTERISTIC VALUES OF THE FC UNIT

The characteristic values used are given in table 6.3.

Tab. 6.3 | characteristic values of the FC unit from Leah et al. [57]

Parameter	value	unit	Description
J_{fC}	12	[-]	amount of discretization units
L_{fc}	0.4	$[m]$	total length of FC unit
W_{fc}	0.1	$[m]$	total width of the FC unit
$d_{channel}$	$1*10^{-3}$	$[m]$	Channel height of both bulk fuel and bulk air
$t_{interconnect}$	$1*10^{-3}$	$[m]$	thickness of interconnect
$t_{support}$	$3*10^{-4}$	$[m]$	thickness of support
t_{hole}	$1.25*10^{-4}$	$[m]$	space between holes in support
t_{anode}	$1.5*10^{-5}$	$[m]$	thickness of anode
$t_{cathode}$	$5*10^{-5}$	$[m]$	thickness of cathode
$t_{electrolyte}$	$1.5*10^{-5}$	$[m]$	thickness of electrolyte
t_{pen}	$1.38*10^{-3}$	$[m]$	Lumped thickness all layers in the PEN and the bulk fuel channel
ρ_{pen}	7700	$[\frac{kg}{m^3}]$	lumped density of all layers in the PEN and the channels
$c_{p_{pen}}$	460	$[\frac{J}{kgK}]$	lumped heat capacity of all layers in the PEN and the channels
$k_{s_{pen}}$	15.1	$[\frac{W}{mK}]$	Thermal conductivity of all layers in the PEN and the channels

6.4. THERMODYNAMIC MODEL

The thermodynamic model exists out of 2 governing first order ODEs. They determine the temperature of the air gas and the lumped fuel gas and solid. The main reason why it is assumed that the fuel gas and the solid can be lumped is that the reaction heat is assumed to take place on the surface of the solid, therefore non of the heat is directly put into the fuel gas. The only route to the fuel gas will be through heat transfer of the solid. The heat capacity of the solid differs an enormous amount compared to the fuel gas due to the fact that the heat capacity is defined proportional to $\propto \frac{1}{kg}$ or $\propto \frac{1}{mol}$ as it is defined as $\frac{J}{kgK}$. Therefore, the more weight available in a certain volume the more energy should be added to raise the medium with one Kelvin, i.e. the solid is able to store more heat than the gas. Another reason that it can be lumped is because experimental data often shows that the temperature of the fuel gas and the solid are indeed about the same and have the same transient [58]. From now it is important to mention, that when a variable is addressed with the the group category $_{fuel}$, it holds for the lumped group of fuel gas and the solid structure.

The 2 governing equations, 6.13 & 6.18, are given below

$$\frac{dT_{air}}{dt} = \frac{1}{\sum c_{p_{air}} C_{out}} \left(q_{a_{in}} - q_{a_{out}} + h_a \frac{T_{fuel} - T_{air}}{d_{channel}} - 0.5 R_{ox} \Delta H_{ox} \right) \tag{6.13}$$

This equation, 6.13, exist out of a couple of components. The first term is the product of the heat capacity and the amount of moles of each air component, i.e. 21% oxygen and 79% nitrogen. This is proportional to $\propto \frac{m^3 K}{J}$, this is used as an multiplying factor for the three components in the brackets to get a form proportional to $\propto \frac{K}{s}$.

The first term between brackets, $q_{a_{in}} - q_{a_{out}}$ is the heat flux in minus the heat flux out. This is calculated via the following equations.

$$q_{a_{in}} = \sum N_{a_{in}} \Delta H_{a_{j-1}} \tag{6.14}$$

$$q_{a_{out}} = \sum N_{a_{out}} \delta H_{a_j} \tag{6.15}$$

It should be noted that only the difference in enthalpy, ΔH_a is used, not the absolute amount of enthalpy. So the heat flux is the sum of the entalpy times the molar flow in the system. How enthalpy is determined will be further explained in section 6.4.2. To calculate the molar flow the following equations are needed

$$N_{a_{in}} = y_{a_{in}} \frac{P_a \dot{V}_{a_{in}}}{R_u T_{a_{j-1}}} \frac{1}{V_j} \tag{6.16}$$

$$N_{a_{out}} = y_{a_{out}} \frac{P_a \dot{V}_{a_{out}}}{R_u T_{a_j}} \frac{1}{V_j} \tag{6.17}$$

Note that the molar flow is proportional to $\propto \frac{mol}{m^3 s}$, so the factor $V_j \propto \frac{1}{m^3}$ is added.

The second term between brackets, $h_a \frac{T_{fuel} - T_{air}}{d_{channel}}$ is the heat transfer of the lumped fuel component to the air. Note that the heat transfer coefficient is already defined per surface area, so it is proportional to $\frac{1}{m^2}$. The heat transfer coefficient is a complex parameter that hard to capture in a single constant. In this case, however, simplifications are made. This will be further explained in subsection 6.4.2

The third and last term of equation 6.13 is a compensation term for the heat increment due to mass increment. Note that due to hydrogen oxidation, the hydrogen molecules change to water molecules. If there is no term in heat flux accounts for the change in molecules, then energy is created or destroyed due to molecule differences and there will be an increase or decrease in temperature. Therefore the difference in enthalpy gained through hydrogen oxydation is subtracted from the system.

$$\frac{dT_{fuel}}{dt} = \frac{1}{\rho_s c_{p_s} (t_{int} + t_{PEN} + d_{channel})} \big((q_{f_{in}} - q_{f_{out}})(t_{int} + t_{PEN}) - \sum \Delta_f H^{\Theta} R_{react} + k_s x_s \frac{d^2 T_{fuel}}{dt^2} + h_a (T_{air} - T_{fuel}) + (-UI_j) \tag{6.18}$$

This equation, 6.18, describes the change in temperature of the lumped unit of fuel gas and the solid structure. As for equation 6.13, a multiplication factor is added to rewrite the components proportional to $\propto \frac{K}{s}$. The factor itself is proportional to $\propto \frac{m^2 K}{J}$ and is defined by one divided by the product of the density, the heat capacity and the height of the components adding to the density that is considered. Only in the case of $d_{channel}$ it is not directly the height of the bulk gas channel. If one looks closely at the schematic representation of the FC in figure 6.1, one notices that the bulk channel, logically, is not a solid layer, but a layer with channels. Since it is assumed that the effective width of the channels are $W_{eff} = 0.5$ for both the fuel gas as the air gas, it is assumed that $d_{channel}$ is exactly equal to the height of the channel.

As for the air gas temperature, the heat flux $q_{f_{in}} - q_{f_{out}}$ is determined through the sum of the products of the molar flow and the change in enthalpy per species as shown below. More on the calculation of enthalpy in section 6.4.2

$$q_{f_{in}} = \sum N_{f_{in}} \Delta H_{f_{j-1}} \qquad q_{f_{out}} = \sum N_{f_{out}} \delta H_{f_j}$$

$$N_{f_{in}} = y_{f_{in}} \frac{P_f \dot{V}_{f_{in}}}{R_u T_{f_{j-1}}} \frac{1}{V_j} \qquad N_{f_{out}} = y_{f_{out}} \frac{P_f \dot{V}_{f_{out}}}{R_u T_{f_j}} \frac{1}{V_j}$$

The second term is the change in heat due to the formation energy released or drawn depending on the reaction. Only three reactive equilibriums are considered, methanol decomposition, water gas shift, and the hydrogen oxidation. The equations are already given in section 6.2. The formation energy however is considered to be constant, they are given in table 6.4.

Note how the endothermic reaction, like methanol decomposition, have a positive heat of formation since the reaction needs energy to happen. A exothermic reaction releases energy which is then noted as a negative

Tab. 6.4 | Total heat of formation of reactions

Type of reaction	**Chemical equation**	$\Delta_f H^{\Theta}[\frac{KJ}{mol}]$
Water-gas shift	$CO + H_2O \rightarrow CO_2 + H_2$	-41.17
Methanol Decomposition	$CH_3OH \rightarrow CO + 2H_2$	90.64
Hydrogen Oxidation	$H_2 + O^- \rightarrow H_2O$	-286.00

heat of fromation. For this reason the second term in the governing equation is denoted with a minus since releasing energy heats the system as a result.

The third term is the second order central difference derivative that represents the conductive heat of the neighbouring discretization units. Note that in the first and the last discretization unit the heat input of the unit itself and the neighbouring unit is used which result in the following equations.

$$\left.\frac{d^2T_{fuel}}{dt^2}\right|_{j=1} = \frac{T_j + T_{j+1} - 2*T_j}{L^2_{disc}} = \frac{T_{j+1} - T_j}{L^2_{disc}} \qquad \textbf{Boundary at } L_{fc} = 0 \tag{6.19}$$

$$\left.\frac{d^2T_{fuel}}{dt^2}\right|_{j=12} = \frac{T_j + T_{j-1} - 2*T_j}{L^2_{disc}} = \frac{T_{j-1} - T_j}{L^2_{disc}} \qquad \textbf{Boundary at } L_{fc} = 1 \tag{6.20}$$

The fourth term is the heat transfer between the bulk air and the lumped bulk fuel and solid. Note that again the heat transfer coefficient is proportional to $\propto \frac{1}{m^2}$, so no variable of length needs to be added.

Lastly the term UI_j is subtracted from the total heat. Note that I_j is the current density, which result in a power density that is proportional to $\propto \frac{W}{m^2} = \frac{J}{m^2 s}$. This term is added to correct for the amount of electrical energy produced by the system, therefore it cannot be added as heat. One should know that this term is smaller than the energy released per hydrogen oxidised, therefore drawing more energy will inevitably not cool the stack based on the subtraction of electrical energy produced.

6.4.1. HEAT TRANSFER OF AIR

Heat transfer between the lumped fuel gas and solid to the air gas is, in theory, rather complex. Therefore some assumptions have been made. First of all, the equation used to determine the heat transfer is the following 6.21.

$$h_a = Nu\frac{\lambda_a}{d_h} \tag{6.21}$$

h_a is the heat transfer coefficient of the bulk air to the lumped solid and fuel, Nu is the Nusselt number, λ_a is the conductive heat transfer of the bulk air and lastly the d_h is the hydraulic diameter. The hydraulic diameter is needed to relate the Reynolds number to the geometrical shape of the channels.

Although the Reynolds number is not visibly present in equation 6.21, it defines the Nusselt number. The Reynolds number Re itself however is defined as equation 6.22

$$Re = \frac{\rho u d_h}{\mu} \tag{6.22}$$

Where ρ_j is the density of the medium, u_j the flow speed, d_h the hydraulic diameter of the channel, and μ the viscosity of the medium. Now another way to look ath the determination of the Reynolds number is that the nominator states the intertial forces and the demoninator the viscous forces. The hydraulic diameter of the channel is calculated using the height and the width of the channel. In this particular case, becase the effective width of $W_{eff} = 0.5$ is assumed, the height is equal to the width of the channel. Therefore both the height and the width are noted as a.

$$d_h = \frac{4a^2}{4a} = a \tag{6.23}$$

d_h is a very small constant, the density is also very low and the flow speed is relatively low between $4-8[\frac{m}{s}]$. As a result, the flow is very laminar and the reynolds number is low. Concluding, the Nusselt number can be assumed to be constant, a value of 4 is chosen [58].

Looking back at equation 6.21, the only unknown variable remaining is the heat conduction of air. Some assumptions has been made regarding the heat conduction. First of all, air is a gas mixture of several components which has already been simplified to a two component mixture of nitrogen and oxygen. Both components in the air gas have different heat conduction values, although they do not differ that much. For example the heat conductivity of nitrogen at $600K$ is $44.0[\frac{mW}{Km}]$ mili Watt per kelvin meter, and oxygen 48.1. As a result, the simplified air has a heat conduction of 44.861. Now in the case of this FC system, the composition of the air mixture changes due to the reduction of oxygen. Lets assume an oxygen reduction 25% of the partial pressure of oxygen p_{O_2}, then the new value of $\lambda_a = 44.574$. Which is and effective change of about 0.6% in heat conductivity. For this reason an empirically determined heat conductivity of air has been used which depends on the temperature of the air gas only. The empirical values are given in table 6.5

Tab. 6.5 | Thermal conductivity of air on different temperatures from [10]

Temperature in $^\circ C$	**Thermal conductivity in** $\frac{mW}{Km}$
100	31.52
200	38.25
300	44.41
412	50.92
500	55.79
600	61.14

The increase of thermal conductivity along the temperature is about linear. Therefore the equation derived from the values given in the table 6.5 is given in equation 6.24. Note that the model uses Kelvin to describe the temperature and the empirically derived relation is in Centigrade, this is why a correction factor is subtracted from the input temperature $(T_a - 273.15)$.

$$\lambda_a = 27.427 + 0.0544(T_a - 273.15) \tag{6.24}$$

As a result the heat transfer coefficient can finally be determined shown in equation 6.25. Note that a factor $\frac{1}{1000}$ is added to go from miliwatt to Watt and a factor $\frac{1}{W_{fc}}$ to go from $\propto \frac{1}{m}$ to $\propto \frac{1}{m^2}$.

$$h_a = Nu\frac{\lambda_a}{d_h} = \left(4\frac{27.427 + 0.0544(T_a - 273.15)}{d_{channel}}\frac{1}{W_{fc}}\right)\frac{1}{1000} \qquad [\frac{W}{Km^2}] \tag{6.25}$$

6.4.2. HEAT CAPACITY AND ENTHALPY

As for the 1-D reformer model, the 1-D FC model uses the NIST chemistry Webbook also to determine the heat capacity c_p and change in enthalpy δH. For a detailed explanation, the theory behind some simplifications or assumptions is explained in detail in section 5.3.2. For now it is important to know that the equations have a form shown in table 6.6. Variables $A - F$ are the empirically derived constants from which the required thermochemistry is derived.

Tab. 6.6 | NIST Chemistry Webbook equations

Variable	**Equation**
c_p	$= A + BT_{f,a} + CT_{f,a}^2 + DT_{f,a}^3 + E/T_{f,a}^2$
$H^\circ - H^\circ_{298.15}$	$= AT_{f,a} + BT_{f,a}^2/2 + CT_{f,a}^3/3 + DT_{f,a}^4/4 - E/T_{f,a} + F - H$

This equation gives temperature in $\frac{K}{1000}$, which means that the input temperature should be divided by 1000 before entering the equation.

6.5. THE ELECTROCHEMICAL MODEL

The fourth and last model that defines the FC stack is the electrochemical model. This model is needs thorough explanation on how it works, why some choices have been made and what it does. First of all there are three governing equations that need to be satisfied at any moment shown in equations 6.26 - 6.28.

$$U_{tot} = U_{j=1,2,3...,J} \tag{6.26}$$

$$I_{tot} = \sum_{j=1}^{J} I_j \tag{6.27}$$

$$U_j = U_{cell_j} = U_{Nernst_j} - (V_{act_j} + V_{con_j} + V_{ohm_j}) \tag{6.28}$$

As explained in chapter 3, equation 6.28 is highly non-linear. The voltage in a cell depends on $U_{cell}(P_f, P_a, y_{H_2}, y_{H_2O}, y_{O_2}, T_f, I_j)$. Note that every I_j can be different (which it most likely is), but since the equation 6.27 needs to be satisfied, it could be that when the current density rises in cell $j = 1$ it has consequences on the amount of hydrogen left in cell $j = J$. Also, the higher the current density, the higher the local temperature, and this influences the local electrical resistance, at the same time this influences the mass model on the local reaction rates and the volumetric flow since it is assumed that the pressure in constant and that the ideal gas law is applied. In summary, the entire FC model could behave differently if the local current density is chosen differently.

To make sure it is clear how equation 6.28 is defined. All 4 components are elaborated on, for the theoretical explanation, please go to chapter 3. The first equation is the Nernst potential shown in equation 6.29.

$$U_{Nernst} = -\frac{\Delta G_f^0}{2F} - \frac{R_u T_f}{2F} \ln\left(\frac{p_{H_2O}^{inter}}{p_{H_2}^{inter}\sqrt{p_{O_2}^0}}\right) \tag{6.29}$$

The first term gives the Gibbs free energy divided by the amount of electrons that pass per hydrogen reacted in the process. Simply put, this value shows the amount of available energy to do external work. With the assumption that hydrogen oxidation is the main contributor to the the external work, an activity term is added to the equation depending on the universal gas constant divided by the amount of electrons passing per hydrogen reacted times faraday's constant. This term adds to the total Gibbs free energy.

The term ΔG_f^0 is derived from the following table 6.7 and put in this linear relation given in equation 6.30.

$$\Delta G_f^0 = \frac{0.0532 * T_{f_j} - 231.06}{1000} \left[\frac{J}{mol}\right] \tag{6.30}$$

Tab. 6.7 | Gibbs free energy for reaction $H_2 + \frac{1}{2}O_2 \rightarrow H_2O$ [10]

Temperature $[°C]$	$\Delta G_f^0 \left[\frac{kJ}{mol}\right]$
100	-225.2
200	-220.4
400	-210.3
600	-199.6
800	-188.6

The activation losses and the concentration losses have been thoroughly explained in chapter 3, but once

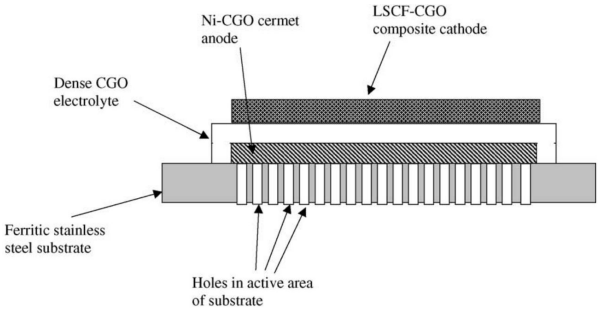

Fig. 6.6 | Schematic representation of Metal Supported PEN structure [57]

more given in equations 6.31 - 6.36.

$$V_{con} = \frac{R_u T_f}{2F} \exp\left(\frac{p^{inter}_{H_2O} p^0_{H_2}}{p^o_{H_2O} p^{inter}_{H_2}}\right) \tag{6.31}$$

$$V_{act} = V_{act_{anode}} + V_{act_{cathode}} \tag{6.32}$$

$$V_{act_{anode}} = \frac{R_u T_f}{\alpha_a F} \sinh^{-1}\left(\frac{I_j}{2I_{0,a}}\right) \tag{6.33}$$

$$I_{0,a} = \sqrt{p^{inter}_{H_2}} K_A \frac{R_u T_{f_j}}{2F} \exp\left(\frac{-E_{AA}}{R_u T_{f_j}}\right) \tag{6.34}$$

$$I_{0,a} = K_C \frac{R_u T_{f_j}}{2F} \exp\left(\frac{-E_{AC}}{R_u T_{f_j}}\right) \tag{6.35}$$

$$V_{act_{cathode}} = \frac{R_u T_f}{\alpha_c F} \sinh^{-1}\left(\frac{I_j}{2I_{0,c}}\right) \tag{6.36}$$

Lastly the ohmic resistance is defined as follows in equation 6.37.

$$V_{ohm} = \left(\frac{\tau_{anode}}{\sigma_{anode}} + \frac{\tau_{cathode}}{\sigma_{cathode}} + \frac{\tau_{electrolyte}}{\sigma_{electrolyte}} + R_{contact}\right) I_j \tag{6.37}$$

All terms have been measured separately representing the ohmic resistance in the PEN structure. The anode and cathode are given as the resistence to an electronic current flow as the electrolyte depends on the ionic conductivity. As explained earlier, the PEN structure looks as follows in figure 6.6. It is assumed that the metal supported plate does affect the resistance. The anode and cathode current collectors are assumed to be constant irrespective of the temperature assuming operating temperatures between $450-600^{\circ}C$. A $R_{contact}$ is added for the any losses between between the cathode current collector and the cathode of the stack. Lastly the ionic conductivity is estimated like shown in equation 6.38. Note that this empirically derived relation is merely dependent on the temperature of the CGO electrolyte.

$$\sigma_{electrolyte_{ionic}} = K_i \frac{\exp\left(\frac{-0.64}{8.6173*10^{-5} T_{f_j}}\right)}{T_{f_j}} \tag{6.38}$$

In table 6.8 the characteristics of the model are given.

6.5.1. CALCULATION OF ELECTRONIC LEAKAGE CURRENT DENSITY I_{leak}

In order to calculate the electronic conductivity of the CGO electrolyte the following empirical equations have been used. The relation for the electric conductivity, given in equation 6.39 [57].

$$\sigma_{electrolyte_{electric}} = 3.459 * 10^{11} \frac{\exp\left(\frac{-2.475}{8.6173*10^{-5} T_{f_j}}\right) p^{-0.25}_{O_{2local}}}{T_{f_j}} \tag{6.39}$$

In this equation the conductivity depends on both the partial pressure of the oxygen inside the electrolyte and the local temperature. A dense CGO material as an electrolyte has a negligible electric conductivity

Tab. 6.8 | Input values of electrochemical model for electrical current density calculations

Parameter	value	unit	Description
σ_{anode}	$8 * 10^4$	$[\frac{S}{m}]$	electrical conductivity anode
$\sigma_{cathode}$	$8.4 * 10^3$	$[\frac{S}{m}]$	electrical conductivity cathode
K_i	$2.706 * 10^6$	$[\frac{SK}{m}]$	pre-exponential factor for electronic conductivity
E_{AA}	$1.294 * 10^5$	$[\frac{J}{mol}]$	activation energy anode
E_{AC}	$1.309 * 10^5$	$[\frac{J}{mol}]$	activation energy cathode
K_A	$3.2 * 10^{13}$	$[\frac{S}{m\sqrt{\text{bar}}}]$	pre-exponential factor anode
K_C	$7.0 * 10^{11}$	$[\frac{S}{m^2}]$	pre-exponential factor cathode
$D_{eff_{anode}}$	$1.495 * 10^-6$	$[\frac{m^2}{s}]$	effective anode diffusivity
R_{cont}	$8.46 * 10^-6$	$[\Omega m^2]$	contact resistance

in a oxidising environment and temperatures below $450°C$. However, in a oxygen reducing environment with local partial pressures of oxygen ranging between 10^{-20} to 10^{-30} bar, it actually is able to develop an electronic conductivity depending on the temperature. The leakage current density, however, is a very complex mechanism depending on various factors like the thickness of the electrolyte, the temperature of the electrolyte, the purity of the CGO at the grain boundary of the electrolyte which reduces the ionic conductivity significantly, the oxygen partial pressure gradient across the electrolyte (which is assumed to be negligible), but the most interesting is the the current density. As shown in equation 6.39 the electric conductivity decreases if the local partial pressure of oxygen increases which it actually does in the case of a high current density. So if the the operating current density is sufficiently high, the electronic leakage current density is considered to be negligible.

To calculate the electronic leakage current density some relations have to be made. First the two following statements are assumed to be true

$$p_{O_2 local} = p^{\theta}$$
$$\sigma_{electrolyte_{ionic}} = \sigma_{electrolyte_{electric}}$$

This creates a relation to determine p^{θ}, which is the local partial pressure of oxygen. When substituted, it gives the relation to calculate the electronic leakage current density I_{leak} in equation 6.40

$$I_{leak} = \left(\frac{p^{\theta}}{\exp\left(\frac{-4R_u T_{f_j}}{F(V_{0,c} + \Delta V_{act,c})} \right)} \right)^{\frac{1}{4}} I_j \frac{\exp\left(\frac{F}{R_u T_{f_j}} - 1 \right)}{1 - \exp\left(-\frac{F}{R_u T_{f_j}} I_j \frac{\tau_{electrolyte}}{\sigma_{electrolyte}} \right)} \tag{6.40}$$

This is a derivation which needs an explanation that goes far beyond the scope of this thesis project. If, for some reason, it is considered important to know how this is derived, please see [57]. The only yet unknown variable used in equation 6.40 is the cathode potential $V_{0,c}$ which is given in equation 6.41.

$$V_{0,c} = -\frac{R_u T_{f_j}}{4F} \ln\left(p_{O_2}^{inter} \right) \tag{6.41}$$

6.5.2. NUMERICAL $U_{guesser}$

The main input of the BoP considered is the power required for an operational profile. The power is defined as $P = IV$. As shown earlier with relations 6.26 - 6.28, both the U_{tot} and I_{tot} are related to each other via equation 6.28 since $\mathbf{U_{cell}}(P_f, P_a, y_{H_2}, y_{H_2O}, y_{O_2}, T_f, \mathbf{I_j})$, which is shown again below in equation 6.42. More important is to understand that it is mathematically extremely difficult to rewrite U_{tot} as a function of I_j to I_j as a function from U_{tot}. This has to do with the hyperbolic and logarithmic relations of the current density to the over potentials shown in relations 6.31 - 6.36 .

$$U_j = U_{cell} = U_{Nernst} - (V_{act} + V_{con} + V_{ohm}) \tag{6.42}$$

In other words, the route to satisfy $U_{tot} = U_{1,2,3,...,J}$ and $I_{tot} = \sum_{j=1}^{J} I_j$ at the same time is a numerical problem, which could be done via the following diagram shown in figure 6.7. The input variables are taken from time step $t = t-1$. As a result, in highly dynamic situations, this numerical solver will be off. In the case of this model, however, the relevant timescale is in orders of 10 seconds and the dynamic behaviour, due to the limiting thermal transients in the system and the conditions the overall numerical solver 'ode45' is fixed to this is not a problem.

In the first step an initial guess is made which starts at $U_{tot}^{initial}(t=0) = 0.7$ and from then it is $U_{tot}^{initial}(t) = U_{tot}^{optimal}(t-1)$. Then, for every discretization unit $j = 1,2,3,...,J$ equation 6.42 is solved for $U_{tot}^{initial}$. For every cell, the a current density I_j is produced based on the initial operating voltage. Except for the last one, because if the initial voltage was right, then the total current drawn, calculated by multiplying the active surface A_{fc} and the total current density I_{tot} should hold. Therefore, the 'remaining' current for I_J should then give the $U_J = U_{tot}$ as the final answer. Note that this rewriting of the last step results in one less equation to solve for the solver.

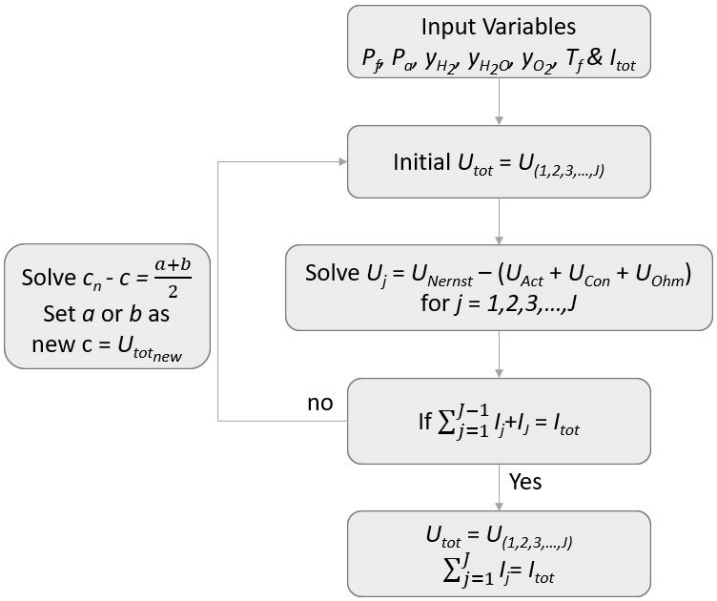

Fig. 6.7 | Iterative numerical solver for current density distribution $I_{1,2,3,...,J}$ along the FC based on [59]

If $U_J > U_{tot}$ it means that the chosen current is too low and if $U_J < U_{tot}$ its the other way around. This is solved with the bisection method. This method is very rigid and converges to the answer with an error up to 1% in about $n = 8 to 9$ iterations. The idea is that boundary values a and b slowly move towards each other. In this case $a = 0$ and $b = 1.4$. If the first iterations shows $U_J > U_{tot}$, then $\frac{a+b}{2} = 0.7$ is chosen as the new a and b stands. The new $U_{tot}^{initial}$ will be $\frac{a_1+b}{2} = 1.05$. Lets say the following iterations shows $U_J < U_{tot}$, then the new initial guess is $U_{tot}^{initial}$ determined by adopting the previous value as new upper boundary condition $b = 1.05$ and new initial guess is $U_{tot}^{initial} = \frac{a_1+b_2}{2} = 0,875$ and so on. The error can be determined by allowing the last cell to be off. In this model however, when I_{tot} is reached with an error of $\epsilon < 0.3\% I_{tot}$, the entire model is solved again simultaneously for every j so the error is effectively spread out over all discretization units. This prevents sudden numerical jumps in the last discretization unit.

7

0-DIMENSIONAL MODULES

This research is mainly about the interaction between the reformer and the MS-SOFC. The heat produced by the SOFC is redirected through the system which preheats the fuel and heats the reformer. Other components have been simplified because their physical interaction with the performance of the BoP is limited.

7.1. HEATERS

Heaters use exhaust heat to heat system. A 0-D model is used for all heaters except the heater in the reformer which is a 1-D parallel heater. The 0-D heaters shows no losses in heat conductivity, have a heat loss of 1% of the total heat passed through the system, and have no flow resistance or pressure loss. The model is shown in figure 7.1

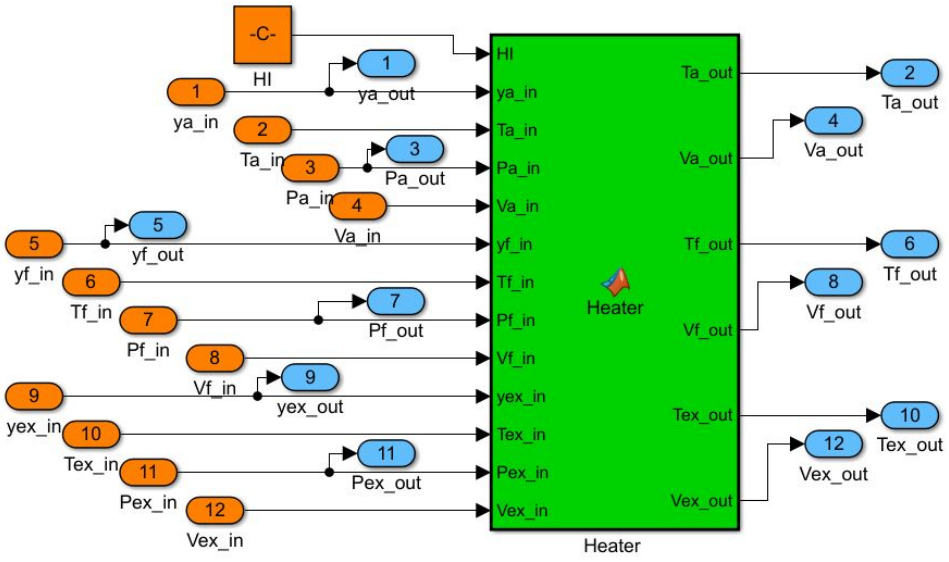

Fig. 7.1 | Schematic representation of the heater model

The colours are according to the colour convention explained in table 4.5. As one see the fuel, the air and the exhaust go into the system. Since pressure loss and flow resistance is neglected, the pressure is no output of the system. y_x is the molar concentration of the species, T_x the temperature, P the pressure and V the volumetric flowrate. Inside the system the heat is transfered by substracting the heat from one the exhaust gasses and adding it to the fuel and air gasses. The volumetric flowrate is recalculated with respect to the ideal gas law.

7.2. BURNER

Before the burner module, the anode off gas and cathode off gas are mixed together with ambient air. The latter is 0 if the amount of air supplied to the system contains enough oxygen to burn all molecules. It is assumed that all methanol, hydrogen and carbon monoxide molecules are burned in the burner module. It is assumed that methanol is reformed via methanol decomposition to hydrogen and carbon monoxide first and then all hydrogen and carbon monoxide is burned with the remain oxygen. The amount of energy released corresponds to the Low Heating Value (LHV) of that particular molecule. The change in enthalpy is given in table 7.1.

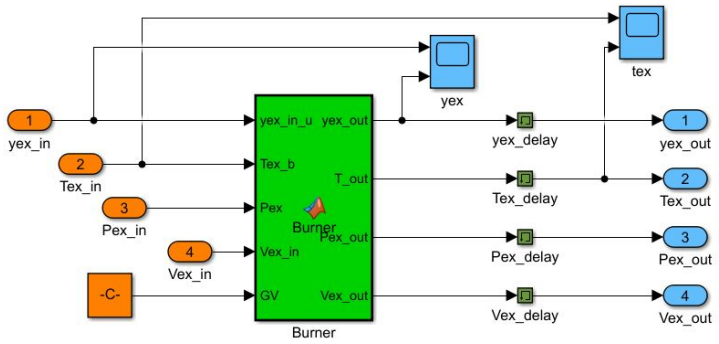

Fig. 7.2 | Schematic representation of the burner model

Figure 7.2 gives a schematic representation of the burner model. y_{ex} is the molar concentration of the exhaust, T_{ex} the temperature, P_{ex} the pressure and V_{ex} the volumetric flowrate. Note that a delay is added to the system. This has two reasons. First the system needs an initial condition of the exhaust gas before actual exhaust gas is produced by the system. The heater in the reformer and the pre-heaters for the FC unit do not work if there is no exhaust gas. The second reason is that the initial conditions for the system are predefined. Especially in the 1-D reformer the spatial exhaust temperature initial condition changes per test to minimise numerical difficulties. Therefore the burner exhaust is delayed to make sure the reformer initial condition is not overwritten. This results in less accurate dynamic results, however, this is at the scale of milliseconds. Steady state solutions do not change as a result of this delay.

Tab. 7.1 | Change in enthalpy for burner reactions $\Delta H[\frac{kJ}{mol}]$

Molecule	Change in enthalpy $\Delta H[\frac{kJ}{mol}]$
Methanol	99.47
Hydrogen	-241.83
Carbon monoxide	-282.99

7.3. PIPES AND CONNECTIONS

The pipes between the system have no dimensions and a friction loss of 0.2%. The size of the pipes can be determined after the model testing. The system itself looks like 7.3. The y_x is the molar concentration of the species, T_x the temperature, P the pressure and V the volumetric flowrate. This particular pipe is the connection between the pre-heater and the reformer unit. Therefore the subscribtion $_f = _{fuel}$ is added.

7.4. FUEL INPUT WITH PUMPS AND TURBINES

The tanks are not modelled. The pumps and turbines 'generate mass' with a volumetric flow rate. The main reason why is because the tanks hardly adds to the dynamic behaviour of the system. Besides, the model is build to evaluate the system based on its operational profile, so the tank sizes are yet unknown. It is assumed that the pump and turbine operations do not change during the run regarding, for example, pressure differences from a tank.

Ambient air is assumed to be 25°C if nothing says differently. Air is also assumed to be of a consistent composure as shown in table 7.2. The main reason is that the only reacting species is oxygen. The real value of oxygen is 0.054% less then the assumed amount. The air feed is usually determined by the heat it needs

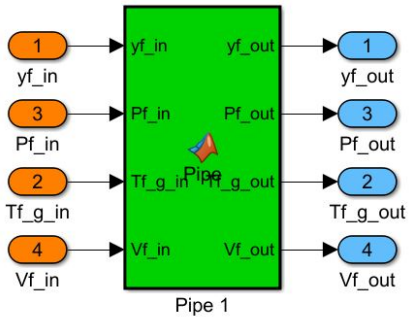

Fig. 7.3 | Schematic representation of the pipe model

to withdraw rather than the amount of oxygen it supplies, therefore this very small surplus is negligible. The species other than nitrogen and oxygen make up about 1% of the species. The reason why these have been neglected is that these species add to the enthalpy and heat capacity calculations only for heat transfer. The heat capacity of argon is about half the heat capacity of nitrogen, which would imply that the heat transfer rate is about +0.5%. On the other hand, the gain on neglecting other minor species is that fewer calculations have to be made and smaller species vectors run through the system.

Tab. 7.2 | Air composition in species

Species	**Reality**	**Model**
Nitrogen	78.08%	79%
Oxygen	20.946%	21%
Argon	0.9340%	-
Minor species	0.04338%	-

Methanol and water are also assumed to be $25°C$ if nothing says differently. Only in the case of water this assumption could have a noticeable effect compared between a real life system and this modelled system. The water is mainly extracted from the exhaust gasses in the water recovery system as shown in fig 8.12. The recovery system should cool the gasses down to a level where at least water has a liquid phase, but it will most likely not cool down up to ambient temperatures. The phase change is the most important characteristic in order to use a pump instead of a turbine. In reality, less heat is added to the mixture for methanol and water, so the system is considered conservative on this part.

8

RESULTS

In this chapter the results of the reformer, the fuel cell and the entire BoP will be analysed. Due to the dynamic behaviour of the 1-D components and the varying operational requirements, multiple 'optimal' designs are possible. Therefore, the emphasis of this research is on reviewing the operating range of the components and how they can be used best.

8.1. REFORMER

The reformer unit is already quite a complex unit to optimise, even though its purpose is rather straight forward. Since the reformer is part of the BoP, it is taken out for this specific part of the results. However, multiple runs have been made with a total current density drawn of $I_{total} = 2500 A/m^2$ and a voltage of $V_{system} = 0.68$ which resulted in a exhaust gas temperature of $T_{exhaust} = 1400$ after the heat was extracted to preheat the fuel gasses in between the reformer and the FC. Note that different fuel feeds for the reformer unit results in different FC current densities. Therefore it is not possible to rate the performance of the reformer itself only.

In every test case, the fuel feed will only exist out of water and methanol. Therefore, only the amount of methanol into the system is given, which then could easily be recalculated to the total amount with the following equation $y_{H_2O} = 1 - y_{Me}$. The mixture ranges from $y_{Me} = 0.4 - 0.6[\frac{mol}{mol}]$ The mass flow through the system is given in $\dot{m}_f$ ranging from $0.1 - 0.5[\frac{m}{s}]$. Note that this is the mass flow going into the system. Because the ideal gas law is assumed, the mass flow rises significantly due to a rise in temperature and in atoms. Methanol steam reforming is a phenomena that goes from two atoms to 4, so in essence doubling the mass flow rate if everything would react at equal feed. Due to the nature of the reformer unit, it is not possible to assume that the entire reformer unit has a specific targeted temperature. Therefore the system is targets various temperatures ranging from $T_{ref} = 558.15 - 598.15[K]$ in steps of 10 at the end of the reformer. This is $T_{ref} = 285 - 325[^\circ C]$ in celcius. Note that the entering temperature of the reformer unit is put on $T_{fuel_{enter}} = 550.15[K]$, which is $T_{fuel_{enter}} = 277[^\circ C]$.

The chosen parameters could be different for an optimal performance of the reformer in the BoP. However, this section is about the characteristics of the reformer and how the reformer behaves under different circumstances. Therefore this chapter is specifically for reviewing the reformers behaviour. For all cases in this section 8.1, the reformer model is considered as a stand alone.

8.1.1. REFORMING CAPABILITIES

In figure 8.1 two graphs are depicted. The left figure, 8.1a, shows the change in methanol along the non-dimensional length of the reformer. Note that multiple mass flows are depicted. One sees that when the mass flow rises, the amount of converted methanol decreases. The figure on the right, 8.1b, has the same mass flow rates and over the same non-dimensional length, but here the change in temperature is given. The mass flow rate is descending in figure 8.1b instead of ascending as in figure 8.1a.

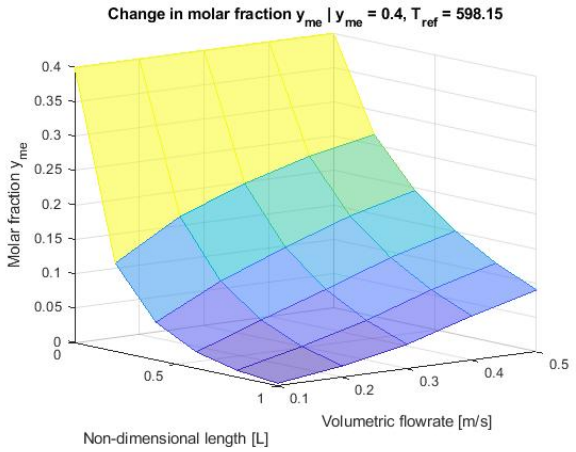

(a) Change in methanol molar fraction along the reformer

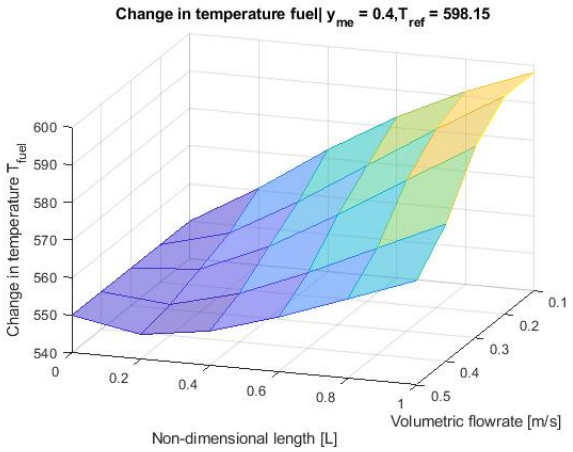

(b) Change in fuel temperature along the reformer

Fig. 8.1 | Varying the mass flow rate at a temperature of $T_{goal} = 598.15[K]$ and $y_{Me} = 0.4$

LOWER BOUND OF METHANOL REFORMED

There are several very remarkable outcomes to the testing of the reformer. The first interesting outcome is that the amount of methanol reformed. It shows that when the mass flow rate is down to $\dot{m}_{fuel} = 0.1\frac{m}{s}$, the reformer is able to reform nearly all the methanol to hydrogen gas with a methanol to water ratio of 0.4 to 0.6. The actual amount of methanol remaining in the system is $y_{Me} = 0.00414$, which is about negligible. This gives the first physical boundary of the system. It means that when the temperature is $T_{fuel} = 598.15[K]$ or $325[^{\circ}C]$ and the flow rate $\dot{m}_{fuel} = 0.1\frac{m}{s}$, all the methanol can be reformed. However, it should be noted that the system already reduced the amount of methanol to 1% at 75% of the length of the reformer unit. However, when the different amount of fuel mixtures are tried like shown in figure 8.2. In figure 8.2a, where the input flow is an equal devided mixture of methanol and water, the system reaches a methanol molar fraction of $y_{Me} = 0.0285$ at $\dot{m}_{fuel} = 0.1\frac{m}{s}$ and $T_{fuel} = 598.15[K]$ or $325[^{\circ}C]$. In the other case shown in figure 8.2b, the remaining methanol is $y_{Me} = 0.1056$ at $\dot{m}_{fuel} = 0.1\frac{m}{s}$ and $T_{fuel} = 598.15[K]$ or $325[^{\circ}C]$. In this particular case however, the amount of water left in the system is $y_{H_2O} = 0.0046$. This does not mean that the system is unable to reform methanol, since methanol decomposition is still able to take place, but it shows that at this temperature the system heavily relies on the presence of water.

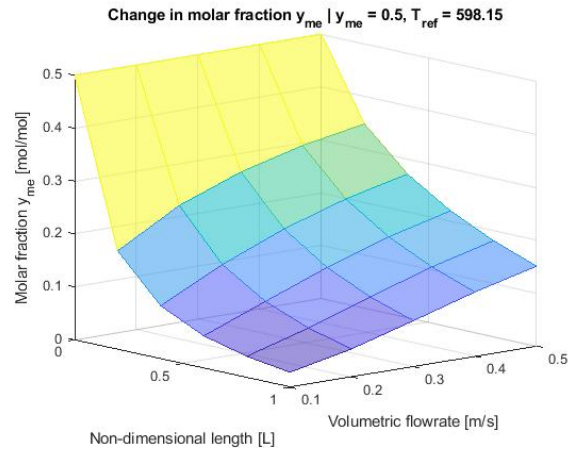

(a) Change in methanol molar fraction along the reformer at $y_{Me} = 0.5$

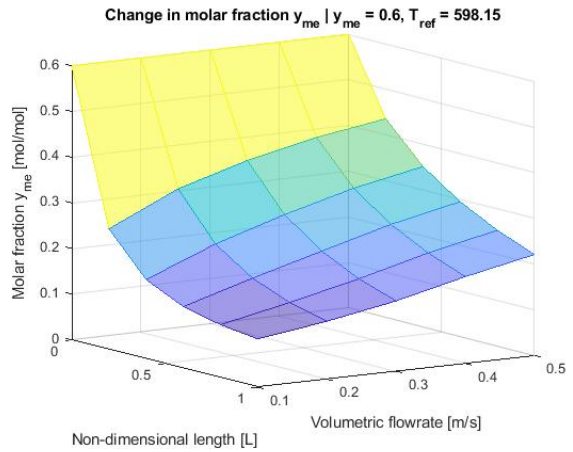

(b) Change in methanol molar fraction along the reformer at $y_{Me} = 0.6$

Fig. 8.2 | Varying the mass flow rate at a temperature of $T_{goal} = 598.15[K]$ and $y_{Me} = 0.6$

UPPER BOUND OF METHANOL REFORMED

Reviewing the upper bound of the system, shown in figure 8.1, it shows that even though the system is programmed to receive enough heat to make sure that the leaving temperature of the fuel gas is $T_{fuel} = 598.15[K]$ or $325[^{\circ}C]$, the system is not able to make it. The mass flow is too high to actually heat up the fuel gas to the required temperature. Note that in figure 8.1b, the temperature even drops slightly. Although the system is still heating up, the requirement of a leaving temperature of $T_{fuel} = 598.15[K]$ is not met. The leaving temperature however is $T_{fuel} = 567.7[K]$ or $294.6[^{\circ}C]$. Keep in mind that this result could still be the preferred configuration for the BoP. If it is decided that the FC system could receive up to $y_{Me} \leqslant 0.10$ without noticeable drop of performance, it could significantly reduce the physical size of the BoP. Note that in figure 8.2a, the amount of methanol remaining is $y_{Me} = 0.151$, which may be more than in the case of the feed of $y_{Me} = 0.4$, but the amount of hydrogen present is higher.

Comparing the results in figure 8.3, it seems that the outcomes are similar, but they are not. The left figure, 8.3a, shows a feed with $y_{Me} = 0.4$ while the right figure, 8.3b, shows a feed of $y_{Me} = 0.6$. The model shows that actually the configuration with $y_{Me} = 0.4$ yields more hydrogen and reformers more methanol then the $y_{Me} = 0.6$ feed. On first sight this is actually strange since the heat capacity of methanol is lower which results in that it is easier to heat up methanol. However, as a result, the higher temperature directly yields in a higher mass flow as the ideal gas law is applied, this results in a lower residence time in the reformer system due to a higher mass flow. All in all, the outcomes of the system are about the same and not too much emphasis should be laid upon the minor differences since they do not considerably influence the system in the grand scheme of things.

Another interesting remark is that in the case of figure 8.3b, is that the amount of potential hydrogen present in the system is higher then in the case of figure 8.3a. This makes, arguably, the system with a mixture of $y_{Me} = 0.6$ preferable since it will result in a higher yield throughout the FC system which could results in a higher current density. If that is the case however, will be discussed in section 8.2.

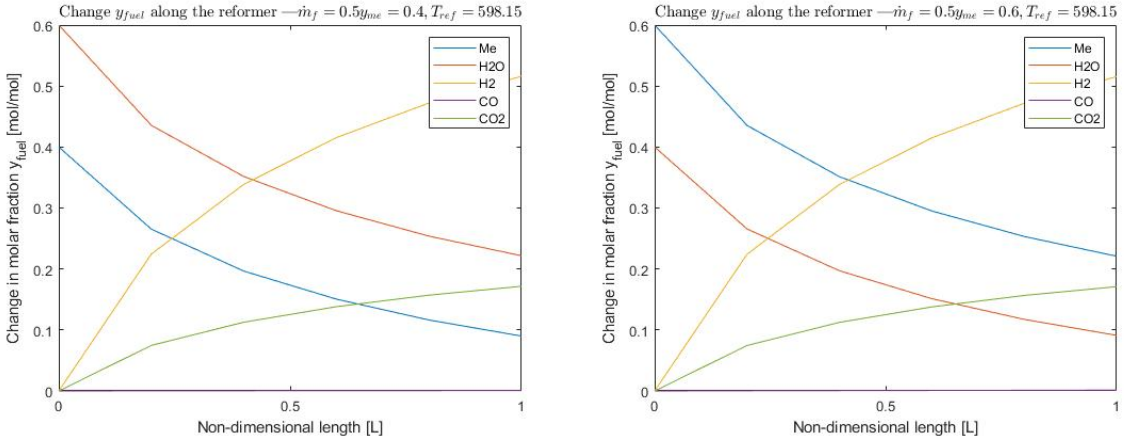

(a) Change in methanol molar fraction along the reformer at $y_{Me} = 0.4$

(b) Change in methanol molar fraction along the reformer at $y_{Me} = 0.6$

Fig. 8.3 | The change in molar fraction for different fuel mixtures at $\dot{m}_f = 0.5$ and $T_{ref} = 598.15$

8.1.2. EXHAUST GAS HEATING LIMITATIONS

The exhaust heat used is fixed on $T_{exhaust} = 1400$ since the reformer is considered a stand alone in this part of the results. However, one should know that this value actually changes heavily throughout the system. Especially when the fuel cell system is optimised properly, there is not that much hydrogen, carbon monoxide or methanol left to burn, which will result in a lower exhaust temperature. However, the actual volumetric rate in which the exhaust gas is flowing through the system is limited at lower volumetric rates of the fuel gas, which means that the upper bound of the exhaust heat is not met at lower fuel gas volumetric rates.

EXHAUST ON VARYING OUTPUT TEMPERATURE $T_{ref} = 558.15 - 598.15$

In figure 8.4, the temperature of the fuel gas is shown in figure 8.4a and the temperature of the exhaust heat is shown in figure 8.5b. In this particular case, the inlet mass flow rate is kept constant at $\dot{m}_f = 0.3$ and the fuel mixture is set on $y_{Me} = 0.5$. The varying variable T_{ref} is the targeted temperature of the fuel gas at the end of the reformer at $T_{fuel} = 558.15 - 598.15$ in steps of 10. The first thing that is noticable is that only the cases of $T_{fuel} = 558.15 - 578.15$ reach their targeted temperature, $T_{fuel} = 588.15$ is a couple of Kelvin off, while $T_{fuel} = 598.15$ is not met at all. However, the amount of exhaust gas that is put through the system differs per case. This is given in table 8.1.

Tab. 8.1 | The amount of exhaust flow passed through the reformer system.

Targeted temperature [K]	Throttle opening
558.15	0.5069
568.15	0.6377
578.15	0.8225
588.15	1.000
598.15	1.000

Lowering or the Throttle value means that the volumetric flow decreases which effectively decreases the amount of exhaust gas that flow through the system. The result of a lower mass flow rate results in that the exhaust gas residence time increases which results in that the fuel gas itself is able to release more heat. This is phenomena is clearly visable in figure 8.5b. Note how the increasing targeted temperature results in a lower leaving temperature of the exhaust gas while it expelled more heat to the system as the temperature of the fuel gas, despite having a higher volumetric rate also, is higher. Especially the case of $T_{ref} = 598.15$ shows the physical limitation of the reformer unit to receive heat from the exhaust gas. In the current chosen design of the reformer unit, it is unable to draw more heat.

Another interesting result is visible in the case of $T_{ref} = 558.15$ in figure 8.4a. Although the system requires a leaving temperature of $T_{ref} = 558.15$, it would be preferable if the entire system would operate on that temperature. In this, case the methanol decomposition rate will rise significantly with higher temperatures, due to its endothermic nature, resulting in higher conversion rates. However, the design of parallel flowing exhaust gas heating the system is unable to succeed in maintaining a constant temperature. This shows that the 1-D modelling of the reformer unit is a necessary to acquire realistic reforming results.

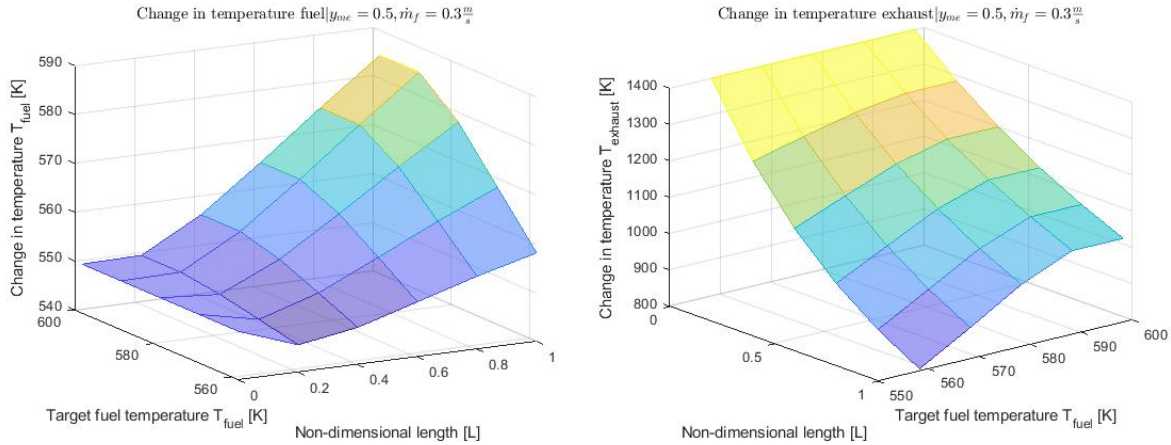

(a) Change in methanol molar fraction along the reformer at $y_{Me} = 0.4$ **(b)** Change in methanol molar fraction along the reformer at $y_{Me} = 0.6$

Fig. 8.4 | The change in targeted fuel temperature at the end of reformer for constant $\dot{m}_f = 0.3$ and $y_{Me} = 0.5$

8.1.3. OUTPUT FLOW RATES

First of al, the volumetric flow rate is the amount of fuel gas and exhaust gas that goes through the system per second measured in volume. In the left figure 8.5a, the fuel gas flow rate is shown. It is measured along the non-dimensional axis L at different target temperatures. In the right figure, 8.5b, the exhaust volumetric flow

rate is given. Note that the right figure is twisted and the axes are different.

The first noticeable result is shown in the left figure 8.5a. Note how the rise in flow rate is the steepest in the first part of the reformer, while in figure 8.4a it was shown that the temperature hardly rises or even slightly decreases. This has to do with the conversion of methanol into hydrogen and carbon monoxide. Due to the ideal gas law, a change in the amount of molecules at constant temperature and constant pressure results in a change in volumetric flow rate. As the fuel gas flows further into the reformer, it is shown that for the case of $T_{ref} = 558.15$ the volumetric flow rate is indeed less than the volumetric flow rate at $T_{ref} = 598.15$. In the latter case the amount of methanol remaining is $y_{Me} = 0.0867$ where the first named has $y_{Me} = 0.1227$ remaining. The flow rates are $\dot{V}_f = 0.0683$ and $\dot{V}_f = 0.0614$ respectively.

$$y_{result} = \frac{y_{Me_{in}} - \left(y_{Me_{T_{ref}=598.15}} - y_{Me_{T_{ref}=558.15}}\right)}{y_{Me_{total}}} = \frac{0.5 - (0.1227 - 0.0867)}{0.5} * 100\% = 92.80\%$$

$$\dot{V}_{result} = \frac{\dot{V}_{in} - \left(\dot{V}_{T_{ref}=598.15} - \dot{V}_{T_{ref}=558.15}\right)}{\dot{V}_{in}} = \frac{0.0378 - (0.0683 - 0.0614)}{0.0378} * 100\% = 81.75\%$$

As a result, the difference between what went in to what goes out is more than twice as large in the volumetric flow rate as compared to the molar fraction. If it would be twice as large, then the only addition to the system would be the change in molecules. Since all carbon monoxide is converted, it means that water and methanol converted into three hydrogen and one carbon dioxide, which effectively doubles the amount of molecules present. Now looking back at the difference in flow rates, it is concluded that the difference between the lower temperature and the higher temperature case must be because of a higher temperature resulting in a higher flow rate. This is completely expected since the ideal gas law was applied.

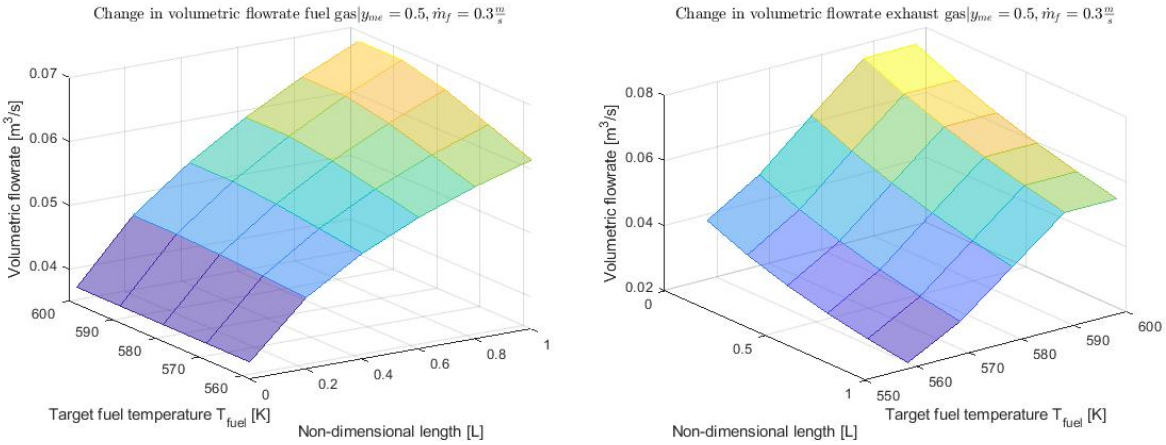

(a) Change in volumetric flow rate of fuel gas varying T_{ref}

(b) Change in volumetric flow rate of fuel gas varying T_{ref}

Fig. 8.5 | The change in volumetric flow rates of both gasses varying the targeted temperature T_{ref} from 558.15 – 598.15 at constant $\dot{m}_f = 0.3$ and $y_{Me} = 0.5$

EXHAUST FLOW RATE AND THROTTLE INTERACTION

In figure 8.5b one sees different starting values at the non-dimensional length $L = 0$. This has to do with the throttle as shown in table 8.1. Note that at the maximum opening of the throttle, the amount of exhaust gas that enters the system is slightly higher in flow rate then the fuel gas. This is unexpected since the burner even adds mass to the system due to the cathode air. The reason that this system is chosen like this is because a physical representation of a tubular reformer unit is chosen in this particular case. Therefore the reformer is not able to take more exhaust gasses than this. However, if the reformer would be designed for this particular case, one should note that there still is untouched valuable exhaust heat left. The decrease in the exhaust gas flow rate is a result of the decrease of the temperature of the gasses. Note that in figure 8.5b the exhaust gas temperature is reduced due to the heat that it expels towards the reformer.

8.1.4. TEMPERATURE IN SOLID STRUCTURE OF THE REFORMER

The last result is the change in temperature of the solid structure along the non-dimensional axis of the structure. Note how this particular figure has 5 data points only along the non-dimensional axis where all other figures in this section 8.1 have 6 datapoints. This is due to the fact that there is no initial feed of heat to the solid structure. The solid structure is just a result of the exhaust gasses heating it and the fuel gasses cooling it. This is also the reason why there are different temperatures at the entrance of the solid structure.

Looking back at the previous figures, it is clear that the reformer has a difficulty heating the fuel gas to the targeted temperature for higher mass flow rates. Figure 8.6 shows how the solid is heated over the different massflows along the length. For the lowest mass flow rate at $\dot{m}_f = 0.1$, it is actually noticeable that the incoming heat is able to heat the entrance of the system and keeping a rather constant temperature along the reformer unit itself. Note that the decreasing exhaust gas temperature and the increasing fuel gas temperature apparently keep the structure in an equilibrium. The structure itself however, is also able to draw or give heat to the adjacent sections of solid structure. For higher mass flow rates, up to $\dot{m}_f = 0.3$, the targeted heat values of $T_{ref} = 598.15$ is reached is still reached, but the solid structure is nearly 100 degrees higher to acquire the desired fuel gas temperature. For higher mass flow rates, $\dot{m}_f \geqslant 0.4$, the amount of heat that is drawn from the exhaust heat is not enough to heat the solid. The solid is even cooler at these higher rates due to the cooling effect of the fuel gas which comes at an entering temperature of $T_{fuel_{entering}} = 550[K]$. Together with the endothermic reactions that take place, the solid is not able to keep up the heat.

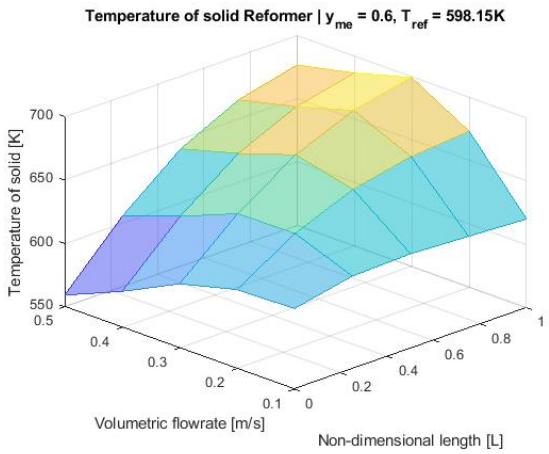

Fig. 8.6 | The change in temperature of the solid structure for various mass flow rates at constant targeted temperature $T_{ref} = 598.15$ and $y_{Me} = 0.6$.

8.2. FUEL CELL

The FC model has enormous amounts of variables that define its performance. To make sure the characteristics of the FC unit are shown properly, the results are bound to several basic input components. To do so, the FC is analysed as a stand alone. All results come from steady state solutions with the pre-defined fuel flow, fuel temperature, fuel molar concentrations as the same for air. The required current density is another main input from the model. The output voltage and corresponding power output is calculated by the model.

There are multiple phenomena that must be captured before the entire BoP can be analysed. For the FC however, most of these phenomena actually influence each other, so it is rather difficult up to impossible to keep all input values constant and vary one single variable while gaining insightful outputs. For example, when the fuel and air feed, temperature, and composition are kept constant, but the current density varies, then there will be too much fuel inside the system at lower current densities. However, when one tries to capture the feed on a constant amount of hydrogen used, for example a fuel utilisation of $H_{2_{consumed}} = 70\%$, then the air feed has to differ to keep make sure that the temperature output does not exceed $T_{solid} \leqslant 873.15[K]$ or $\leqslant 600[^\circ C]$. This influences the behaviour along the length of the FC unit, which can only be managed by varying other parameters also. Nevertheless, all these relations and interactions actually are the defining characteristics of the FC. Therefore, interactions like these are analysed in this

section.
An important note to the reader, which is explained in previous chapters also; there are two temperatures, the temperature of the air T_{air} and the temperature of the fuel and all cell components lumped referred to as T_{solid} or T_{fuel}. However, along the FC cell $T_{solid} = T_{fuel}$ for $j = 1,2,3,...,12$, but for $j = 0$, which is the initial condition, $T_{solid} \neq T_{fuel}$. Here $T_{fuel} = T_{fuel_{enter}}$ which is the temperature of the fuel that enters the system coming from the pre-heater. For all cases in this section 8.2, the FC model is considered as the stand alone unit.

8.2.1. COMPARING PERFORMANCE FOR DIFFERENT FUEL FEEDS

In figure 8.7 two experiments are shown. These are the characteristics of the FC performing at steady state. The local current densities are spatially distributed along the non-deminsional length. The two experiments are executed under different fuel feeds. Before analysing these results, some understanding is needed. For every case, a tailored feed has been determined.

FEED AND TEMPERATURE OPTIMISATION

Since it is desired to use an FC in its most optimal point, it was decided to run the FC with the most optimal feed. This is determined by running the model in steady state situations and slowly decreasing the fuel feed. At a certain moment, it was found that the concentration losses were so dominant at the exit of the FC, that the system 'crashed'. The main reason for the high concentration losses is that due to the metal support, it is slightly more difficult to actually access the PEN structure. This is explained in section 6.5. The reduced spatial partial pressure of hydrogen and the increased spatial partial pressure of water due to holes in the metal support cause the concentration losses to rise.

Table 8.2 shows the amount of effective hydrogen is used. These values are calculated shown in equation 8.1. It must be noted that the molar fraction of methanol and carbon monoxide at the end of the FC unit are $y_{Me_{j=12}}, y_{CO_{j=12}} \leqslant 0.0002$ in all cases, so they can be neglected. Therefore it is save to assume all methanol and carbon monoxide reacted to hydrogen, and thus the remaining hydrogen is the total amount of remaining fuel. Thus equation 8.1 gives the effective amount of hydrogen available. Note that the molar mass of methanol is multiplied by a factor 3. This is since a complete methanol steam reforming reaction yields 3 hydrogen atoms for one methanol atom. Besides, the discretization unit is noted with $j = 0$, this means that it is the initial value, and not after the first discretization unit.

Tab. 8.2 | The amount of hydrogen used after passing $j = J = 12$ effectively

$I_{total}[A/m^2]$	η_{H_2} for $y_{Me} = 0.1$	η_{H_2} for $y_{Me} = 0.3$
2100	0.7552	0.6965
2300	0.7197	0.6623
2500	0.6497	0.6536
2700	0.6406	0.5866
2900	0.6330	0.6104

$$\eta_{H_2} = \frac{\frac{\dot{V}_{fuel_{j=0}} * P_{fuel}}{R_u T_{fuel_{j=0}}} \left(3y_{Me_{j=0}} + y_{H_2 j=0} + y_{CO_{j=0}}\right) - \frac{\dot{V}_{fuel_{j=12}} * P_{fuel}}{R_u T_{fuel_{j=12}}} \left(3y_{Me_{j=12}} + y_{H_2 j=12} + y_{CO_{j=12}}\right)}{\frac{\dot{V}_{fuel_{j=0}} * P_{fuel}}{R_u T_{fuel_{j=0}}} \left(3y_{Me_{j=0}} + y_{H_2 j=0} + y_{CO_{j=0}}\right)} \tag{8.1}$$

Note that the feed is only addressed with the amount of methanol fed to the system, i.e. $y_{Me} = 0.1$ or $y_{Me} = 0.3$. However a small calculation is need to actually know how much methanol is fed to the system. To keep matters simple, for all test results of the FC, unless told differently, the initial feed for the reformer unit is an equal split of water and methanol, thus $y_{Me} = 0.5$ and $y_{H_2O} = 0.5$. Now when 80% of all methanol is reformed, the remaining methanol and water are $y_{Me} = 0.1$ and $y_{H_2O} = 0.1$. However, this is not true since the amount of hydrogen produced is 3 times higher. The actual feed is given in table 8.3. This table shows the feed input how it is denoted in the model, and then how it is normalised to a molar fraction. The main reason the feeds are written in the non-normalised vectors is because it is easier to observe how the feed was

reformed by the reformer.

Tab. 8.3 | Normalised feeds for the FC for both test cases

Species [-]	Fuel feed of $y_{Me} = 0.1$		Fuel feed of $y_{Me} = 0.3$	
	Feed input $[\frac{mol}{mol}]$	normalised $[\frac{mol}{mol}]$	Feed input $[\frac{mol}{mol}]$	normalised $[\frac{mol}{mol}]$
Me	0.1	0.0556	0.3	0.214
H_2O	0.1	0.0556	0.3	0.214
H_2	1.2	0.6667	0.6	0.429
CO	0.0	0.0	0.0	0.0
CO_2	0.4	0.2222	0.2	0.143

Going back to the results shown in table 8.2, it shows that the effective hydrogen used in the system decreases when the current density increases. This is effect is fully tracked back to the limiting concentration losses of the system measured by decreasing the fuel feed flow. This is a result of higher current densities, the spatial partial pressure of hydrogen is too low in the metal support and too high for water. As an effect, it shows that even more hydrogen is needed in the system to make sure the local hydrogen partial pressure is high enough.

The effective amount of hydrogen entering the system for $y_{Me} = 0.1$ is actually lower than for $y_{Me} = 0.3$ for the same volumetric flow rate due to the fact that 1 molecule of methanol carries 3 potential hydrogen molecules. For this reason alone it is explained why the volumetric flow of fuel $\dot{V}_{fuel_{j=0}}$ for the case of $y_{Me} = 0.1$ is higher then $y_{Me} = 0.3$ which is observed in table 8.3. Note how the airflow in the case of $y_{Me} = 0.1$ is also slightly higher then in the case of $y_{Me} = 0.3$. This is because the stack needs slightly more cooling because of the absence of the endothermic reactions of methanol.Because the volumetric flow rate of fuel is so much lower for the case of $y_{Me} = 0.3$ compared to $y_{Me} = 0.1$, the factor is higher. However, the volumetric flow rate will increase in the case of $y_{Me} = 0.3$ and will become the same as $y_{Me} = 0.1$.

Table 8.4 shows the fuel feeds in volumetric flow rate for both $y_{Me} = 0.1$ and $y_{Me} = 0.3$. The factor is the fuel flow proportional to the air flow. Note that for a higher methanol feed, $y_{Me} = 0.3$, the air flow rate factor is bigger. This is expected since one methanol carries more hydrogen, which is reformed internally. Since the temperature stays somewhat the same compared to the fuel feed of $y_{Me} = 0.1$, the volumetric fuel flow will rise due to an increase in molar fraction.

Tab. 8.4 | Volumetric flow $[\frac{m^3}{s}]$ rate of the fuel feeds $[\frac{mol}{mol}]$ per current density $[\frac{A}{m^2}]$

$I_{total}[\frac{A}{m^2}]$	Fuel feed of $y_{Me} = 0.1$			Fuel feed of $y_{Me} = 0.3$		
	$\dot{V}_{fuel_{j=0}}[\frac{m^3}{s}]$	$\dot{V}_{air_{j=0}}[\frac{m^3}{s}]$	factor [-]	$\dot{V}_{fuel_{j=0}}[\frac{m^3}{s}]$	$\dot{V}_{air_{j=0}}[\frac{m^3}{s}]$	factor [-]
2100	4.20E-05	8.82E-05	2.1	3.50E-05	8.75E-05	2.5
2300	4.80E-05	1.01E-04	2.1	4.00E-05	9.60E-05	2.4
2500	5.70E-05	1.14E-04	2.0	4.40E-05	1.06E-04	2.4
2700	6.20E-05	1.18E-04	1.9	5.20E-05	1.14E-04	2.2
2900	6.80E-05	1.29E-04	1.9	5.40E-05	1.22E-04	2.25

8.2.2. COMPARING CURRENT DENSITIES $I_{total}[\frac{A}{m^2}]$

This section analyses the local current densities spatially distributed along 12 discretization units of two experiments that differ in fuel feed. The feeds are shown in table 8.2 - 8.4. The main difference in both feeds is that in the case of $y_{Me} = 0.1$, 80% of the methanol is reformed to hydrogen. The feed of $y_{Me} = 0.3$ only 40% of the methanol is reformed to hydrogen. All experiments have a fuel feed temperature of $T_{fuel_{enter}} = 773.15[K]$ and an exiting temperature of $T_{fuel_{exit}} \leqslant 873.15[K]$. The entering air temperature is $T_{air_{enter}} = 743.15[K]$. A range of current densities is tested from $I_{total} = 2100, 2300, ..., 2900$ jumping $200\frac{A}{m^2}$ per experiment. A total of 10 experiments have been performed, 5 for each fuel feed. Every result shows a single cell performance, the cell itself is defined in chapter 3.3.

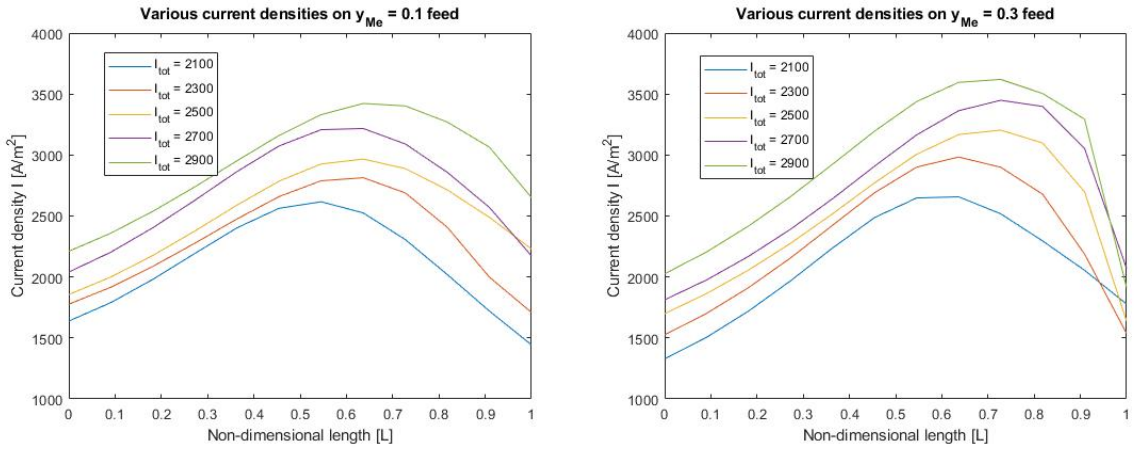

(a) Current density with $y_{Me} = 0.1$ feed

(b) Current density with $y_{Me} = 0.3$ feed

Fig. 8.7 | Steady state spatial distribution of various current densities

Before analysing the results, it must be noted that the optimisation of the correct volumetric flow rates for the fuel feed and air feed to increase the fuel utilisation on hydrogen used η_{H_2} has been done manually. As a consequence, the results are not exactly the optimal outcome. The jumps in volumetric flow rate were of the magnitude of about $4-5\%$ of the previous value. However, since multiple experiments per fuel feed have been made, clear trends show up. These trends will be looked upon closely.

The first trend is the skewing of the peak in local current density towards the exit of the FC at higher current densities. This is actually directly an effect of the metal support. As explained in chapter 3, the activation losses and ohmic resistance losses are inversely proportional to the temperature, which already explains why the majority of the current density is at $L \geqslant 0.5$, however, the concentration losses are logarithmic inversely proportional to the current density $V_{con} \propto ln\left(1-\frac{i}{i_o}\right)$ this causes the local current density to drop rapidly when the concentration of hydrogen reduces. Taking this information into account, if the fuel feed volumetric flow rate of the experiment with the largest current density $\dot{V}_{fuel_{I_{tot}=2900}}$ would be equal for every experiment $I_{tot} = 2100, 2300, ..., 2900$, then the peak local current density would actually move towards the exit for lower current densities. However, the opposite is the case. This is because all experiments were performed under optimised flow rates, as a result it shows that the concentration losses are the governing loss component that determines the optimal fuel feed volumetric flow rate. Because of the spatial partial pressure distribution of the hydrogen and water in the metal support, higher and less efficient volumetric flow rates are needed to overcome this boundary, thus skewing the local current density for that particular experiment peak to the exit. Therefore, the higher the overall current density of the FC system in optimised situations, the further the local current density peak skews towards the exit.

Another trend is difference between distribution of the local current density along the length $L(0,1)$. This can be explained by analysing figure 8.8. This figure shows the molar fraction of the five components in the discretization units $j = 1, 2, 3, ..., 12$. Note that this figure does not show $j = 0$, which is the initial fuel feed shown in table 8.3. The most obvious difference is the higher molar fraction of hydrogen and lower molar fraction of water near the entrance of the fuel cell. This is expected due to the difference in feed. In this part of the reformer concentrations are favourable for lowering concentration losses. Thus showing why the feed of $y_{Me_{I_{tot}=2700}} = 0.1$ yields a higher local current density then $y_{Me_{I_{tot}=2700}} = 0.3$. The current density however rises while the concentrations of hydrogen get lower in case of $y_{Me_{I_{tot}=2700}} = 0.1$. This is a result of the local governing losses which are bound to temperature. In the case of $y_{Me_{I_{tot}=2700}} = 0.3$ the molar fraction of hydrogen stay somewhat equal due to the production of hydrogen of the methanol reforming process. As a result it shows that the increment of the local current density is higher due to a rather constant concentration loss and lower activation-, and ohmic losses. Both experiments have a convex progression in the distribution of the local current density between from the entrance up to the middle. In the case of $y_{Me_{I_{tot}=2700}} = 0.3$ this seems to be longer than in the case of $y_{Me_{I_{tot}=2700}} = 0.1$. This can be explained due to the endothermic process of methanol decomposition which cools the FC cell,

along the length the amount of methanol decomposition decreases and the amount of hydrogen oxidated increases. As a result the convex distribution slowly turns to a concave distribution. The point where the convex progression turns into a concave progression is also where the concentration losses begin to rise. As expected, the molar fraction of hydrogen in the case $y_{Me_{I_{tot}=2700}} = 0.1$ is lower near the end of the FC cell compared to $y_{Me_{I_{tot}=2700}} = 0.3$, the other way around for water. Thus resulting in a higher local current density.

Due to the distribution, which its origin is explained in the previous paragraph, the peak current density is higher. However, comparing figure 8.7a to figure 8.7b purely based on peak current density, it shows that the difference in peak current density is lower for the cases of $I_{total} = 2100$ compared to the cases of $I_{total} = 2900$. This is actually a result of the efficiency of the system. The more the peak current density is skewed towards the end of the FC unit, the lower the effective hydrogen consumption. Due to the nature of internal reforming, the case of $y_{Me_{I_{tot}=2700}} = 0.3$ needs to overcome its local current density deficit at the entrance of the FC by yielding higher local current densities near the end where the concentration losses are higher, especially at $j = 12$. Thus resulting in a high peak current density between $j = 7, 8, 9, and 10$.

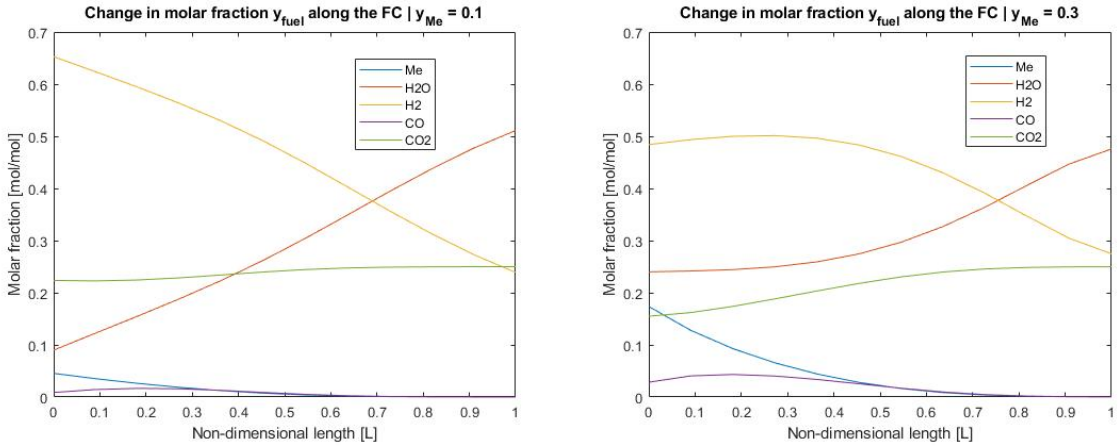

(a) Change in molar fraction along the length with $y_{Me} = 0.1$ feed

(b) Change in molar fraction along the length with $y_{Me} = 0.3$ feed

Fig. 8.8 | Change in molar fraction along the length for the testcase of $I_{total} = 2700[\frac{A}{m^2}]$

8.2.3. THERMODYNAMIC BEHAVIOUR OF THE FC CELL

The temperatures along the FC cell have different values for the fuel feed. This is shown in figure 8.9a. Both cases start with the same entering temperature of air $T_{air_{enter}} = 743.15[K]$ and fuel temperature of $T_{fuel_{enter}} = 773.15[K]$. Due to the endothermic methanol decomposition reactions, which mainly happens at the entrance of the FC cell, the stack is cooled. As one can see, this cooling effect is bigger for the feed containing more methanol. This also explains the lower local current densities at the entrance of the fc for the $y_{Me} = 0.3$ experiments. Because lower temperatures give higher ohmic and activation losses. It is also noticeable that the temperature gradient rises around $L = 0.6 - 0.8$ more heavily for the $y_{Me} = 0.3$ than for the case of $y_{Me} = 0.1$, this is also expected due to the peak in local current density at this part of the FC cell shown in figure 8.7b. Finally the temperature gradient decreases near the exit due to a lower local current density.

One of the major drawbacks for IT-SOFC systems is the relative high activation and ohmic losses due to the lower temperature compared to HT-SOFC. The limitation of $T_{solid} \leqslant 873.15[K]$ causes serious limitations to the system. During all cases it is assumed that maximising the exit temperature $T_{solid_{exit}}$ is preferable for the performance. These assumptions show to be true when figure 8.9b and corresponding table 8.5 is analysed. Three experiments were carried out on identical feeds $y_{Me} = 0.1$, identical current densities $I_{tot} = 2500\frac{A}{m^2}$ and identical volumetric flow rates $\dot{V}_{fuel} = 5.70E-05\frac{m^3}{s}$ and $\dot{V}_{air} = 1.14E-04\frac{m^3}{s}$. Although steps of 20 degrees are taken, it significantly influences the overall performances of the cell. The ohmic and activation losses increase significantly compared to the concentration losses. The voltage drops significantly, which affects the efficiency of the system. This is shown in figure 8.10.

Figure 8.10 does not only show the differences in losses due to temperature, but it also shows the distribution of losses along the FC cell. In figure 8.10a the operating voltage is shown for a test case of

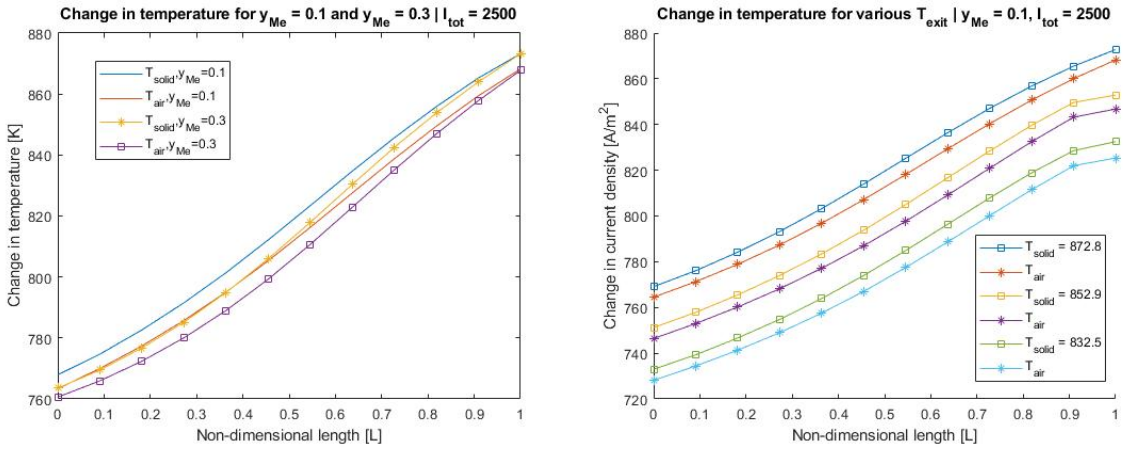

(a) Operating temperatures of experiments with $y_{Me} = 0.1$ and $y_{Me} = 0.3$ | $I_{tot} = 2500$ and $T_{exit} = 873.15[K]$

(b) Operating temperatures of experiments with $y_{Me} = 0.1$ varying the entrance and exit temperature at $I_{tot} = 2500$

Fig. 8.9 | Influence of temperature differences on system

Tab. 8.5 | Operating temperature and corresponding operating voltage at $I_{tot} = 2500 \frac{A}{m^2}$

Operating temperature [K]	Operating voltage [V]
872.8	0.7607
852.9	0.6857
832.5	0.5918

$I_{tot} = 2500$, which is also used in the previous figures. This figure shows the local losses. The green area is the operating voltage, the purple area is the amount of concentration loss, the yellow area the ohmic loss and the orange area gives the activation loss. The interface of the orange and blue area is the open circuit voltage. The open circuit voltage becomes lower along the length due to the increase of temperature. This is a result of the decreasing Gibbs free energy. The activation losses become less significant due to the increasing temperature and the increasing current density. If looked closely, one can see that the rate of decreasing lowers toward near the exit due to, this is a result of the increasing temperature but the decreasing current density, this shows also that the temperature is more significant for activation losses than temperature. The ohmic losses are somewhat constant because of higher temperatures but also higher current densities, near the end the current density lowers and thus the ohmic losses also. The concentration losses rise near the end due to the decreasing local partial pressure of hydrogen in the metal support.

Figure 8.10b shows the same operating experiment, but with a temperature of $T_{exit} = 832.5[K]$ or $559.4[^{\circ}C]$. For this particular experiment, it was chosen not to reduce the volumetric flow rate. As a result however, the amount of moles entering the system is higher due to the ideal gas law $\frac{P\dot{V}}{RT} = \dot{n}$. Nevertheless, the decreasing concentration losses do not compensate for the increasing ohmic and activation losses due to the lower temperature. Besides, the concentration losses are distributed differently since the peak power density is skewed towards the exit. This effect is already explained in figure 8.7.

8.2.4. POWER DENSITY, OPERATING VOLTAGE AND SYSTEM EFFICIENCY

Lastly a scatter plot is made of the total current density against the operating voltage and the current density against the power density in figure 8.11. The model made prediction trendlines through the scatter plot. For the current density against voltage trendline, the input value of the average open circuit voltage V_{OC} distributed over the length of the FC, shown in figure 8.10, is used at $I_{tot} = 0$. For the current density against the power density an input value of $P_{cell} = 0$ at $I_{tot} = 0$ is used.

Figure 8.11b shows that the operating voltage prediction curve is more concave as figure 8.11a. Meaning that the the system has a lower power density at various voltages, especially when the current density increases. As a result, it seems that in the case of $y_{Me} = 0.3$, the power density significantly drops as an effect

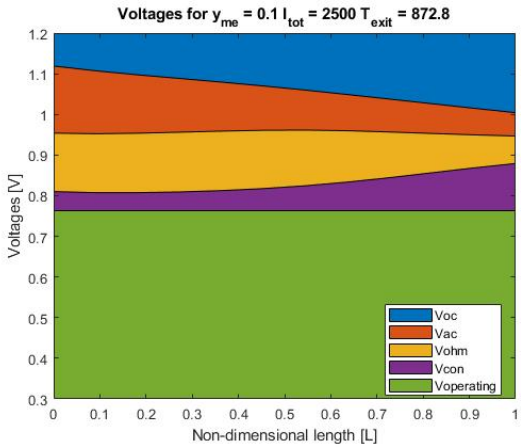

(a) Operating voltage after reduction of losses for $T_{exit} = 872.8[K]$

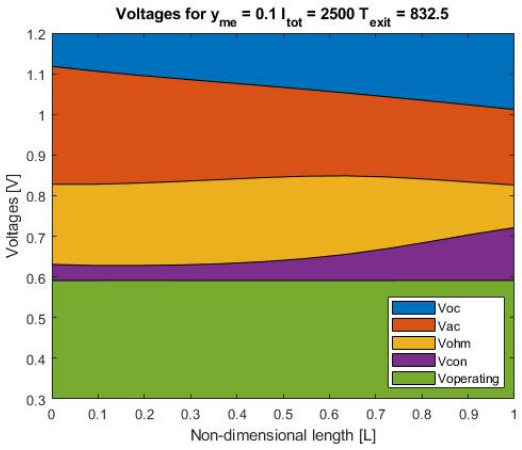

(b) Operating voltage after reduction of losses for $T_{exit} = 832.5[K]$

Fig. 8.10 | Operating voltages at different temperatures at constant $y_{Me} = 0.1, I_{total} = 2500, \dot{V}_{fuel} = 5.70E-05, \dot{V}_{air} = 1.14E-04$

of the internal reforming process of the methanol. A concluding remark is that the FC unit is more optimal for a more pure hydrogen feeds.

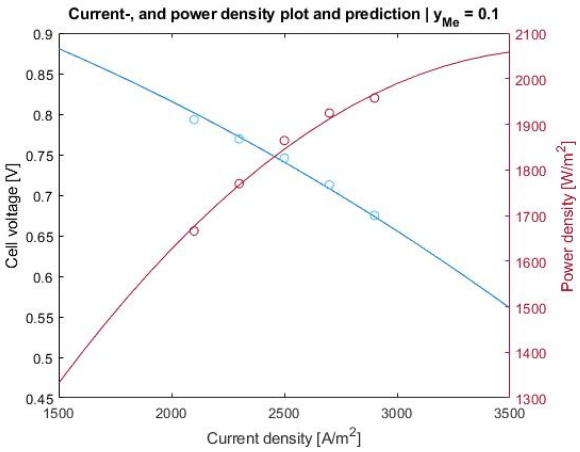

(a) Current and power density with $y_{Me} = 0.1$ feed

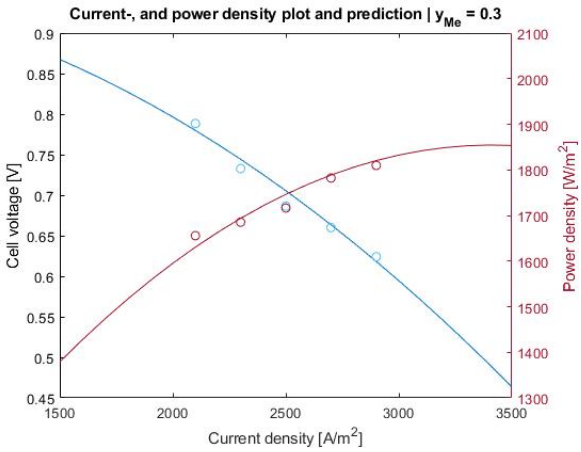

(b) Current and power density with $y_{Me} = 0.3$ feed

Fig. 8.11 | Scatter plots of experimental model data and model prediction curves for $I_{total} = 2700[\frac{A}{m^2}]$. The model prediction curves do not have any physical meaning.

The FC cell efficiency, which is determined by equation 8.2, is shown in table 8.6. The operating voltage $V_{operating}$ is constant along the the length of the FC, the open circuit voltage V_{OC} however is not. This is due to temperature differences and partial pressure differences. An average of the open circuit voltage distribution is taken for every experiment to determine the cell efficiency η_{FC}. The maximum thermodynamic efficiency $\eta_{thermodynamic}$ is calculated by dividing the change Gibbs free energy by the change in enthalpy. Lastly, the fuel utilisation η_{H_2} is calculated by dividing the reacted fuel by the total input fuel.

Table 8.6 shows that the efficiency of the FC drops when the power density of the system increases, however, approaching the maximum power density of the system, the efficiency seems to approach a lower limit of η_{FC} also. This is visible when then intervals are observed going from lower current densities to higher current densities for both fuel feeds. Table 8.6 also gives that a fuel feed of $y_{Me} = 0.1$ makes the FC cell about 10% more efficient compared to $y_{Me} = 0.3$.

$$\eta_{FC} = \eta_{H_2} \eta_{thermodynamic} \frac{V_{operating}}{V_{OC}} \tag{8.2}$$

Tab. 8.6 | The system efficiency and power density for two types of fuel feed for various current densities

	Fuel feed of $y_{Me} = 0.1$		Fuel feed of $y_{Me} = 0.3$	
Current density $\frac{A}{m^2}$	Power density $\frac{W}{m^2}$	Efficiency η_{FC}	Power density $\frac{W}{m^2}$	Efficiency η_{FC}
2100	1665.8	0.479	1655.8	0.439
2300	1769.8	0.443	1685.3	0.388
2500	1864.3	0.388	1716.3	0.359
2700	1924.6	0.365	1782.1	0.310
2900	1957.6	0.342	1809.7	0.305

8.3. BALANCE OF PLANT BEHAVIOUR AT OPERATIONAL PROFILES

There are five different operational profiles with two having the same parameter requirements, which are the Operations and Economical Transit profile. So there will be four test cases of different alignments of the system. Please look back at chapter 3 and 3 for the operational profile and scoping of the type of operations. During the testing it happened to be that reforming more methanol is preferable for the operations of the FC system. To make sure the results are somewhat comparable, it is chosen to set the reformer at reforming 80% of the methanol.

Figure 8.12 shows the BoP containing various indicators which lead back to the fuel flow or the system dynamics which are explained in the tables. Table 8.7 explains all labels given to the flows.

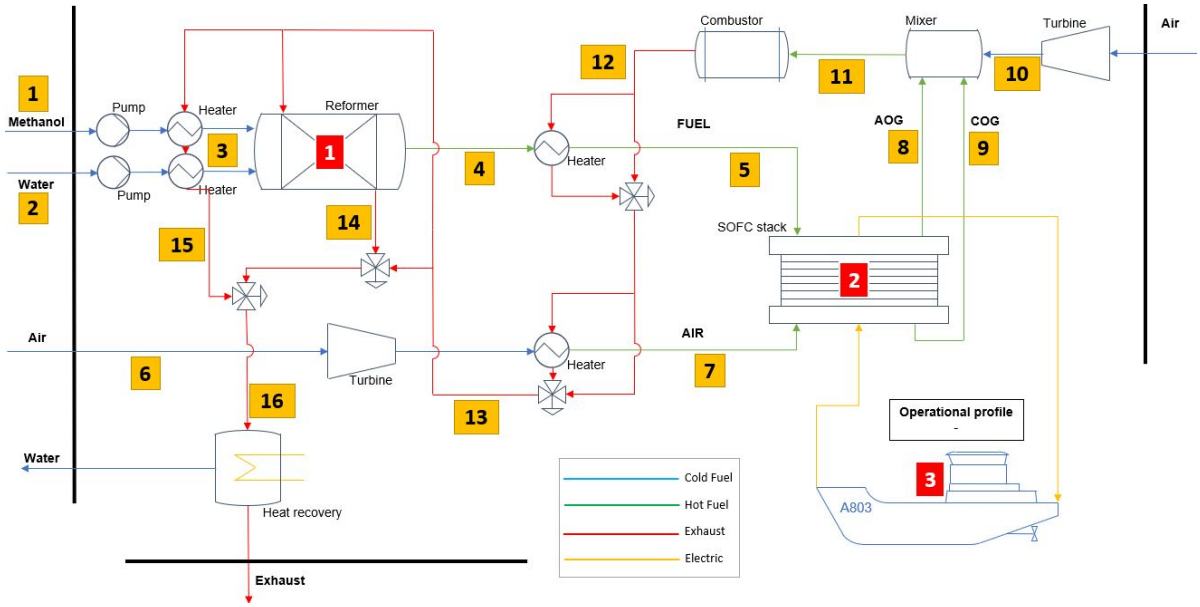

Fig. 8.12 | Balance of Plant

Tab. 8.7 | Description of yellow labels from figure 8.12

Label& Description flows in yellow	
1	Methanol feed to pre-heater
2	Water feed to pre-heater
3	Methanol and water feed temperature
4	Fuel feed to heater
5	Fuel feed to fuel cell
6	Air feed to turbine and heater
7	Air feed to fuel cell
8	Anode off gas to mixer
9	Cathode off gas to mixer
10	Air feed to mixer
11	Exhaust feed to combustor
12	Exhaust feed to heaters
13	Exhaust heat to reformer and pre-heaters
14	Exhaust feed after reformer
15	Exhaust feed after pre-heaters
16	Final exhaust heat to heat-, water recovery
Label & Description systems in red	
1	Reformer output
2	Fuel Cell output
3	Operational profile

8.3.1. MAXIMUM SPEED TRANSIT

The first set of results determine the size of the the entire BoP. According to the functional scoping a required $P_{installed} = 1485kW$ must be installed to produce enough power for the entire load of the BoP. Note that the maximum propulsion load is $P_{propulsion} = 1150kW$. However, parasitic loads of the turbines, pumps or other components have not been taken into account yet. Note that the recovery of water and heat is also not taken into account. There are too many assumptions needed to properly scope the operational profile which would make the detailed results of the reformer and FC redundant.

All major results are shown in tables 8.8 and 8.9. The FC system is pushed to its maximum, which is at $I_{tot} = 3100\frac{A}{m^2}$ and $V_{operating} = 0.656$. Pushing the voltage to lower levels decreases the η_{H_2} and η_{FC} heavily. This configuration requires 18252 individual cells for this operation. Ceres produces stacks with 140 individual cells which results in 131 stacks required [57]. The reformer unit has an entrance speed of $\dot{m}_f = 0.2[\frac{m}{s}]$ in which 80% of the methanol needs to be reformed. This results in a volumetric flow rate of $\dot{V}_{fuel} = 1.314\frac{m^3}{s}$. The reformer input volumetric flow rate is $\dot{V}_{fuel_{reformer,input}} = 0.1257\frac{m^3}{s}$, but considering the decomposition of methanol yielding more mole and increasing the temperature and thus increasing the volumetric flowrate, it is $\dot{V}_{fuel_{fc,input}} = 0.3179\frac{m^3}{s}$. As a result, this means that the current reformer is too small by a factor 4.13. Note that the current reformer has a diameter of $D_{ref} = 0.4m$, so there is room to scale.

Tab. 8.8 | Flow values | $I_{tot} = 3100[\frac{A}{m^2}], y_{Me} = 0.1[\frac{mol}{mol}], \dot{m}_f = 0.2[\frac{m}{s}]$

Label	Temperature [K]	Pressure [Bar]	Mass flow [g/s]
1	293.15	1.013	185.6
2	293.15	1.013	104.4
3	550.00	1.013	185.6 / 104.4
4	593.15	1.020	289.9
5	773.15	1.019	289.9
6	293.15	1.013	1142.5
7	753.15	1.200	1142.5
8	875.25	1.018	449.3
9	869.82	1.199	983.1
10	293.15	1.200	0
11	871.52	1.152	1432.4
12	1355.40	1.152	1432.4
13	1021.52	1.149	1432.4
14	740.27	1.148	573.0
15	966.63	1.149	1432.4
16	817.39	1.148	1432.4

Tab. 8.9 | Operating values of system | $I_{tot} = 3100[\frac{A}{m^2}], y_{Me} = 0.1[\frac{mol}{mol}], \dot{m}_f = 0.2[\frac{m}{s}]$

[1] Reformer molar fractions		[2] Fuel Cell	
Me	0.056	$I_{operating}$	124 [A]
H_2O	0.058	$u_{operating}$	0.656 [V]
H_2	0.667	$P_{percell}$	81.36 [W]
CO	0.002	Cells	18,252
CO_2	0.222	Stacks	131
		η_{H_2}	0.632
		η_{FC}	0.332

8.3.2. HIGH SPEED TRANSIT

See tables 8.10 and 8.11 for the results of the high speed transit profile. Since the amount of FC stacks is capped at 131, as determined with the max speed transit, it can be assumed that the system needs to operate below this threshold. The higher the operating voltage, the higher the efficiency of the system (at constant hydrogen utilisation). It was found that the system can operate at $I_{tot} = 2300 \frac{A}{m^2}$ to achieve the high speed transit required power of $P_{Highspeedtransit} = 1230kW$. Note that the mass flow is considerably lower compared to the maximum speed transit. The system is also considered with fewer active stacks working.

Tab. 8.10 | Flow values | $I_{tot} = 2300[\frac{A}{m^2}], y_{Me} = 0.1[\frac{mol}{mol}], \dot{m}_f = 0.2[\frac{m}{s}]$

Label	Temperature [K]	Pressure [Bar]	Mass flow [g/s]
1	293.15	1.013	117.8
2	293.15	1.013	66.2
3	550.00	1.013	117.8 / 66.2
4	593.15	1.020	184.0
5	773.15	1.019	184.0
6	293.15	1.013	823.1
7	753.15	1.200	823.1
8	872.80	1.018	296.7
9	865.73	1.199	710.5
10	293.15	1.200	0
11	867.13	1.158	1007.1
12	1329.83	1.158	1007.1
13	980.99	1.154	1007.1
14	727.68	1.151	453.2
15	904.06	1.153	1007.1
16	762.20	1.150	1007.1

Tab. 8.11 | Operating values of system | $I_{tot} = 2300[\frac{A}{m^2}], y_{Me} = 0.1[\frac{mol}{mol}], \dot{m}_f = 0.2[\frac{m}{s}]$

[1] Reformer molar fractions		[2] Fuel Cell	
Me	0.056	$I_{operating}$	92 [A]
H_2O	0.058	$u_{operating}$	0.769 [V]
H_2	0.667	$P_{percell}$	70.75 [W]
CO	0.002	Cells	17,376
CO_2	0.222	Stacks	125
		η_{H_2}	0.720
		η_{FC}	0.443

8.3.3. OPERATIONS- & ECONOMIC TRANSIT

See tables 8.12 and 8.13 for the results of the high speed transit profile. This result shows how the FC system would operate at $I_{tot} = 1700\frac{A}{m^2}$. Note that the system efficiency is again higher for this operational state compared to previous operations. the amount of fuel is considerably lower also. The amount of stacks used is also lower, not that is has to, but to compare results also. For this specific operational profile it needs to produce $P_{installed} = 780kWS$, the system is easily able to cover this,

The operational requirements are that the vessel is able to sail $5000nm$, this vessel is able to sail $9knots$ in the economic transit operational profile, which means that it should be able to sail for about 23.15 days straight. With the fuel mass flow of $61.1[g/s]$, it should be able to bunker $L_{bunker} = 154.5m^3$ litre of methanol with the weight of methanol $m_{methanol} = 0.7914kg/L$. The current design of the hydrographic survey vessel has a bunker capacity of $L_{bunker} = 387m^3$. As a result, the bunker capacity can be lowered, however, tanks for water storage have not been considered yet. Nevertheless, the bunker capacity of a water day tank for operational requirements is not in the order of $L_{water} = 200m^3$.

Tab. 8.12 | Flow values | $I_{tot} = 1700[\frac{A}{m^2}], y_{Me} = 0.1[\frac{mol}{mol}], \dot{m}_f = 0.2[\frac{m}{s}]$

Label	Temperature [K]	Pressure [Bar]	Mass flow [g/s]
1	293.15	1.013	61.1
2	293.15	1.013	34.4
3	550.00	1.013	61.1 / 34.4
4	593.15	1.020	95.5
5	773.15	1.019	95.5
6	293.15	1.013	467.7
7	753.15	1.200	467.7
8	870.52	1.018	160.3
9	865.75	1.199	402.9
10	293.15	1.200	0
11	867.11	1.158	563.2
12	1305.67	1.157	563.2
13	963.10	1.154	563.2
14	689.03	1.151	276.0
15	884.07	1.152	563.2
16	739.57	1.151	563.2

Tab. 8.13 | Operating values of system| $I_{tot} = 1700[\frac{A}{m^2}], y_{Me} = 0.1[\frac{mol}{mol}], \dot{m}_f = 0.2[\frac{m}{s}]$

[1] Reformer molar fractions		[2] Fuel Cell	
Me	0.056	$I_{operating}$	68 [A]
H_2O	0.058	$u_{operating}$	0.848 [V]
H_2	0.667	$P_{percell}$	57.68 [W]
CO	0.002	Cells	13,523
CO_2	0.222	Stacks	97
		η_{H_2}	0.812
		η_{FC}	0.551

8.3.4. LOW SPEED TRANSIT

See tables 8.14 and 8.15 for the results of the high speed transit profile. This operational profile shows that sailing at low speed is very efficient. The efficiency of the system could even be higher if more FC stacks would be used. However, in this configuration, it could also fulfil the economic transit operational requirements, which means the vessel needs to bunker $L_{bunker} = 86.0m^3$ litre of methanol to sail $5000nm$ at $9knots$. This shows that the part-load capabilities of the system is extremely efficient.

Tab. 8.14 | Flow values | $I_{tot} = 1300[\frac{A}{m^2}], y_{Me} = 0.1[\frac{mol}{mol}], \dot{m}_f = 0.2[\frac{m}{s}]$

Label	Temperature [K]	Pressure [Bar]	Mass flow [g/s]
1	293.15	1.013	34.0
2	293.15	1.013	19.1
3	550.00	1.013	34.0 / 19.1
4	593.15	1.020	53.1
5	773.15	1.019	53.1
6	293.15	1.013	271.6
7	753.15	1.200	271.6
8	870.52	1.018	91.5
9	865.75	1.199	233.3
10	293.15	1.200	0
11	867.11	1.158	324.8
12	1274.94	1.158	324.8
13	937.27	1.154	324.8
14	671.98	1.151	165.6
15	868.34	1.153	324.8
16	728.55	1.152	324.8

Tab. 8.15 | Operating values of system | $I_{tot} = 1300[\frac{A}{m^2}], y_{Me} = 0.1[\frac{mol}{mol}], \dot{m}_f = 0.2[\frac{m}{s}]$

[1] Reformer molar fractions		[2] Fuel Cell	
Me	0.056	$I_{operating}$	52 [A]
H_2O	0.058	$u_{operating}$	0.909 [V]
H_2	0.667	$P_{percell}$	47.27 [W]
CO	0.002	Cells	10,294
CO_2	0.222	Stacks	74
		η_{H_2}	0.841
		η_{FC}	0.645

8.4. TRANSIENT BEHAVIOUR

The four operational profiles are considered in steady states. Note that there are two boundaries to which the steady state must comply; the maximum temperature of the solid must not exceed $T_{solid} \leqslant 600°C$ and the required power is at least the delivered power $P_{installed} = P_{deliverd}$. The model, however, was not able to do dynamic testing due to numerical failure. Therefore the transients between operational profiles and the system start up could not be tested dynamically.

Nevertheless, the steady state results do tell something about the behaviour of the system during the transients. First of all, the entering temperature of both the fuel and the air is kept constant, as is the boundary condition of $T_{solid} \leqslant 600°C$. In figure 8.13a the change in temperature of the solid for the four operational profiles are depicted descending with their corresponding current densities; $I_{operation}$ = [3100 2300 1700 1300] relative to the I_{low} = 1300. Therefore, the relative temperature of $T_{I_{low}=1300} = 0$ for all spatial distributions.

The most interesting result is that the higher the total current density, shown in figure 8.13b, the lower the temperature around $L_{fc} = 0.6 - 0.8$. This effect is a result of the current density distribution which is skewed towards the exit. A higher current distribution means more hydrogen oxidised. This releases heat near the exit and thus more cooling is needed near the exit of the stack. As a result, the temperature of the solid needs to be lower in advance of the exit, around $L_{fc} = 0.6$, to comply with the maximum exit temperature boundary. To make sure the stack is cool enough, higher air flow is needed.

Higher air supply for a skewed current density distribution has another consequence which is negative for the stack performance. When the relative temperatures are observed in figure 8.13a, it is noticeable that for the lowest total current density I_{tot} = 1300 the relative temperature is the highest. As shown in the results in section 8.2.3, slight temperature differences have a major impact on the efficiency of the system. Therefore, besides having a lower fuel utilisation at higher total current densities, the internal temperature is relatively lower as well. Making the system even more inefficient.

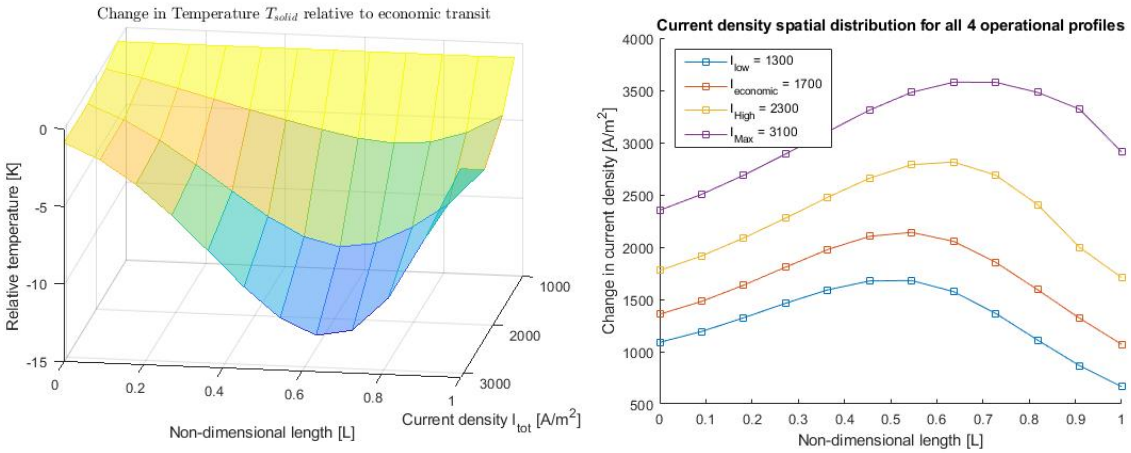

(a) The relative change in temperature of the solid T_{solid} for all four operational profiles.

(b) Change current density for all operational profiles

Fig. 8.13 | The relative temperature and the current densities of all four operational profiles.

However, for the transient behaviour it is shown that the relative differences in temperature of the stack are small. The largest difference in temperature is $\Delta T_{solid} = 12.6[K]$, which is at $L_{fc} = 0.64$. Although the temperature gradient limits are unknown for the MS-SOFC used in this research, it is safe to assume that the difference in temperature gradients alone is not the problem. Ceres Power did MS-SOFC test whith higher total current densities and lower initial fuel and air temperatures [57]. Meaning the system is able to cope with even higher temperature gradients, assuming the temperature gradient relations shown in figure 8.13a apply for that MS-SOFC stack also, and having a higher gradient due to the lower entrance temperature.

8.5. SYSTEM COMPARISON TO CONVENTIONAL SYSTEM AND ENVIRONMENTAL IMPACT

The operational requirements are shown again in table 8.16 and 8.17. Note that the operational profiles are based on table 8.17, and the bunker capacity is based on the range transit. The endurance of the vessel is 14 days in which it should be able to cover the requirements shown in table 8.17.

Tab. 8.16 | Principal design characteristics [9]

Parameter	**HOV**
High speed transit	8 kts
Maximum speed	12 kts
Installed power	1546 kw
Range transit speed	5000 nm
Displacement	1814 t
Payload	≈ 800 t
Design life	30 years
Endurance	14 days
Operational Days	200 p/y

The middle part of the table shows power required, the efficiency of the stack and the fuel used total for the 14 day endurance. According to the estimation of the percentage of time of the operations, the total fuel used is $L_{fuel} = 93.666[m^3]$. Also, as previously mentioned, the amount of fuel needed for a $5000nm$ transit is $L_{fuel} = 86.0m^3$. Note that the vessel either operates for 14 days or it sayls 5000 nm. Therefore the largest tank size is determined on the operation with the largest fuel consumption. The currently available bunker size is $L_{bunker} = 387[m^3]$. So the amount of fuel needed is about 4 times less.

Tab. 8.17 | Operational profile family design [9]

	Type of operation	**Power**	**Time**	**Speed**	$P_{installed}[kW]$	η_{FC}	**Fuel used**$[m^3]$	Emissions $[g/kWh]$
1	Low speed	33%	15%	4kts	495	0.645	6.169	345.512
2	Operations	52%	40%	6-10kts	780	0.551	11.086	387.35
3	Economic transit	52%	15%	9kts	780	0.551	29.563	387.35
4	High speed transit	82%	25%	12kts	1230	0.443	35.623	473.84
5	Maximum speed	99%	5%	15kts	1485	0.332	11.225	618.04

The amount of stacks that need to be installed are 131 based on the max speed transit operational profile. The size of a stack module however is unknown. Therefore it is unable to estimate the size of the BoP. Considering every stack module is of a dimension of a big suitcase with a volume of $W * D * L = 0.4 * 0.3 * 0.6 = V_{fc} = 0.0720m^3$ and surface of $W * D = A_{fc} = 0.4 * 0.3 = 0.12$ requires a floorspace of $A_{fc,total} = 15.7m^2$ and a volume of $9.432m^3$. Note that this estimation is highly inaccurate and should not be taken as an estimation for the BoP size. But it does give an order of magnitude for the floorspace an FC system requires.

Considering the results of table 8.17, it can be concluded that this BoP configuration based on the reformer and FC system is able to replace the current system. This is based on performance only.

8.5.1. ENVIRONMENTAL IMPACT OF EXHAUST GASSES

Table 8.17 shows the emissions of CO_2 gram per kilowatt hour. Note that in this system, the absolute maximum temperature is reached inside the reformer which is below $T_{max} \leqslant 1400[K]$. The formation of NO_x is mostly present in combustion processes exceeding $T_{max} \geqslant 1600[K]$, therefore it is assumed that NO_x formation can be excluded. At the same time, due to the excess of oxygen in the exhaust gasses, it is assumed that all remaining methanol and carbon monoxide are burned also. Besides, the amount of methanol and carbon monoxide are already reduced to a molar fraction of $y_{Me}, y_{CO} \leqslant 0.002$ leaving the FC. The particle matter (PM) emissions is non-existent also. Taking this into account, the only emission this system produces

is CO_2.

Considering the percentage of operation time to determine a mean distribution of the CO_2 emissions results in an $\eta_{CO_2} = 414.23[g/kWh]$. Note that this system only produces CO_2 emissions, which can be recovered during the production of methanol via carbon capture. This would make methanol a carbon neutral fuel.

For comparison, a $3000kW$ marine generator on MDO of 2020 from MAN is taken. This generator complies with all tier II norms set by IMO. However, only the exhaust pollution is compared [**MAN2020GenSet**]. The generator produces approximately $\eta_{CO_2} = 590[g/kWh]$, note that this is one of the cleanest marine generators currently available by MAN [**MAN2020GenSet**]. The carbon dioxide equivalent of NO_x is a factor 298, for the MAN generator set this is about $\eta_{NO_x} \leqslant 12[g/kWh]$ resulting in an addition equivalent to $\eta_{CO_{2_{equiv}}} = 3576[g/kWh]$. Besides it pollutes sulphur oxide SO_x and other hydrocarbons HC larger than CO_2 which is combined $\eta_{other} = 14[g/kWh]$. The FC considered produces no NO_x, SO_x or other HC $\eta_{other} = 0[g/kWh]$.

9

DISCUSSION

The discussion chapter has the same structure as the results. The assumptions, results and concluding remarks will be evaluated.

9.1. REFORMER ANALYSIS

It is shown that as a part of the BoP, the current model used is too small by a factor 4.13. Since there is no methanol reformer in the literature that reforms about 80 – 90% of the methanol, it is unable to assume its size on literature only. Therefore it is also difficult to assume its optimal temperature because size and temperature are intertwined with flow rate and the reaction rate. What can be concluded is that, according to literature, the reformer temperature should be between 558.15 – 598.15[K] for material consideration and optimal reforming. The model showed that the optimal reforming temperature is at 598.15[K]. This yields the highest flow rate and thus reduces the size of the reformer. Another note is that it take quite long to reform all methanol, but partly reforming it can be done at way higher rates, up to twice as fast. Therefore partly reforming methanol up to 80%, according to this study, is considered possible with a relative small installation of 1 meter long, and 0.4 meter wide. Four installations would be enough to reform all methanol required.

The reformer model shows that when the methanol water ratio is 60/40, about all water is reformed $y_{H_2O} \leqslant 0.02$, but not all methanol $y_{H_2O} = 0.19$. Because of the absence of water, the methanol reforming is slowed down. When the temperature rises in the FC system, it could even be that the reverse water gas shift is dominant over the water gas shift. This would mean that carbon formation is highly likely to be present. However, when the methanol is mixed with water in a ratio of 50/50 or less, the amount of water will never drop below the methanol molar fraction during the reforming process. During this study, carbon formation is not considered, however, all operations shown in the results do avoid situation where carbon formation is likely. This however, cannot be concluded from this study alone.

The reformer results shown have two drawbacks, the initial temperature and the volumetric flow of the exhaust gas. After a considerable amount of testing it has shown that the volumetric flow of the exhaust was nearly a factor 8 bigger as initially used, but the temperature was about 400 kelvin lower. This has been taken into account in the BoP results, but not in the results from the reformer section. Even though the results of the reformer section are not used in any result further along this research, the behaviour stayed the same.

Another note is that the physical design of the heater in the reformer influences the characteristics of the reformer. This has mainly to do with the amount of heat captured in the exhaust gas. If the exhaust gas temperature is high, about $T_{exhaust} = 1400[K]$, then the volumetric flow rate at the entrance will be lower resulting in extreme peaks of heat conduction. If the exhaust gas temperature is lower, about $T_{exhaust} = 1000[K]$, the reformer units temperature distribution is much more stable. The results of the operational profile tests showed that the reformer could conduct enough heat to get the fuel gas exit temperature at the desired $T_{fuel_{exit}} = 598.15[K]$ while using less of half of the exhaust fuel gas, meaning there was enough heat.

9.2. FUEL CELL ANALYSIS

The FC model initially should consist out of $J \geqslant 14$ discretization units if the model of Handa & Xi was followed regarding the spatial distribution of the FC losses [59]. Although this is not the case in this research, it is still detailed enough to show the behaviour of the FC regarding the losses, local current densities and operational temperatures. Together the characteristics of the MS-SOFC can be described detailed enough to make a decision on whether the MS-SOFC is capable of delivering the required power.

The FC model numerical solver for the current density distribution along the length of the FC cell required extreme computational time and therefore lowered the time step to extremely low steps $t_n = 0.00001s$. When the time step was forcibly increased, the system would crash. It was never found why this numerical solver required so much computational time and why it slowed the system immensely. As a result, this model was not able to run transient conditions. It is very likely that something goes wrong regarding the switch towards a Matlab environment from a SIMULINK environment. The ode45 solver optimises function blocks known to the SIMULINK environment, but most probably the solver is unable to optimise a non-predefined Matlab environment.

The biggest drawback of the metal support is the lowered local partial pressure of hydrogen and higher local partial pressure of water. As a result, this system behaves poorly at higher current densities. At lower current densities the system behaved greatly in terms of efficiency, but then the question remains if the system is preferable since a great amount of space is required for the amount of stacks that should be fitted, and having a system that is able to work great at lower power densities only is not great. To overcome this problem, a couple of solutions remain, either having an amount of batteries that are slowly charged during low speed transit and economic transit and discharged during the high speed transit. Another solution would be installing an ICE which has an operational profile for high power demands. Or have no high speed or max speed transit at all. All cases influence the design and the operational profile of the vessel and are therefore considered not applicable.

The system showed that methanol as a fuel would do good from an FC fuel feed perspective. As shown in the voltage losses section, a great amount of losses come due to low temperatures. Methanol steam reforming is not extremely endothermic due to methanol decomposition and not very exothermic due to the water gas shift, as a result, the temperature gradients are subtle considering an internal reforming FC. It did show that when 40% of the methanol was reformed, that the FC already behaved less optimal, therefore partly reforming is considered better. At lower current densities this model showed that the effective hydrogen used η_{H_2} would rise, as a result, the amount of air relative to the fuel should increase also to maintain the required temperature distribution. Another method would be to increase the molar fraction of methanol to the system, however this did led to a lower power density and lower η_{H_2} since the peak load was still skewed towards the exit. Therefore, have a pure hydrogen feed with more air would be beneficial for the FC power density instead of more methanol with less air.

9.3. BALANCE OF PLANT ANALYSIS

The first note is that this research mainly focused on the reformer, the FC, and the flows through the system. Losses due to pumps, turbines, or heaters have been highly simplified. At the same time energy production from a heat recovery system or water gained from the exhaust was neglected also. As a result, concluding remarks about the entire BoP are difficult. However, since all flows have been determined at every stage of the BoP, it is possible to further design the BoP regarding the results of this research. Therefore this research is able to guide the BoP design based on its characteristics.

The operational profiles are limited, since they only give insights in the total power required. Besides, there is a big debate on how much power the vessel actually needs. The difference between the former functional requirements or the family function requirements is an increase of required power of about 40%, which is a lot for the system design. Therefore, the actual size of the system is less important since the operational profile is not that detailed either. However, the power density, the current density and the

system efficiency are important. These values cover whether the system can or cannot be used for maritime applications.

Reviewing the power density of the FC, there are many limiting factors. However, there is one factor that seems to dominate its performance significantly, and that is the metal support. Due to the metal support and thus the lower partial pressure of hydrogen, the fuel optimisation is limited. This directly results in either low power densities or high fuel usage. To a certain extend this is acceptable, but this research showed that this particular FC is not able to perform well under high current densities.

The system expels high quality exhaust heat. Much of the heat is used for the system itself. At the bigger the fuel utilisation, the lower the expelled heat is. Therefore the amount of heat used differs per operational profile from $45\% to 73\%$. Nevertheless, this heat could drive up the total efficiency of the system and even make it very interesting. The system already showed that it could perform greatly under low current densities, if the exhaust heat could be captured in some way for higher current densities, it could be of great interest for maritime applications.

9.4. TRANSIENT BEHAVIOUR

Although the model was not able to perform actual transient behaviour, it seems that the temperature gradients itself were physically all right. The rate in which a temperature gradient could change is not know, but assuming the vessel goes from low speed to max speed in 1 minute would result in a temperature gradient of $\Delta T_j = 0.21[\frac{K}{s}]$ or $\Delta T_j = 12.6[\frac{K}{min}]$. There have been studies about ramp up and ramp down characteristics of MS-SOFC units with $\Delta T_j = 10[\frac{K}{min}]$ which showed hardly any degradation [**Heenan2018InvestigatingCells**]. Heenan even suggests that ramp-up or ramp-down rates of $\Delta T_j = 20[\frac{K}{min}]$ are possible without significant degradation.

So theoretically, the system is able fully perform in the scope of marine applications regarding the operational profile of a vessel and its ramp-up and ramp-down characteristics. However, the airflow must be carefully controlled to maintain the desired temperatures. The temperature of the solid must be controlled by the air feed which implies that there is a response time of the air turbine to the air feed when a higher flow rate is needed for better cooling. This problem is actually the main challenge regarding the ramp-up and ramp-down characteristics for an MS-SOFC. Although this challenge requires a strong control system because of the sensitivity of the FC to temperature changes, it is safe to conclude that the MS-SOFC on methanol based BOP is able to perform in all required operational profiles. The amount of oxygen required for the system is less sensitive than the change in heat due to the excess of oxygen relative to the cooling capacity of the air.

9.5. SYSTEM COMPARISON TO CONVENTIONAL SYSTEM AND ENVIRONMENTAL IMPACT

The comparison with the BoP of this research to a conventional system is difficult due to the unknown size of the reformer and the FC system. The supporting systems can be estimated, however this is still difficult since they are sized based on the dimensions of the reformer and the FC system. It could be that either the reformer or the FC system changes in size which would result in different flow rates, different fuel ratios or different current densities due to a yet unkown reason. Still, regarding the efficiency of the system, the power density of the stack and the mass-, volumetric flow rates, it can be concluded that this system is able to deliver the functional requirements. Therefore, a design study should be held to further investigate this BoP.

Because of the low TRL, it is difficult to do make any conclusions about safety, reliability, maintenance, economics, scalability or signatures. What can be concluded is that the materials used in this system are capable to endure for a long operational endurance and that carbon formation is limited. These assumptions are however purely based on literature and cannot be proven with this model. However, since it is proven that this model is able to perform in the suggested configuration, it is needed to further investigate the design of the BoP.

The emissions of the system only exist out of CO_2. This is an assumption since it could be that the burner does not burn all methanol or carbon monoxide. However, this is unlikely since the burner is not bound to fast burning rates, it should burn everything. Giving such an exposure to heat with an excess of oxygen, it is very well likely that all matter is burned. Thus the assumption that CO_2 is the only emission is grounded. Then the mean CO_2 emission is caped at $\eta_{CO_2} = 414.23[g/kWh]$.

The comparison with the marine ICE generator showed that the amount of carbon dioxide is reduced with 30%. However, the biggest win is the absence of any nitrogen oxides, which is $\eta_{NO_x} = 0[g/kWh]$ for the MS-SOFC due to the low temperatures. In this research, the operational states have tested for various current densities, but the system has not been optimised yet, leaving room for even bigger carbon dioxide reductions using methanol.

10

CONCLUSION

An MS-SOFC on methanol based BoP for power generation applications on a naval vessel could look like the schematic representation shown in figure 10.1. The system configuration utilises its own heat, the main parasitic subsystems are the pumps and turbines. The green and red arrows, representing the hot fuel and exhaust gasses respectively, are considered the hot part of the BoP. Heat losses could be minimised if these systems could be put together in a 'hot box'.

10.1. THE SYSTEM EFFICIENCY

The efficiency is high at lower operational profiles but low at higher profiles. The MS-SOFC overall efficiency regarding all operational profiles is $\eta_{FC} = 0.527$. The amount of heat used from the exhaust gasses to heat the fuel, air and reformer unit is about 73% of the available heat. Meaning from highest reached temperature in the system to ambient temperature. A lot of heat is used in the reformer and preheating the liquid fuel to a gaseous fuel of $T_{reformer_{entrance}} = 550[K]$. It is unlikely that the system efficiency will rise much due to heat recovery.

Compared to an conventional ICE, the system efficiency is about the same. Therefore the MS-SOFC on methanol based BOP is viable in terms of system efficiency regarding marine applications.

10.2. THE POWER DENSITY

The power density of the system is moderate. It is determined that the system exists out of 131 units requiring a floorspace of $A_{fc,total} = 15.7m^2$ and a volume of $9.432m^3$. The system needs 4 reformer units of 1 meter long and a width of 0.5 meter including the heater. The amount of fuel needed for transit is $L_{methanol} = 93.7m^3$ which is 24.2% of the current bunker size. Note that a water tank is required for the fuel feed. However, due to active recovery of water, this tank size is not bigger than $L_{water} \leqslant 2m^3$. The system requires an air turbine which is able to supply $L_{air} = 0.66m^3/s$ at max.

At higher power requirements $P_{required} \geqslant 0.85P_{max}$ the system gives FC efficiencies of $\eta_{FC} \leqslant 0.443 - 0.332$. This is a result of the metal support which lowers the local partial pressure of hydrogen near the PEN structure. It is assumed that the maximum power density is about $P_{max} = 2100W/m^2$, however the system seems to operate best, in terms of efficiency, for $P_{required} \leqslant 0.55P_{max}$ with a power density of $P_{max} = 1300 - 1700W/m^2$.

10.3. THE LOAD TRANSIENTS

The maximum transient from the low speed transit to the max speed transit is $\Delta T_{solid} = 12.6K/min$. Studies show that transients up to $\Delta T_{solid} \leqslant 20K/min$ have no severe degredation and should be possible with an MS-SOFC. The coefficient of thermal expansion of the metal support is about the same as the PEN structure $CTE_{400ss} = CTE_{YSZ,CGO,LSGM} = 10-12ppm/K$. The biggest challenge is to actively control the air feed, which cools the stack to $T_{exit} \leqslant 873.15$. Thus it can be concluded that the MS-SOFC is physically capable to perform

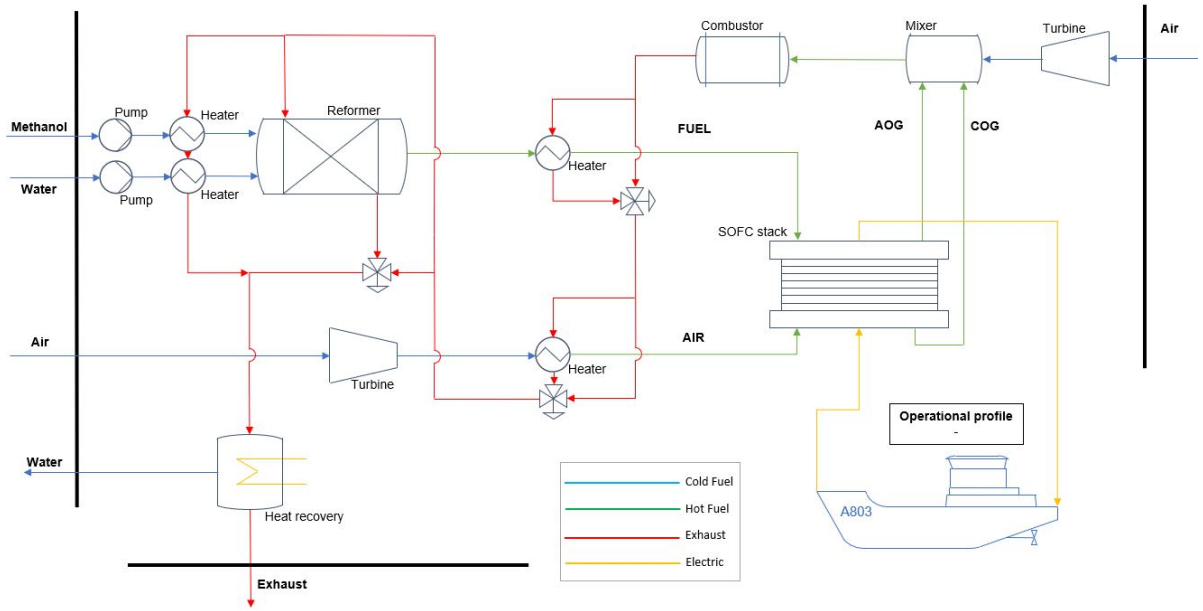

Fig. 10.1 | Schematic representation of BoP containing a reformer, FC system and their supporting systems

transients for marine applications due to the maximum temperature change of $\Delta T_{solid} = 12.6K/min$. A challenge in designing a control system for smooth transients remains.

10.4. THE EMISSIONS

The system carbon dioxide emission is $\eta_{CO_{2,FC}} = 414.23g/kWh$ for all operational profiles combined. Compared to a ICE this is a reduction of 30%. Besides the FC system has no nitrogen oxide emissions $\eta_{NO_{x,FC}} = 0g/kWh$ which are about $\eta_{NO_{x,ICE}} = 12g/kWh$ for the ICE. NO_x has a carbon dioxide equivalent of 298, which effectively adds another $\eta_{CO_{2,ICE}} = 3576g/kWh$ to the ICE system. As a result, this MS-SOFC system is a lot less polluting than a modern ICE.

Using methanol could be carbon neutral when methanol is synthesised using carbon capture methods. Also methanol is diluted in water easily, as a result it is relatively harmless for the sea environment when spilled.

10.5. VIABILITY

The combination of partly reforming methanol for an MS-SOFC is viable as a replecement of the ICE for marine applications. Especially for the relative low power applications with a power density of $P_{required} \leqslant 1700W/m^2$. The system utilises the fuel up to $\eta_{fuel} = 0.841$ in for lower power requirements and is suitable for all operations required for the HOV. However, the system is not efficient in the higher power range $P_{required} \geqslant 2900W/m^2$. It must be noted that the power density of the tested MS-SOFC could rise since the system has a TRL of about 5.

It was also found that partly reforming methanol is possible in relative small systems, however when all methanol needs to be reformed, the system quickly gets bigger. An MS-SOFC does suffer if it needs to reform a lot, it was found that when the reformer unit pre-reformed about 80% of the methanol, then the performance of the MS-SOFC is hardly touched. At the same time, the temperature of the MS-SOFC should kept as high as possible since it greatly affects the power density of the system. For this specific BoP configuration, about 4 reformers are required. All in all it can be concluded that partly reforming methanol for MS-SOFC applications is a solution for the tank-to-wake challenges.

11

RECOMMENDATIONS

The recommendations for future work can be distinguished in three main parts, the design of the BoP and the FC, the control system for transients of the MS-SOFC and the well to tank analysis of the fuel.

11.1. BOP DESIGN

The design of the entire BoP has not been touched. The main reason is the unknown size of the reformer unit and the FC unit. If these values are known, then the system can be sized. Trade offs between inlet temperature compared to turbine and heater size can be made, trade offs between methanol molar fraction for the inlet fuel of the FC and the size of the reformer can be made, a heat recovery system can be designed, tank sizes can be determined etc. All these systems can be determined based on the performance modelled in this research. Since this model proves the viability of the system based on performance, going into the design phase is the next step.

A BoP design is also restricted to a vessel and its operational profile. Therefore it is important to chose a vessel beforehand. It is advised to consider a vessel with a relative low power density requirement. The main challenges are the following.

The consideration of the air turbine for the cathode inlet, the amount of air required at maximum power is $\dot{m}_{fuel} \approx 0.9 kg/s$ at ambient pressure. Note that the pressure could be higher due to the rigidness of the metal support inside the MS-SOFC. However, not much is known about the pressure differences between air and fuel yet.

The consideration of the size of the reformer unit. This model provides a stand alone unit which is able to determine the volumetric flows, temperature and molar fraction for a dimensionless reformer. However, for design purposes it could be preferred to have more small reformers instead of a larger reformer. Larger reformers could have more difficulties with heat transfer of the exhaust gas due to uneven spatial distribution of heat. This could result in hot-spots and damage the reformer unit.

The consideration of the MS-SOFC system size. Note that the MS-SOFC performs well in part-load conditions regarding its fuel utilisation and overall efficiency. Therefore it could be that the system designer chooses to install more stacks. More stacks however lead to more complex system since, as for now, it is unable to scale the MS-SOFC in size significantly. The MS-SOFC is built from relative cheap metals, therefore the price of an MS-SOFC against the methanol used is also interesting.

The consideration of a pumps, combustor, tubes and heaters is also important for the total size of the BoP. Especially the heater in which the phase change of liquid fuel to gaseous fuel is interesting to analyse, although the size of this particular heater will not be significant. The flows in the system are considered to be at ambient pressure with little pressure drop, therefore it is important to size the system properly. Big temperature differences ranging from $\Delta T_{system} = 550 - 1355[K]$ and methanol reforming, resulting in more moles, result in large volumetric flow fluctuations. Therefore it is important to size the piping system accordingly.

The consideration of an extra power generation system. Because of the excellent part-load but poor high-load capabilities, another power generation system could be considered. An ICE next to the MS-SOFC system could be such a solution. The fuel utilisation of the MS-SOFC system decreases significantly when the power

density increases, it could even drop below $\eta_{fuel} \leqslant 0.6$. As a result, an ICE could support the MS-SOFC system and use the MS-SOFC exhaust gas as a fuel. Some researches in combining an SOFC system and an ICE have already been conducted [**Sapra2020PotentialShips**]. For the MS-SOFC in particular it has not, but it could be a great solution. Note that one of the drawbacks of the MS-SOFC is the low local partial pressure of hydrogen inside the metal support resulting in a lower fuel utilisation compared to HT-SOFCs at high current densities.

11.2. TEMPERATURE CONTROL IN FC TRANSIENTS

The transients could not be modelled dynamically. However, due to the optimisation towards temperature of the solid, it can be concluded that the temperature gradients do not differ greatly. However, this would take a dynamic study which should be done at FC level only. When the dynamic study shows the dynamic behaviour accordingly, it can be implemented in the model used for this study and a BoP design can be made.

The emphasis of the transient study should be about the control system. The change in current density spatially distributed over the system is considered instant relative to the change in temperature of the solid. Then again, due to the metal parts of the FC, the change in temperature should be actively controlled by the air supply. Note that a change in temperature affects the distribution of the current density of the stack. Especially when the stack is optimised to fuel utilisation, the system is bound to an amount of hydrogen available.

The control system should consider the amount of fuel available spatially distributed along the FC, it should consider the change in current density, and it should consider the temperature of the fuel, air, PEN structure, metal support and interconnect. Note that the hydrogen oxidation happens inside the holes of the metal support, therefore the interconnect is latent to the metal support. Although the differences are small, in the order of 1 to 5 degrees for the solid parts, the metal support is the biggest contributor to high concentration losses near the exit.

It is suggested that during a transient time-step, the fuel and air feed are increased first so the fuel utilisation is less optimal. This prevents the system from crashing due to fuel shortage because of higher current densities.

11.3. METHANOL FROM WELL-TO-TANK

This study shows that methanol as a fuel for tank-to-wave purposes is viable from a performance perspective. However, the well-to-tank challenges are left open. Besides, methanol regulations have not yet matured for marine applications as a bunker fuel. An economic study about production and supply of methanol and a study about regulations towards the use of methanol as a fuel is needed also. Literature suggests that many companies already experiment with marine applications using methanol as a logistic fuel also, that will complement this research.

The emphasis of this study should lie in the compliance, the economic feasibility and the logistic challenges that methanol has. Currently methanol widely shipped as a liquid good. However, the rules for transporting something compared to using it as a fuel differ. Also, the long term effects of using methanol from a logistic point of view regarding deterioration of fuel tanks or health issues working in environment with methanol as a fuel are also unknown. The transition to methanol seems to be relatively easy due to its liquid nature, however effects like corrosion or being hygroscopic have not been studied extensively.

The fuel of the future depends as much on well-to-tank performance as for tank-to-wave performance regarding costs, safety and ease to use for a logistic fuel in general. It could even be said that the well-to-tank performance is directive [4]. The biggest drawback of methanol is that it emits carbon dioxide, something ammonia does not for example. However, this particular BoP and MS-SOFC configuration is specifically built for methanol. The performance will be significantly different when other fuels are considered. Therefore it is advised to stick to methanol regarding this research. If other fuels are preferred, then the BoP and MS-SOFC combination should be reviewed as well.

BIBLIOGRAPHY

1. IMO. Adoption of the Initial IMO Strategy on Reduction of GHG Emissions From Ships and Existing Imo Activity Related To Reducing Ghg Emissions in the Shipping Sector. *Mepc 72,* 27 (2018).
2. Serra, P. & Fancello, G. Towards the IMO's GHG goals: A critical overview of the perspectives and challenges of the main options for decarbonizing international shipping. *Sustainability (Switzerland)* **12.** ISSN: 20711050. doi:10.3390/su12083220 (2020).
3. DNV GL. Energy Transition Outlook 2020 - A global and regional forecast to 2050. *Dnv Gl Energy Transition Outlook,* 306 (2020).
4. DNV GL. Energy Transition Outlook 2020: Maritime Forecast To 2050, 118 (2020).
5. Niermann, M., Drünert, S., Kaltschmitt, M. & Bonhoff, K. Liquid organic hydrogen carriers (LOHCs)-techno-economic analysis of LOHCs in a defined process chain. *Energy and Environmental Science* **12,** 290–307. ISSN: 17545706. doi:10.1039/c8ee02700e (2019).
6. Hurskainen, M. & Ihonen, J. Techno-economic feasibility of road transport of hydrogen using liquid organic hydrogen carriers. *International Journal of Hydrogen Energy* **45,** 32098–32112. ISSN: 03603199. doi:10.1016/j.ijhydene.2020.08.186 (2020).
7. 't Hart, P. *The Royal Netherlands Navy expresses strong interest in methanol as fuel for its support vessels* 2020.
8. Staten-generaal, T. K. D. Materieelprojecten; Lijst van vragen en antwoorden; Lijst van vragen en antwoorden over het 'Project 'Vervanging hulpvaartuigen CZSK', 1–15 (2020).
9. Division, M. S., Organisation, D. M., Systems, S. & Team, I. Exploring the impact of methanol as an alternative , cleaner fuel for the auxiliary and support vessels within the RNLN (2020).
10. Moseley, P. *Fuel Cell Systems Explained* **1-2,** 285. ISBN: 047084857X. doi:10.1016/s0378-7753(00)00571-1 (2001).
11. Antig. *Types of Fuel Cells*
12. U.S. Department of Energy. *Types of Fuel Cells*
13. Tucker, M. C. Progress in metal-supported solid oxide fuel cells: A review. *Journal of Power Sources* **195,** 4570–4582. ISSN: 03787753. doi:10.1016/j.jpowsour.2010.02.035 (2010).
14. Yang, B. C. *et al.* Direct Alcohol-Fueled Low-Temperature Solid Oxide Fuel Cells: A Review. *Energy Technology* **7,** 5–19. ISSN: 21944296. doi:10.1002/ente.201700777 (2019).
15. Kundu, A., Shul, Y. G. & Kim, D. H. *Chapter Seven Methanol Reforming Processes* 419–472. ISBN: 9780080453941. doi:10.1016/S1752-301X(07)80012-3 (Elsevier Ltd, 2007).
16. Zhang, R. *et al.* Hydrogen production from methanol steam reforming over TiO2 and CeO2 pillared clay supported Au catalysts. *Applied Sciences (Switzerland)* **8,** 1–12. ISSN: 20763417. doi:10.3390/app8020176 (2018).
17. Meng, X. *et al.* Low-temperature ceria-electrolyte solid oxide fuel cells for efficient methanol oxidation. *Journal of Power Sources* **196,** 9961–9964. ISSN: 03787753. doi:10.1016/j.jpowsour.2011.08.002 (2011).
18. Roychoudhury, S. & Mastanduno, R. *Balance of Plant* 517–526. ISBN: 9780444535634. doi:10.1016/B978-0-444-53563-4.10015-X (Elsevier, 2011).
19. Van Biert, L., Godjevac, M., Visser, K. & Aravind, P. V. A review of fuel cell systems for maritime applications. *Journal of Power Sources* **327,** 345–364. ISSN: 03787753. doi:10.1016/j.jpowsour.2016.07.007 (2016).
20. RNLN. *Hydrografische opnemingsvaartuigen* 2021.
21. Brussel, V. Sailplan 2030 (2018).

22. Gaaij, A. E. D. Master thesis. *Mycotoxin Research* **-,** 127 (2019).

23. Geertsma, C. (d. i. & Krijgsman, i. M. Alternative fuels and power systems to reduce environmental impact of support vessels. *Proceedings of Marine Electrical and Control Systems Safety Conference (MECSS)* **1,** 1–9. doi:10.24868/issn.2515-8198.2019.003 (2019).

24. Speight, J. G. *Fuels for Fuel Cells* 29–48. ISBN: 9780444535634. doi:10.1016/B978-0-444-53563-4.10003-3 (Elsevier, 2011).

25. Kaltschmitt, T. & Deutschmann, O. Fuel Processing for Fuel Cells. *Advances in Chemical Engineering* **41,** 1–64. ISSN: 00652377. doi:10.1016/B978-0-12-386874-9.00001-4 (2012).

26. Adamopoulos, A. *Maersk claims progress in carbon neutral methanol hunt* 0.

27. Lloyd's Register & UMAS. Safety considerations for the use of zero-carbon fuels and technologies. *Part of Zero-Emission Vessels: Transition Pathways,* 16 (2019).

28. Dias, V., Pochet, M., Contino, F. & Jeanmart, H. Energy and Economic Costs of Chemical Storage. *Frontiers in Mechanical Engineering* **6.** ISSN: 22973079. doi:10.3389/fmech.2020.00021 (2020).

29. Valento, M., York, N., Booth, S. & Cameron, P. Toxic Alcohol Ingestion : Prompt Recognition And Management In The VISIT US AT ACEP i t i ss Toxic Alcohol Ingestion : Prompt Recognition And Management In The Emergency Department (2017).

30. Cardenas, D. Methanol and Hydrogen Production. *Energy Engineering,* 1–57 (2006).

31. Maritime Knowledge Centre, TNO & TU Delft. Methanol as an alternative fuel for vessels, 1–24 (2018).

32. Ru, Y., Sang, J., Xia, C., Wei, W. C. J. & Guan, W. Durability of direct internal reforming of methanol as fuel for solid oxide fuel cell with double-sided cathodes. *International Journal of Hydrogen Energy* **45,** 7069–7076. ISSN: 03603199. doi:10.1016/j.ijhydene.2019.12.222 (2020).

33. Iulianelli, A., Ghasemzadeh, K. & Basile, A. Progress in methanol steam reforming modelling via membrane reactors technology. *Membranes* **8,** 1–22. ISSN: 20770375. doi:10.3390/membranes8030065 (2018).

34. Choi, Y. & Stenger, H. G. Kinetics, simulation and optimization of methanol steam reformer for fuel cell applications. *Journal of Power Sources* **142,** 81–91. ISSN: 03787753. doi:10.1016/j.jpowsour.2004.08.058 (2005).

35. Li, Q., He, R., Gao, J.-A., Jensen, J. O. & Bjerrum, N. J. The CO Poisoning Effect in PEMFCs Operational at Temperatures up to 200°C. *Journal of The Electrochemical Society* **150,** A1599. ISSN: 00134651. doi:10.1149/1.1619984 (2003).

36. Ilsen Önsan, Z. & Avci, A. K. *Reactor Design for Fuel Processing* 451–516. ISBN: 9780444535634. doi:10.1016/B978-0-444-53563-4.10014-8 (2011).

37. Chiu, Y. J., Chiu, H. C., Hsieh, R. H., Jang, J. H. & Jiang, B. Y. Simulations of hydrogen production by methanol steam reforming. *Energy Procedia* **156,** 38–42. ISSN: 18766102. doi:10.1016/j.egypro.2018.11.081 (2019).

38. Campbell, C. T. The degree of rate control : a powerful tool for catalysis research, 1–27. doi:10.1021/acscatal.7b00115.

39. Shen, Y. *et al.* Hydrogen generation from methanol at near-room temperature. *Chemical Science* **8,** 7498–7504. ISSN: 20416539. doi:10.1039/c7sc01778b (2017).

40. Cambridge, U. o. *Engine*

41. Kee, R. J., Zhu, H., Braun, R. J. & Vincent, T. L. *Modeling the Steady-State and Dynamic Characteristics of Solid-Oxide Fuel Cells* 331–381. ISBN: 9780123868749. doi:10.1016/B978-0-12-386874-9.00010-5 (2012).

42. Sun, C. & Stimming, U. Recent anode advances in solid oxide fuel cells. *Journal of Power Sources* **171,** 247–260. ISSN: 03787753. doi:10.1016/j.jpowsour.2007.06.086 (2007).

43. Wang, Z. *et al.* Dynamic evaluation of low-temperature metal-supported solid oxide fuel cell oriented to auxiliary power units. *Journal of Power Sources* **176,** 90–95. ISSN: 03787753. doi:10.1016/j.jpowsour.2007.10.002 (2008).

44. Blennow, P. *et al.* Manufacturing and characterization of metal-supported solid oxide fuel cells. *Journal of Power Sources* **196,** 7117–7125. ISSN: 03787753. doi:10.1016/j.jpowsour.2010.08.088 (2011).

45. Noren, D. A. & Hoffman, M. A. Clarifying the Butler-Volmer equation and related approximations for calculating activation losses in solid oxide fuel cell models. *Journal of Power Sources* **152,** 175–181. ISSN: 03787753. doi:10.1016/j.jpowsour.2005.03.174 (2005).

46. Gellings, P. J. *et al. The CRC Handbook of Solid State Electrochemistry Library of Congr ess Cataloging-in-Publication Data* ISBN: 0849389569 (1997).

47. Aguiar, P., Adjiman, C. S. & Brandon, N. P. Anode-supported intermediate temperature direct internal reforming solid oxide fuel cell. I: Model-based steady-state performance. *Journal of Power Sources* **138,** 120–136. ISSN: 03787753. doi:10.1016/j.jpowsour.2004.06.040 (2004).

48. Costamagna, P., Selimovic, A., Del Borghi, M. & Agnew, G. Electrochemical model of the integrated planar solid oxide fuel cell (IP-SOFC). *Chemical Engineering Journal* **102,** 61–69. ISSN: 13858947. doi:10.1016/j.cej.2004.02.005 (2004).

49. Van Biert, L., Godjevac, M., Visser, K. & Aravind, P. V. Dynamic modelling of a direct internal reforming solid oxide fuel cell stack based on single cell experiments. *Applied Energy* **250,** 976–990. ISSN: 03062619. doi:10.1016/j.apenergy.2019.05.053 (2019).

50. Deeley, D. T. Positive displacement pumps. *in: Solids and Liquids Conveying Systems, M.V. Bhatia (Ed.), Westport, U.S.a., Technomic Publishing Co. Inc., 1982, Chapter 3* **4),** 110–152. ISSN: 0019-7866. doi:10.1201/9781482296600-16 (1982).

51. Kalikatzarakis, M., Geertsma, R. D., Boonen, E. J., Visser, K. & Negenborn, R. R. Ship energy management for hybrid propulsion and power supply with shore charging. *Control Engineering Practice* **76,** 133–154. ISSN: 09670661. doi:10.1016/j.conengprac.2018.04.009 (2018).

52. Boveri, A., Silvestro, F., Molinas, M. & Skjong, E. Optimal Sizing of Energy Storage Systems for Shipboard Applications. *IEEE Transactions on Energy Conversion* **34,** 801–811. ISSN: 08858969. doi:10.1109/TEC.2018.2882147 (2019).

53. Yu, S. Reformer Using Phase Change Heat Transfer. **3** (2020).

54. Zhu, J., Araya, S. S., Cui, X., Sahlin, S. L. & Knudsen Kaer, S. Modeling and Design of a Multi-Tubular Packed-Bed Reactor for Methanol Steam Reforming over a Cu/ZnO/Al 2 O 3 Catalyst. doi:10.3390/en13030610.

55. *NIST WebBook*

56. Xu, Q., Xia, L., He, Q., Guo, Z. & Ni, M. Thermo-electrochemical modelling of high temperature methanol-fuelled solid oxide fuel cells. *Applied Energy* **291,** 116832. ISSN: 03062619. doi:10.1016/j.apenergy.2021.116832 (2021).

57. Leah, R. T., Brandon, N. P. & Aguiar, P. Modelling of cells, stacks and systems based around metal-supported planar IT-SOFC cells with CGO electrolytes operating at 500-600°C. *Journal of Power Sources* **145,** 336–352. ISSN: 03787753. doi:10.1016/j.jpowsour.2004.12.067 (2005).

58. Xi, H. & Sun, J. Dynamic analysis of planar solid oxide fuel cell models with different assumptions of temperature layers. *Journal of Fuel Cell Science and Technology* **6,** 0110111–01101112. ISSN: 1550624X. doi:10.1115/1.2971055 (2009).

59. Xi, H. & Sun, J. A low-order dynamic model for planar solid oxide fuel cells using online iterative computation. *Journal of Fuel Cell Science and Technology* **5,** 1–12. ISSN: 1550624X. doi:10.1115/1.2931491 (2008).